DYNAMIC SAFETY ANALYSIS OF A SUBCRITICAL ADVANCED BURNER REACTOR

A Dissertation
Presented to
The Academic Faculty

By

Andrew Tyler Bopp

In Partial Fulfillment
of the Requirements for the Degree
Doctor of Philosophy in
Nuclear Engineering

Georgia Institute of Technology

May 2017

DYNAMIC SAFETY ANALYSIS
OF A
SUBCRITICAL ADVANCED BURNER REACTOR

Approved by:

Dr. Weston Stacey, Advisor
Nuclear and Radiological Engineering Program
Georgia Institute of Technology

Dr. Mostafa Ghiaasiaan
School of Mechanical Engineering
Georgia Institute of Technology

Dr. Bojan Petrovic
Nuclear and Radiological Engineering Program
Georgia Institute of Technology

Dr. Anna Erickson
Nuclear and Radiological Engineering Program
Georgia Institute of Technology

Dr. Jim Grudzinski
Nuclear Engineering Division
Argonne National Laboratory

Date Approved: March 30, 2017

ACKNOWLEDGEMENTS

I completed this thesis with the aid of many people. Firstly, I thank my advisor Dr. Weston Stacey for his seemingly infinite patience and open mindedness. I thank Dr. Jim Grudzinski for teaching me all about fuel bowing and the many phone conversations we've had on the subject. I thank Dr. Bojan Petrovic for the use of his cluster B1 which made the computational work of this thesis feasible. I thank Dr. Chris Chapman for creating the MCNP cross section sets I needed. I thank my committee members for their time and technical expertise. I thank my family for years of belief and financial support.

Lastly, I thank Steph Provow. I would not have finished this thesis without the years of her unrelenting love and encouragement.

TABLE OF CONTENTS

LIST OF TABLES

LIST OF FIGURES

SUMMARY

Nuclear power provides the only technically credible option for impacting climate change in the next century. The ultimate disposal of long lived transuranics (TRU) in spent nuclear fuel is the central technical issue preventing the expansion of nuclear power. Georgia Tech's Subcritical Advanced Burner Reactor (SABR) aims to close the back end of the nuclear fuel cycle by destroying TRU. SABR is composed of 10 physically separate but neutronically coupled pool type fast reactors. In this thesis, we develop a customized dynamic safety model and use it to analyze the safety characteristics of SABR. We simulate Loss of Flow Accidents, Loss of Heat Sink Accidents, and Loss of Power Accidents. We analyze the effect of various shutdown mechanisms such as inserting control rods and shutting the fusion reactor off. The core avoids failure (no fuel melting or coolant boiling) for 50% (failure of 1 of 2 pumps) Lost of Heat Sink (LOHSA) and Loss of Flow (LOFA) accidents without any corrective action being taken. For 100% (failure of both pumps) LOFAs and LOHSAs, coolant boiling (1156 K) and fuel melting (1473 K) occur at about 25s and 35s, respectively, after pump failure unless corrective control action is taken before this time, in which case the core can be shut down without fuel melting or coolant boiling by shutting off the plasma power source. The present passive heat removal system is not sufficient to remove the decay heat and both fuel melting and coolant boiling ultimately occur in the 100% LOFAs and LOHSAs (failure of both pumps) unless some other means is provided for decay heat removal. We make recommendations on how to improve the passive safety characteristics of SABR.

CHAPTER 1
INTRODUCTION

1.1 The Waste Problem

If we want to impact climate change over the next century, we need a massive source of clean, carbon-free energy. Nuclear power provides the only technically credible option. The major technical problem preventing the widespread expansion of nuclear power is nuclear waste. The United States government currently has no plan to deal with nuclear waste generated by commercial power plants. Plant operators have been forced to stockpile their waste on site.

The term nuclear waste usually refers to spent nuclear fuel (SNF). Spent nuclear fuel is fuel that has just been removed from a reactor. It contains a mixture of unfissioned uranium, structural mechanics, fission products (FP), and transuranics (TRU). Unfissioned uranium composes the majority of SNF. The fission products decay fairly rapidly and actually generate heat in the fuel despite no longer being in the reactor. Fission products typically decay away within about 100 years. The TRU on the other hand remains radioactive for millions of years.

The common suggestion to deal with this waste is the high-level radioactive waste repository (HLWR). A repository could store this waste for millions of years until it was no longer radioactive. This is easier said than done. Various organizations have proposed several HLWRs, but none of them are close to becoming a reality in the U.S.

Fortunately, there is another way to deal with this problem and dispose of TRU. TRU can be fissioned in a fast burner reactor. The high energy spectrum of a fast reactor enables it to fission TRU and transmute it into the shorter lived FPs. This process destroys TRU and produces more recoverable energy at the same time.

Some TRU elements are fairly reactive, but others are not and will absorb quite a few neutrons before fissioning. A fast burner reactor with TRU will require uranium "driver" fuel to be mixed in for two reasons: safety and reactivity. We discuss the safety aspect in the next chapter. The reactivity aspect is that TRU is not reactive enough to self sustain. It consumes more neutrons than it produces. The driver fuel adds extra neutrons and sustains the fission chain reaction. The requirement for uranium fuel reduces the net amount of TRU we can burn in the reactor, and it produces some TRU in the process. This makes critical fast burner reactors inefficient at burning TRU.

A more efficient way is to fuel a reactor completely with TRU and operate it subcritically by using an adjustable neutron source to maintain the fission chain reaction. This allows each reactor to burn more TRU and decreases the total number of reactors needed to burn a certain amount of TRU.

There are two types of external neutron sources that have been suggested for this. The first is an "accelerator driven system" where accelerated deuterons impinge on a spallation neutron target embedded in the TRU fuel. The second type is a "fission fusion hybrid reactor" where the 14.1 MeV neutrons from deuterium-tritium fusion reactions stream into TRU fuel located outside the plasma chamber.

The subcriticality of a source driven system provides two distinct advantages. The first advantage is burnup. As we deplete the fissionable TRU by burnup and decrease its reactivity, we can maintain the fission chain reaction at the same power by increasing the neutron source as shown in Eq. 1.1. This results in increased fuel burnup. We only have to remove the fuel when it reaches its radiation damage limit instead of removing it when the fuel loses too much reactivity. When the radiation damage limit is reached, the fuel is removed and reprocessed. During reprocessing, any unburned TRU goes back into the fuel, and any fission products are removed and sent to the repository. The deeper the burnup that

can be achieved, the fewer times the fuel will need to be reprocessed.

$$(TRU\ Fission\ Rate) = \frac{k_{source}}{1 - k_{source}}(Plasma\ Fusion\ Rate) \tag{1.1}$$

k_{source} is the number of fission neutrons generated per plasma source neutron emitted.

The second advantage is safety. The reactivity margin to a prompt supercritical power excursion is larger for a subcritical reactor than for a critical reactor. The reasons for this are explained in the next chapter.

1.2 SABR Overview

The Subcritical Advanced Burner Reactor (SABR) is a fission fusion hybrid burner reactor that is intended to close the back end of the nuclear fuel cycle [1]. SABR is a combination of an ITER fusion device and an Integral Fast Reactor (IFR) [2, 3]. A graphical overview is shown in Fig. 1.1. SABR's fusion device is based on ITER's design. It has ITER-like dimensions as shown in Fig. 1.1, and it can breed the tritium it requires for operation. The fission reactor lies just outside the plasma chamber, and it is composed of 10 separate sodium pools each with their own fission core and heat exchanger. One of the pools is shown in Fig. 1.2, and one of the assemblies is shown in Fig. 1.3. Each pool contains a metal fueled, sodium cooled, pool type fast reactor. Reloading a reactor requires removing the entire pool. Fig. 1.4 shows how the pools are rotated around the plasma chamber, removed between the magnets and transported to hot cells for refueling.

SABR's fuel is a 100% TRU-Zr alloy developed by Argonne National Laboratory (ANL). We estimate that each SABR can annually destroy the TRU from 3 LWRs or the minor actinides from up to 25 LWRs [1]. SABR uses a pyro-processing fuel cycle that separates the TRU from the FPs as a single aggregate metal. The plutonium is never separated from the other TRU, and that greatly reduces the risk of proliferation.

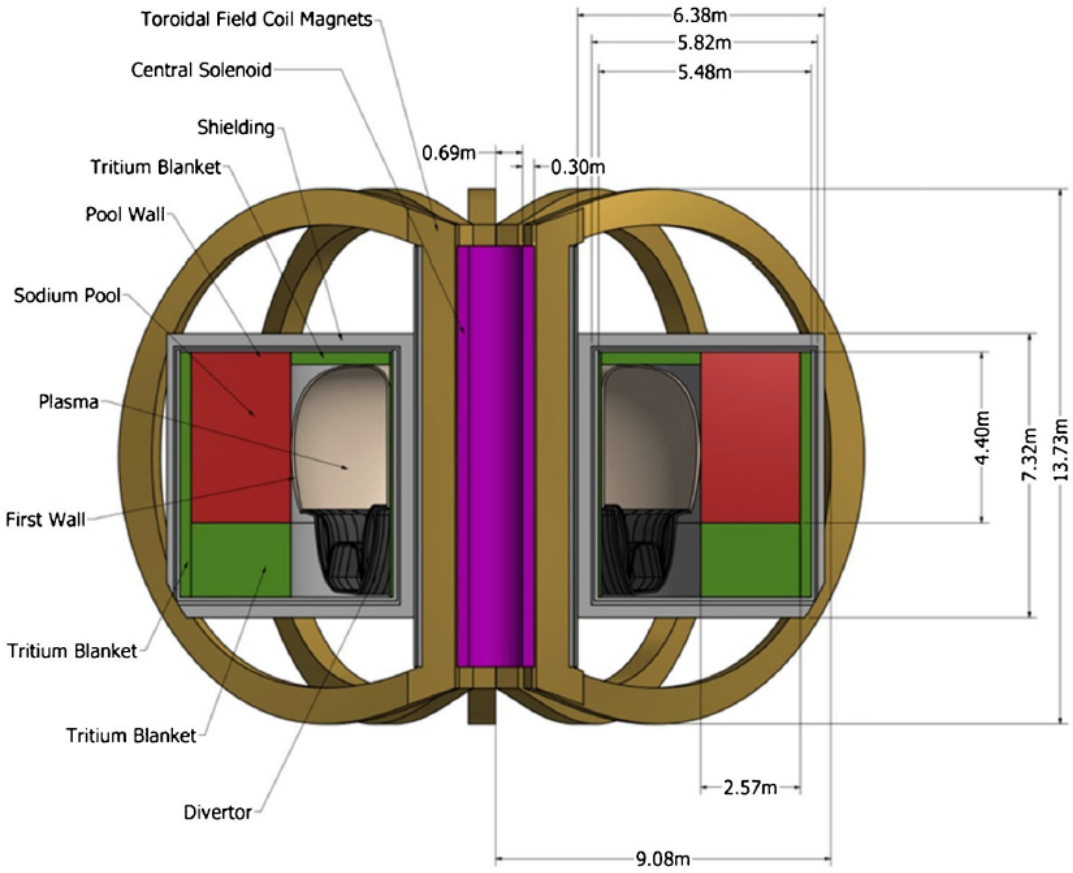

Figure 1.1: Overview of SABR [1]

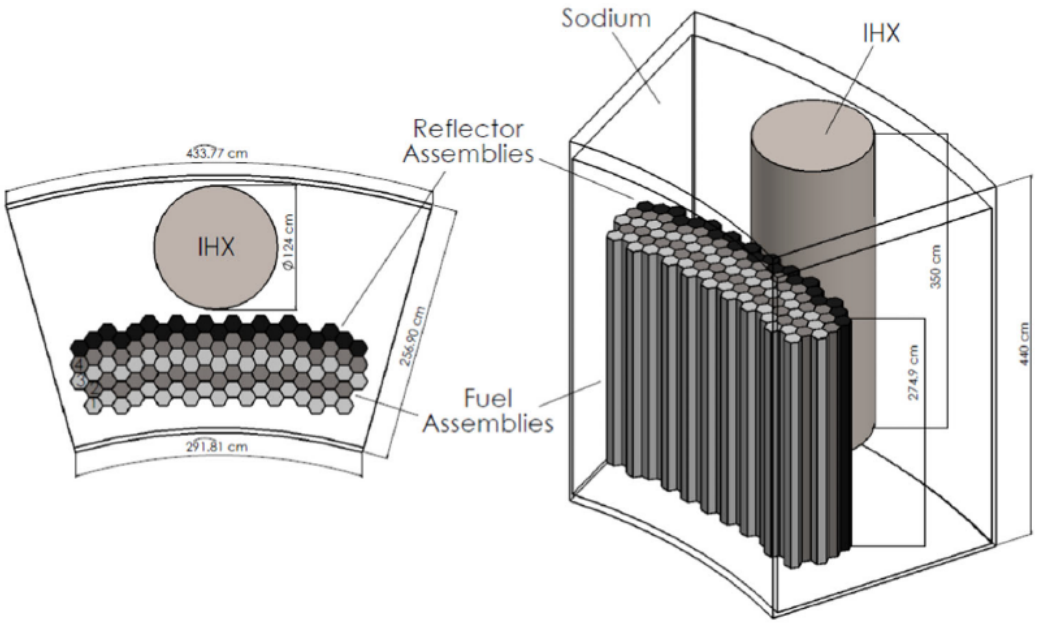

Figure 1.2: SABR Sodium Pool [1]

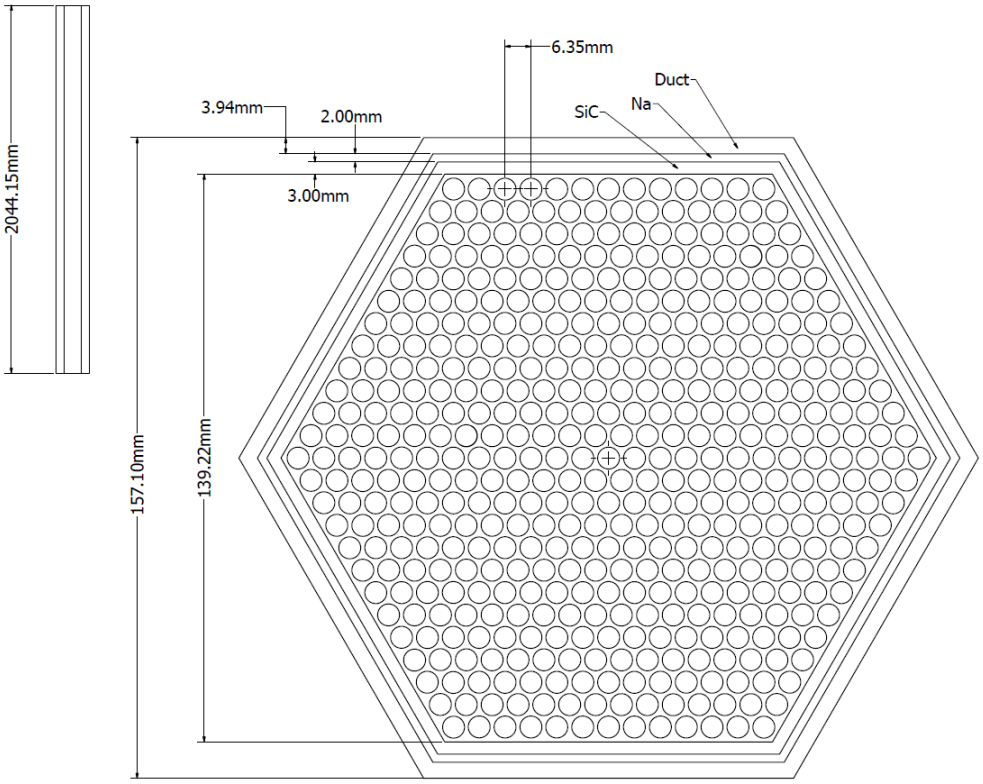

Figure 1.3: SABR Fuel Assembly [1]

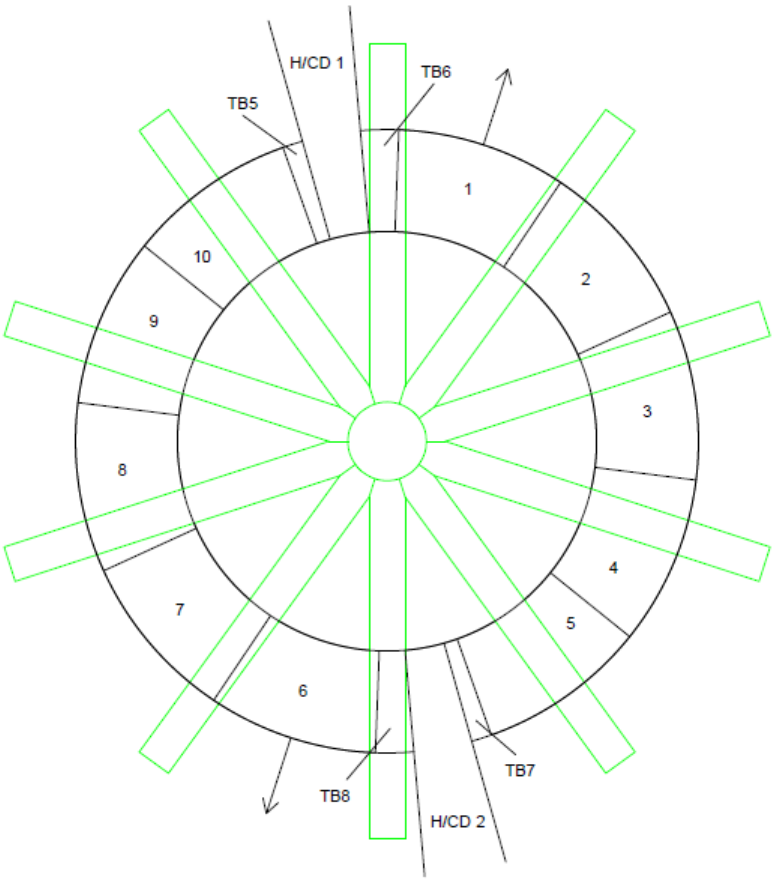

Figure 1.4: SABR Pool Reloading Scheme [1]

The design of the fission reactors borrows heavily from the IFR. ANL designed the IFR to be passively safe [4]. This was based on experimental work done by ANL on the Experimental Breeder Reactors (EBR I and II). EBR-I was built in 1951 and operated until 1965 [5]. It was the first nuclear reactor to produce electricity, the first reactor to demonstrate the breeding gain of fissile material, and the first reactor to use molten metal as a coolant. EBR-I experienced a partial meltdown in 1955. The operators were studying how the power level responded to a change in coolant flow rate. The response was a power spike that caused a partial fuel meltdown. The operators realized the temperature distriubution across the fuel caused it to bow inward toward the center of the core. The fuel caused the power spike by moving into a region of higher neutron flux.

The engineers at ANL kept this fuel bowing in mind as they designed EBR-II in 1965. EBR-II's design used dimples on the outer surface of the fuel assemblies to prevent inward bowing of the fuel during a transient [6]. Doing so reduced the positive reactivity from fuel bowing enough to allow other negative feedbacks to appreciably reduce the reactor power during several planned transients in 1986 [7]. ANL conducted Loss of Flow Accident (LOFA) and Loss of Heat Sink Accident (LOHSA) tests from full power without SCRAM. For all cases, the negative reactivty feedbacks lowered the power enough such that natural circulation could cool the core indefinitely. The IFR incorporates these principles in its design.

We hope that SABR retains some of these passive safety features, but there are several design differences between SABR and IFR. IFR is a single core, critical reactor. SABR is a subcritical, source driven reactor with 10 physically separate but neutronically coupled cores. A change in the power level in one core could affect the power level of the neighboring cores. This is complex behavior, and it is very difficult to model. It is the intention of this PhD thesis to perform a dynamic safety analysis of SABR. The primary objective is to determine is SABR can be safely controlled, and the secondary objective is to determine if it retains and of the IFR's passive safety characteristics.

CHAPTER 2

NUCLEAR REACTOR KINETICS

Nuclear reactors normally operate at a constant power level, but the power level can change due to various factors. A few examples are: a change in core temperature, the removal of a control rod, the addition of neutron absorbers to the coolant, and the depletion of fuel. Changes in power can be anywhere from small and slow to large and instant. It's important to understand how quickly these changes occur. The field of study that models a reactor's time dependent behavior is called nuclear reactor kinetics.

The neutrons produced in a fission reaction do not all show up at the same time. Some neutrons show up about $10^{-14}\ s$ after fission occurs. We call these "prompt" neutrons. Some neutrons show up seconds or even minutes after a fission. We call these "delayed" neutrons. Fewer than 1% of fission neutrons are delayed. This may seem a small number, but delayed neutrons have a huge impact the kinetics of a reactor. Consider the case of supercriticality. A reactor may become supercritical enough to meltdown but avoid doing so because delayed neutrons allow enough additional time for corrective action. To explain how this happens, let's define some key terms.

β is the fraction of fission neutrons that are delayed.

$k_{effective}$, or the more commonly used k, is defined in Eq. 2.1. k is the multiplication factor of a nuclear reactor. Critical reactors have a k equal to one. Supercritical reactors have a k larger than one. Subcritical reactors have a k smaller than one.

$$k_{effective} = \frac{Number\ of\ neutrons\ produced\ in\ generation\ i}{Number\ of\ neutrons\ produced\ in\ generation\ i+1} \tag{2.1}$$

ρ is reactivity, and it is defined in Eq. 2.2. Reactivity is a measure of the change in k. A positive reactivity means an increase k. A negative reactivity means a decrease in k. A

reactivity of zero means no change in k.

$$\rho = \frac{k-1}{k} \tag{2.2}$$

Now back to the case of supercriticality. Something causes our reactor to go supercritical, and we have $\rho > 0$. If the reactivty is positive but smaller than the delayed neutron fraction ($\beta > \rho > 0$), the reactor is operating in the "delayed supercritical" regime. It's power is increasing slow enough such that we have seconds or minutes to respond. If however the reactivity is both positive and larger than the delayed neutron fraction ($\rho > \beta > 0$), then the reactor is operating in the "prompt supercritical" regime. The power will increase so rapidly that the fuel will melt almost instantaneously. This is really a worst case scenario for any reactor.

This is where the safety advantage of a subcritical, source driven system that we alluded to earlier becomes obvious. For a critical reactor, the reactivity margin to promp supercriticality is $\Delta\rho \approx \beta$. On the other hand, for a subcritical reactor, the safety margin is $\Delta\rho = \Delta k_{sub} + \beta >> \beta$.

Nuclear power plants have been operating in the U.S. since 1971, and as of 2015, there were 99 operating reactors [8]. Only a single meltdown has occured at a U.S. power plant, and it wasn't due to prompt supercriticality. It was due to a Loss of Coolant Accident (LOCA). A prompt supercritical meltdown has never occured at a commercial nuclear power plant in the U.S.

On March 28, 1979, one of the reactors at the Three Mile Island power plant in Pennsylvania melted down [9]. A mechanical failure in the secondary system initiated a SCRAM that successfully shut the reactor down. A SCRAM is when all of the neutron absorbing control rods are inserted into the reactor core as quickly as possible. The only heat being generated after a SCRAM is called decay heat. Decay heat results from the decay of fission products, and it slowly decreases over days and weeks. The decay heat caused the water pressure in the reactor core to rise, and plant operators opened relief valves to decrease

the pressure. Due to instrument failure in the control room, the operators removed more coolant from the core than they intended to and left the core without sufficient cooling. A large part of the reactor core melted before the decay heat decreased enough to stop the melting. The radiation released from the plant was minimal, and there was no physical harm to the public or plant workers.

The scenario of a prompt supercritical meltdown sounds scary, but in reality it's easy to avoid. The avoidance of a meltdown is at the forefront of concern when designing a nuclear power plant. EBR-II is an excellent example of how nuclear engineers can design a reactor to avoid melting down during an accident. EBR-II's operators subjected it to severe accidents, and EBR-II did not melt down in any case. It did so without any external help from the operators or emergency equipment. There were no control rods to SCRAM the reactor; the reactivity feedbacks shut it down. There were no backup pumps; natural circulation was enough to cool the core. It was completely passively safe with no threat of a meltdown.

2.1 Point Kinetics

The point kinetics equations shown in Eqs. 2.3 and 2.4 are the most widely used method to determine a reactor's transient neutron behavior. The approach treats the reactor as a single point by assuming the power profile across the core changes only in magnitude and not in shape. It assumes that any change in power scales directly with any change in neutron density [10]. This method works as long a core's size isn't too large or heterogeneous.

$$\frac{dn}{dt} = \frac{\rho(t) - \beta}{\Lambda} n(t) + \sum_{i=1}^{6} \lambda_i c_i(t) \tag{2.3}$$

$$\frac{dc_i}{dt} = \frac{\beta_i}{\Lambda} n(t) - \lambda_i c_i(t) \ , \ for\ i = 1\ to\ 6 \tag{2.4}$$

$n(t)$ is the neutron density, $\rho(t)$ is the reactivity, β is the effective delayed neutron

fraction, λ_i is the decay constant of the i^{th} delayed neutron group, $c_i(t)$ is the neutron density of delayed neutron precursor isotopes for the i^{th} group, β_i is the delayed neutron fraction of the i^{th} delayed neutron group, and Λ is the mean generation time of fission neutrons. These equations are easy to solve, and they even have analytical solutions if a few approximations are made. The real work in setting up an accurate point kinetics model is determining how the reactivity $\rho(t)$ changes with time.

2.2 Reactivity Feedbacks

Reactivity feedbacks quantify how the reactivity of a reactor changes with time. Reactivity is usually a function of temperature, which is a function of time. This could be the temperature of the fuel, the cladding, the moderator, or the coolant. Nuclear engineers exert great effort in making tables of reactivity vs temperature. The hard part about it is that there are so many mechanisms by which temperature affects reactivity. There are different types of reactivity feedbacks. The design of the reactor dictates which feedbacks are relevant, but in general the most prevalent feedbacks are Doppler broadening, moderator voiding, core axial expansion, core radial expansion, and fuel bowing.

2.2.1 Doppler Broadening

Doppler broadening occurs when an increase in fuel temperature broadens the absorption resonances of the fuel [11]. The resonance, or cross-section, is a function of incoming neutron energy. The cross section spikes at very specific neutron energies. The fuel absorbs a neutron only if that neutron is at just the right energy. When the fuel increases in temperature, the thermionic motion of its molecules increases as well. Thermionic motion is the vibration of stationary molecules. As fuel heats up and its molucules vibrate harder, the relative energy of incoming neutrons gets a little randomized and fewer fission reactions occur. It's the Doppler effect. It's the same reason a train whistle sounds higher as it travels towards someone and lower as it travels away from them. Doppler broadening

is the quickest reactivity feedback. A change in power manifests in the fuel and activates Doppler broadening before any other feedback. Sensitivity to Doppler broadening depends on the isotopic composition of the fuel.

2.2.2 Moderator Voiding

Moderator voiding occurs when an increase in moderator temperature causes it to expand and become less dense. The job of the moderator is to interact with neutrons and slow them down so they are more likely to cause fission. If we reduce the density of the moderator, we reduce its ability to interact with neutrons. This effect is most pronounced in water moderated systems where the water density can change so much it changes phases. This is called ”voiding”. This feedback applies to the coolant voiding as well. Some reactor designs include coolant and moderator voiding in the same reactivity coefficient. This is done for reactors that use the same material for the coolant as they do the moderator (usually water). Other reactor designs have no moderator (such as fast reactors like SABR) or use separate materials for their moderator and coolants. Using separate materials for the moderator and coolant may have its advantages, but if the reactor is not carefully designed, this can lead to a positive reactivity feedback. This called a ”positive void coefficient”.

Chernobyl is a perfect example of what a positive void coefficient can do. On April 26, 1986, an unintended power surge destroyed one of the reactors at the Soviet Union’s Chernobyl Power Station [12]. The destruction resulted in the release of massive amounts of radioactive material into the atmosphere and local environment. There were a litany of failures that caused this destruction, both technical and human. One of the technical failures was the reactor design itself. It had a positive void coefficient. It was a graphite moderated, water cooled reactor. Several human errors created a small power spike in the core. The positive void coefficient magnified the spike. The spike flashed the coolant into steam. There was little coolant left in the core, but the graphite moderator remained unchanged. The water coolant was responsible for a small amount of parasitic neutron absorption,

and once this water was gone, so was the absorption. The extra neutrons available turned the small power spike into a large power spike. This was the final stage of the accident before the reactor literally blew the roof off of the building and began releasing radioactive material. The positive void coefficient was not responsible for all of this, but it was huge factor.

2.2.3 Core Axial Expansion

Core axial expansion occurs when an increase in temperature causes thermal expansion in the axial direction of the fuel, reflectors, or control rods. Fuel, reflector, and control rods have high aspect ratios; they are very thin and very long. Radial expansion in these individual components is trivial. Their axial expansion is not. The axial expansion of fuel and reflectors creates negative reactivity by increasing the surface area of the core. Any increase in core surface area will increase neutron leakage. Fast reactors are very sensitive to neutron leakge due to the higher mean free paths of their neutrons. In other words, the neutrons of a fast reactor already have an easy time escaping, so anything that increases this provides negative reactivity. The axial expansion of a control rod creates negative reactivity by increasing neutron absorption in the core. Fast reactors are more sensitive to fuel and reflector expansion, and thermal reactors are more senstive to contol rod expansion.

2.2.4 Core Radial Expansion

Core radial expansion occurs predominantly in fast reactors. The bottom of fast reactor fuel assemblies fit into a large steel grid plate that holds them in place. An increase in grid plate temperature causes it to thermally expand and stretch the core out radially. This increases the surface area of the core and subsequently increases neutron leakage. For a given increase in temperature, this feedback gives more negative reactivity than axial expansion. A fast reactor is shaped like a cylinder. If you increase a cylinder's height by a factor of 2, you will increase its surface area (which is proportional to neutron leakage) by

a factor of 2. If you increase its radius by a factor of 2, you increase its surface area by a factor of 4. The surface area of a cylinder scales linearly with height and exponentially with radius. This is why most fast reactors are designed to be shorter and wider than thermal reactors.

2.2.5 Fuel Bowing

Fuel bowing is exclusive to fuel assemblies with an outer shell. This describes most fast reactor fuel assemblies. Fast reactor fuel assemblies are composed of many fuel pins encased in a large hexagonal duct. Fuel bowing occurs when a temperature gradient develops across one of these ducts. The temperature gradient causes differential thermal expansion across the assembly and causes it to bow. For example, consider the three cases shown in Fig. 2.1. Case 1 shows a rod at a uniform temperature of 600 K. For Case 2, we heat the rod up to a uniform temperature of 800 K, and we see the rod increases in length due to thermal expansion. For Case 3, we put the rod under a non-uniform temperature distribution. The rod is hotter on the right side than it is on the left side. The right side thermally expands to a larger degree than the left side does resulting a deformed shape.

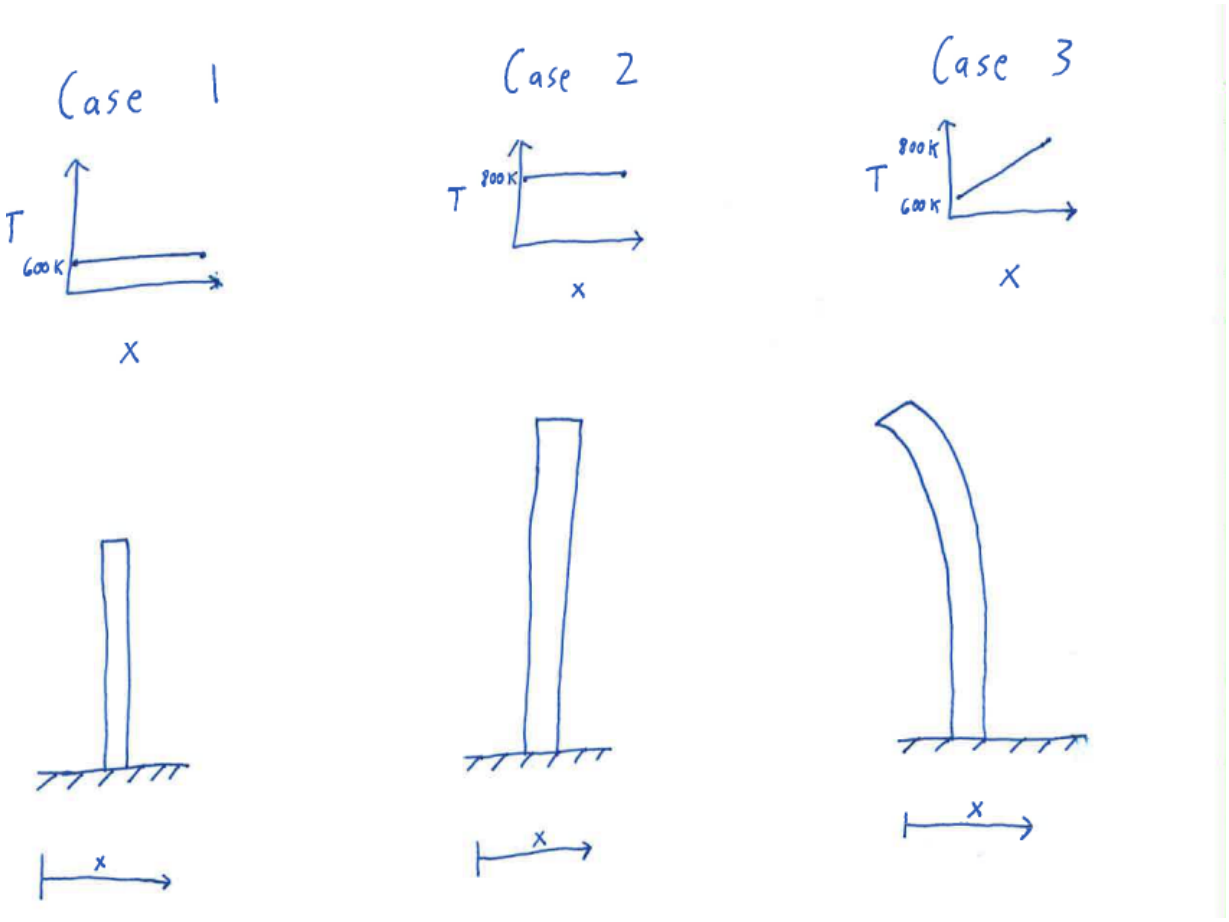

Figure 2.1: Example of Thermal Bowing

The fuel pins inside the assemblies do not contribute to fuel bowing because they are not large enough to develop a big enough temperature gradient. They also don't inhibit fuel bowing. The reason is shear coupling (or rather the lack thereof). When the duct changes shape, it pushes the pins into different positions. The pins are powerless to resist because each individual pin can move up and down relatively freely of one another. The perfect analog to this is a phone book. It's easy to bend a phone book, but if you hold it closed very tightly it's much harder to bend. You are increasing the shear coupling by enhancing the page-to-page friction.

Fuel bowing provides a change in reactivity by moving the fuel pins to a different

position in the reactor core. The neutron flux in a reactor core generally varies with radius. It tends to be much higher in the center of the core and much lower at the edge of the core. If fuel bows toward the center of the core, you get postive reactivity. If fuel bows away from the core, you get negative reactivity. As we mentioned in Chapter 1, fuel bowing was discovered by accident in EBR-I. The clever engineer can design his or her reactor to take advantage of this powerful feedback by ensuring it creates negative reactivity.

2.3 Power Tilts

There is an interesting transient phenomenon in coupled systems: power tilts. A power tilt occurrs when a perturbation of some sort excites higher flux modes in the system. This leads to a change in the eigenvalue and the power distribution. This generally happens in large, heterogenous cores where there is a degree of neutronic decoupling between two regions. It has even been shown that the degree of decoupling is related to the change in eigenvalue during the power tilt [13]. Such power tilts are possible in SABR, and they could lead to standing power oscillations between the cores depending on the feedback mechanisms involved.

2.4 Nodal Kinetics

Some reactors are large and heterogeneous enough that the point kinetics approach is no longer applicable. They require a kinetics model that accounts for changes in power distribution. Engineers use large, computationally expensive, 3D finite difference kinetics codes to model these cores. Nodal kinetics lies on the midpoint between point kinetics and 3D finite difference kinetics. It captures more detail than point kinetics and is more computationally efficient than 3D finite difference. Nodal kinetics works by subdividing a core into an arbitrary number of nodes and homogenizing their contents [11]. The nodes are coupled to one another through the use of coupling coefficients. Nodal kinetics is a natural fit for SABR. Each individual SABR core has a relatively uniform flux because of the long mean

free path of the neutrons.

CHAPTER 3
BACKGROUND REVIEW

3.1 Neutronic Coupling

SABR will likely exhibit some very unique neutronic behavior. SABR's 10 modular fission reactors are physically separate but neutronically coupled. They are close enough so that neutrons can stream from core to core. A perturbation in one core could affect several of the neighboring cores. This makes their time dependent behavior difficult to model. The standard point kinetics model ignores spatially dependent behavior and treats the entire system as a single point. Any perturbation in the system will affect the entire system uniformly. This is not an accurate reflection of SABR.

Each fission reactor needs its own set of point kinetics equations that are coupled to the other cores. This is a perfect application for nodal kinetics. There are many different ways to define and implement nodal kinetics, so it's worth reviewing some published works on the subject.

Avery was the first to suggest the use of nodal kinetics [14]. His underlying approach was energy dependent diffusion theory. He accounts for coupling by breaking down the fission source in each node into multiple components. Each component represents fissions induced by neutrons from another specific node. He solves for the flux in all nodes while setting the fission sources in all but one node to zero. One by one, he does this for all nodes in the system, and then applies superposition to model the full system.

Murray et al. derives some time-dependent power equations for an array of N-coupled cores in a critical system [15]. The equations assume the reactivity feedbacks are intrinsically negative, that prompt neutron kinetics are sufficient, and that all cores in the array have identical charactersitics.

Belleni-Morante discusses the use of coupled kinetics equations with delayed neutrons [16]. His formulation is shown below.

$$\frac{dn_g(t)}{dt} = \frac{(1-\beta_g)k_g(t)-1}{l_g} n_g(t) + \frac{1}{l_g}\sum_{g'=1}^{G} \alpha_{gg'} n_{g'}(t-\tau_{gg'}) + \sum_{d=1}^{D} \lambda_{gd} c_{gd}(t) \tag{3.1}$$

$$\frac{dc_{gd}(t)}{dt} = -\lambda_{gd} c_{gd}(t) + \frac{\beta_{gd}}{l_g} k_g(t) n_g(t) \tag{3.2}$$

$n_g(t)$ is the neutron density in the g-th fuel region, $c_{gd}(t)$ is the precursor density of the d-th group of delayed neutrons in the g-th region, λ_{gd} is the precursor delay constant, β_{gd} is the fraction of delayed neutrons belonging to the d-th group in the g-th region, β_g is the overall delayed neutron fraction for the g-th region, l_g is the mean lifetime of neutrons in the g-th region, $k_g(t)$ is the multiplication factor, $\alpha_{gg'}$ is the coupling coefficient between the g'-th and the g-th region ($\alpha_{gg} = 0$), and $\tau_{gg'}$ is the time lag. We can heavily modify this formulation to create a model applicable to SABR. First, we need an external source. Second, we neglect the core to core streaming time. In SABR, the time of flight of neutrons from core to core is negligible because it's a fast reactor. Third, we redefine several existing terms to ensure we can calculate them.

3.2 Existing Dynamic Safety Codes

Computer codes like TRACE, RELAP, and SAS are the tools of choice when analyzing the dynamic safety of a nuclear reactor [17, 18, 19]. The U.S. Nuclear Regulatory Comission (NRC) maintains TRACE and uses it as their primary tool for thermal hydraulic analysis [17]. TRACE can model two fluid compressible flow in 3D, and it can couple to an NRC 3D kinetics solver called PARCS [20]. Unfortunately, TRACE is not currently capable of modeling sodium-cooled systems.

Idaho National Laboratory (INL) developed RELAP for the NRC [18]. It contains

many features similar to TRACE. RELAP can model multidimensional flow, and it has several built-in kinetics solvers. While most of these solvers rely on point kinetics, there is one solver, NESTLE, that takes the nodal kinetics approach [21]. NESTLE solves the few-group neutron diffusion equation for critical systems. Its implementation in RELAP is incompatible with a source-driven system. Additionally, while NESTLE is a nodal kinetics solver, it does not handle neutronic coupling the way we need it to. The solver uses a diffusion equation that only accounts for neutrons streaming to and from directly adjacent nodes. We require a model that accounts for neutrons from all other nodes. None of RELAP's built-in kinetics solvers can do what we need, but we could couple RELAP to PARCS. PARCS can handle a source-driven system, but it cannot handle the neutronic coupling of multiple nodes.

Argonne National Lab (ANL) developed SAS to model accident scenarios in liquid metal fast reactors [19]. SAS can model the two phase flow of molten metal coolant in 1D, and it has a built-in kinetics solver. This kinetics solver takes the point kinetics approach, so it is not suited to our purposes. In the past, ANL developed a special version of SAS called SAS-DIF3DK. This version couples the thermal hydarulics solvers of SAS with the impressive kinetics solvers of DIF3DK. Not only can DIF3DK model nodal kinetics, it can do so in a source-driven system. Sadly, SAS-DIF3DK is currently listed as "in development" and is not available for distribution [22].

No computer codes currently available are capable of performing a dynamic safety analysis of SABR. This is not surprising because SABR is the only reactor design in the published literature that combines the complexities of a source-driven, fission-fusion hybrid reactor with the physics of nodal kinetics and neutronic coupling. Before we move on to describe the custom dynamics model that is the purpose of this thesis, we review some designs similar to SABR and any dynamic safety analyses performed on them.

CHAPTER 4
REVIEW OF OTHER FISSION-FUSION HYBRIDS

4.1 Other FFHR Designs

Argonne National Laboratory suggests a fission-fusion hybrid for the destruction of TRU, spent nuclear fuel, and highly enriched uranium [23]. The design uses a fusion neutron source surrounded by molten blanket of fuel and coolant. The coolant is a molten salt called Flibe (Li_2BeF_4) that was develeoped for the Molten Salt Breeder Reactor in the 1960s [24]. The fuel is either molten UF_4, ThF_4, or PuF_3 [25]. The authors estimate that a PuF_3 fuel with a weight fraction of 0.56% would be able to destroy up 79.689 kg/(MW year).

Sandia National Laboratory has developed what they call the "In-Zinerator Power Plant" [26]. It uses a 20 MW Z-pinch fusion device to produce 3000 MW of power in a blanket of TRU fuel. The Z-pinch device generates fusion by passing a large amount of current through the plasma which generates magnetic fields strong enough to induce plasma. The In-Zinerator would be able to destroy up to 1280 kg of actinides per year. It uses a molten salt fuel and a liquid lead coolant. It is interesting to note that the fuel specifically excludes plutonium which is often included in TRU burner reactors. The design is fairly thorough, but there is no discussion on safety or modeling accident scenarios.

Researchers at Xi'an University in China have developed a fission-fusion hybrid reactor concept that relies on an ITER fusion device just as SABR does [27]. The fuel is a mixture of spent nuclear fuel and natural uranium oxide. The fuel is a continuous blanket wrapped around the outside of the plasma chamber. Pressurized tubes of water are woven into the fission blanket in order to cool it. The design has a lifetime of only 5 years, and it appears to still be in an early conceptual stage of development.

The ”fusion-fission transmutation system” at the University of Texas is another burner reactor concept[28]. Its fusion neutron source is the ”compact fusion neutron source”, and it is still in the theoretical stage of development. The reactor design does not propose a specific fuel cycle for the destruction of TRU. There is little to no information on thermal hydraulic peformance, power conversion cycles, or safety analyses.

4.2 Other FFHR Safety Analyses

The designs in the preceding section are all similar to SABR in one respect or another, but there is a consistent difference: the lack of any safety analysis. There are few safety analyses on fission fusion hybrids.

Previous researchers in our research group performed a safety analysis of an older version of SABR in 2010 [29]. That version's fission reactor is not divided into ten pools. It is composed of a single loop type core. The core is continuously wrapped around the outside of the tokamak instead of the 10 modular sodium pools showns in Figs. 1.1 and 1.2. It is assumed that any perturbation affects the entire system uniformly. The researcher used RELAP5 to run Loss of Flow Accidents (LOFA), Loss of Heat Sink Accidents (LOHSA), and Loss of Power Accidents (LOPA). He also considered reactivity insertion accidents such as control rod removal and an increase in the fusion neutron source strength. He used point kinetics, and he accounted for Doppler broadening and sodium voiding reactivity feedbacks. The accidents were simulated for Beginning of Fuel Lifetime (BOL), Beginning of Equilibrium Cycle (BOC), and End of Equilibrium Cycle (EOC). Table 4.1 shows the time until coolant boiling or fuel melting, whichever occurs first. SABR was redesigned in 2014, and the designers took these results into account [1].

Table 4.1: Time Until Failure (s)

	BOL	BOC	EOC
25 % LOFA	∞	∞	∞
50 % LOFA	13.2	9.6	7.1
75 % LOFA	8.4	5.7	4.9
25 % LOHSA	∞	∞	∞
50 % LOHSA	∞	∞	∞
75 % LOHSA	58.6	54.1	44.9
100 % LOHSA	29.7	26.4	24.2
LOPA	∞	∞	∞
Single Control Rod Ejection	∞	∞	∞
Increase in Neutron Source	12.6	∞	∞

Researchers at Tsinghua University in China have developed a hybrid concept based on an ITER fusion source [30]. It wraps a homogenized fission blanket around the plasma chamber with water coolant tubes flowing through it. The fuel is a mixture of uranium and TRU. Its designers simulated a Loss-of-Coolant-Accident (LOCA) using RELAP5. They found their design to be passively safe with no fuel melting. Unfortunately, there is no mention of the kinetics models they used or any discussion of reactivity feedbacks. It's possible that the design is not sufficiently mature, and that no reactivity feedbacks were even considered.

We are unable to take from these works any suggestions on how to perform a similar analysis for SABR's current design. The proposed work for SABR is the first of its kind. We believe SABR to be the most developed fission-fusion hybrid concept design in the published literature. No other work combines the dynamic safety analysis of a fission-

fusion hybrid reactor with nodal kinetics and neutronic coupling among the cores. We have shown there are no readily available tools to complete this analysis. So it falls to us to develop a customized and original model.

CHAPTER 5
COMPUTATIONAL METHODOLOGY

Creating a dynamics model for SABR is a complex task. It contains elements from a number of disciplines: nuclear reactor kinetics, fusion plasma physics, structural mechanics, fluid dynamics, and heat transfer. It is certainly possible, in principle, to write a code from scratch that incorporates all of these disciplines. It would take far too long to create, and it would involve reinventing the wheel. The efficient approach would be to an open ended software program that already has built in solvers for many of these disciplines. The software should also have the ability to add in user-written solvers. COMSOL Multiphysics 5.2 fits this description perfectly [31].

COMSOL was designed specifically for cross-disciplinary product development, and it has 25 different physics packages available as shown in Fig. 5.1. Several of these physics packages include solvers for fluid flow through pipes, fluid and solid heat transfer, and structural mechanics. Not surprisingly, COMSOL does not have a built-in solver for the kinetics of a fission-fusion hybrid burner reactor. Fortunately, it has the ability to couple to outside programs like MATLAB, Microsoft Excel, AutoCAD, and SOLIDWORKS. We will use MATLAB to handle the nodal kinetics calculations [32].

Now that we have identified the tools we need, we discuss how we use them to contruct our dynamics model. Fig. 5.2 below shows the overall computational flow of our model.

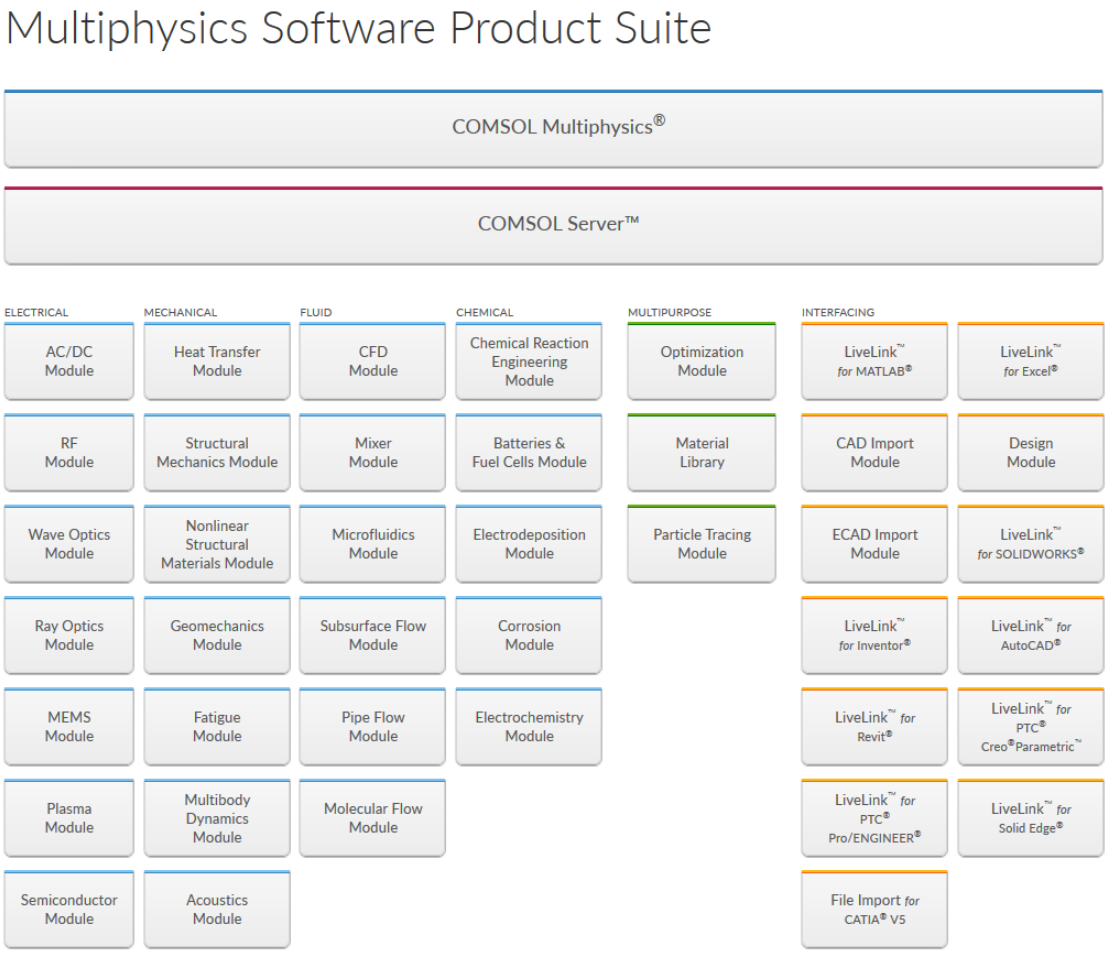

Figure 5.1: COMSOL Multiphysics 5.2 Capabilities

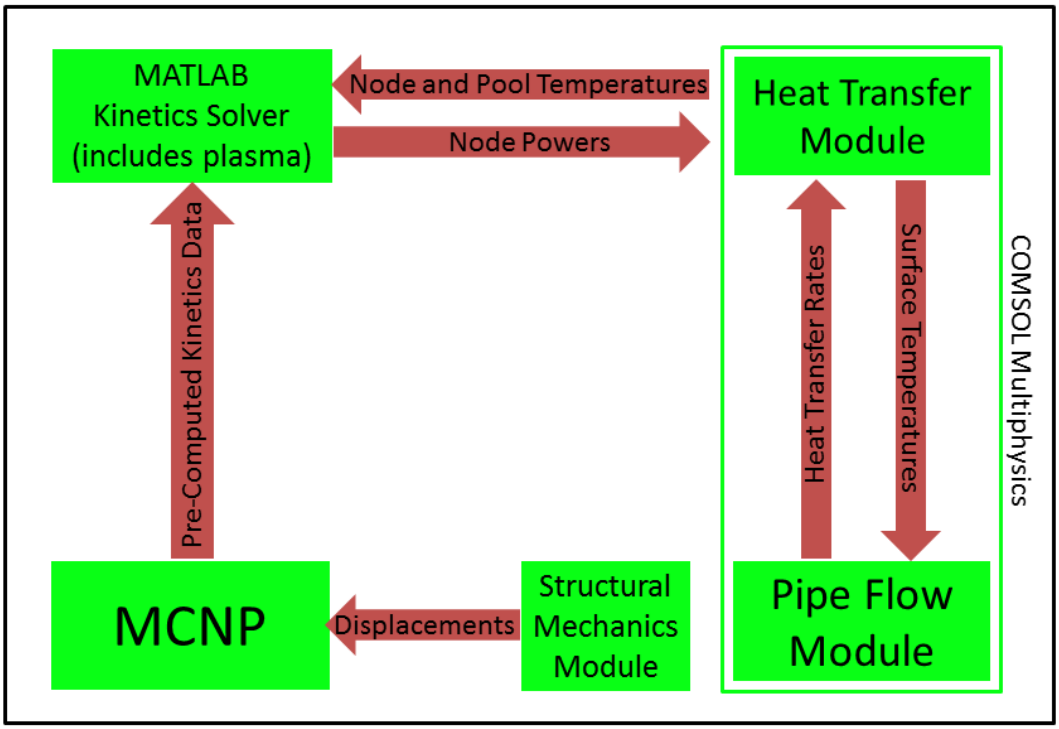

Figure 5.2: Computational Flow of SABR Dynamics Model

For each time step in a transient, COMSOL sends the pool and node temperatures to the MATLAB kinetics solver. The MATLAB kinetics solver uses those temperatures to determine the change in power levels for each node and sends them back to COMSOL. COMSOL uses the new power levels to calculate the new node and pool temperatures for the next time step, and the cycle repeats. The MATLAB kinetics solver uses tables of neutron kinetics data precomputed by MCNP. Our dynamics model does not run MCNP during a simulation. Instead it relies on precomputed MCNP parameters. Now that we've given an overview, we will go into more depth on how we've contructed our kinetics and thermal hydraulics models.

5.1 Thermal Hydraulics Model

The thermal hydraulics component of our dynamics model utilizes COMSOL's Pipe Flow Module and Heat Transfer in Solids Module. We model each of the ten pools separately. When modeling a pool, we consider the entire primary loop (including the temperature distribution in the fuel, cladding, and primary heat exchanger), and we consider only a small part of the secondary loop. In the secondary loop, we only model the flow of sodium through the primary heat exchanger. We place boundary conditions just outside the heat exchanger's secondary side inlet and outlet. We assume the remaining power conversion and heat rejection cycles match that of a typical pool type, sodium coolded fast reactor.

We use the Pipe Flow Module to create what is essentially a loop-type model of a SABR core. A special boundary condition in the loop accounts for additional heat capacity of the sodium pool. The structure of the loop-type model is similar to a RELAP5 model. It is a loop composed of sodium filled pipes. Various boundary conditions simulate heat transfer from the core, across the heat exchanger, and into the sodium pool. A diagram of one of the ten loops in our model is shown below in Fig. 5.3.

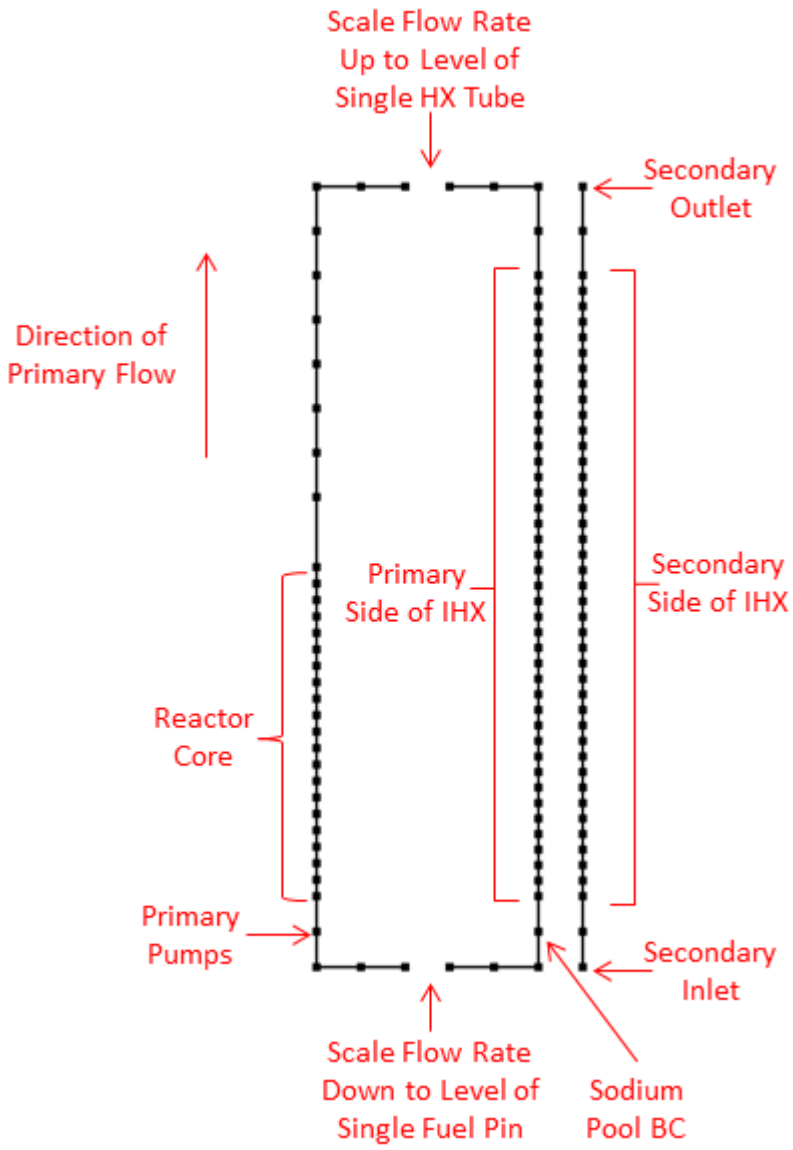

Figure 5.3: Diagram of Sodium Loop

5.1.1 Modeling the Core

For each core, we model a single characteristic fuel pin. We assume 2D axisymmetry as shown in Fig. 5.4. The nodal kinetics model sets the power level in each of the ten different characteristic pins, and the Heat Transfer in Solids Module calculates the temperature distribution across the pins and cladding by solving the conduction equation in Eq. 5.1 for

the case of 2D axisymmetry [33].

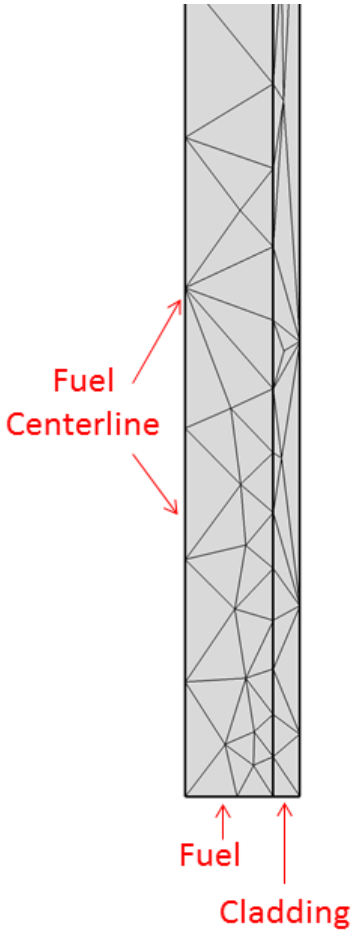

Figure 5.4: Geometry of Fuel Pin

$$\rho C_p(\frac{\partial T}{\partial t} + \overline{u}_{trans} \cdot \nabla T) + \nabla \cdot (q + q_r) = -\alpha T : \frac{d\overline{S}}{dt} + Q \tag{5.1}$$

ρ is the density, C_p is the specific heat capacity at constant stress, T is the absolute temperature, u_{trans} is the velocity vector of translational motion, q is the heat flux by conduction, q_r is the heat flux by radiation, α is the coefficient of thermal expansion, S is the second Piola-Kirchhoff stress tensor [34], and Q is the heat source.

For every point shown in Fig. 5.4, the Pipe Flow Module calculates the heat transfer to

the sodium coolant by solving the convection heat transfer equation:

$$q'' = hA(T_s - T_\infty) \tag{5.2}$$

q'' is the heat flux, h is the heat transfer coefficient, A is the surface area, and T_s is the surface temperature. It also solves the continuity, momentum, and energy equations shown in Eqs. 5.3 - 5.5 for the 1D case [33]. This approach requires various empircal correlations that are described in a later section.

$$\frac{\partial \rho}{\partial t} + \nabla \cdot (\rho \overline{u}) = 0 \tag{5.3}$$

$$\rho \frac{\partial \overline{u}}{\partial t} + \rho(\overline{u} \cdot \nabla)\overline{u} = \nabla \cdot [-p\overline{I} + \overline{\tau}] + \overline{F} \tag{5.4}$$

$$\rho C_p(\frac{\partial T}{\partial t} + (\overline{u} \cdot \nabla)T) = -(\nabla \cdot \overline{q}) + \overline{\tau} : \overline{S} - \frac{T}{\rho}\frac{\partial \rho}{\partial T}|_p(\frac{\partial \rho}{\partial T} + (\overline{u} \cdot \nabla)p) + Q \tag{5.5}$$

ρ is the density, $\overline{u}$ is the velocity vector, p is the pressure, τ is the viscous stress tensor, F is the volume force vector, C_p is the specific heat capacity at constant pressure, T is the absolute temperature, q is the heat flux vector, Q is the heat source, and S is the strain-rate tensor.

5.1.2 Modeling the Heat Exchanger

We use the same procedure and equations described above to model the heat transfer in the heat exchanger. We model a single heat exchanger tube and assume 2D axisymmetry as shown in Fig. 5.5. The Pipe Flow Module calculates the surface temperatures on both sides of the tube. The Heat Transfer in Solids Modules uses the surface temperatures to calculate the temperature distribution and heat transfer across the tube. This gives us the inlet and

outlet temperatures for both sides of the heat exchanger.

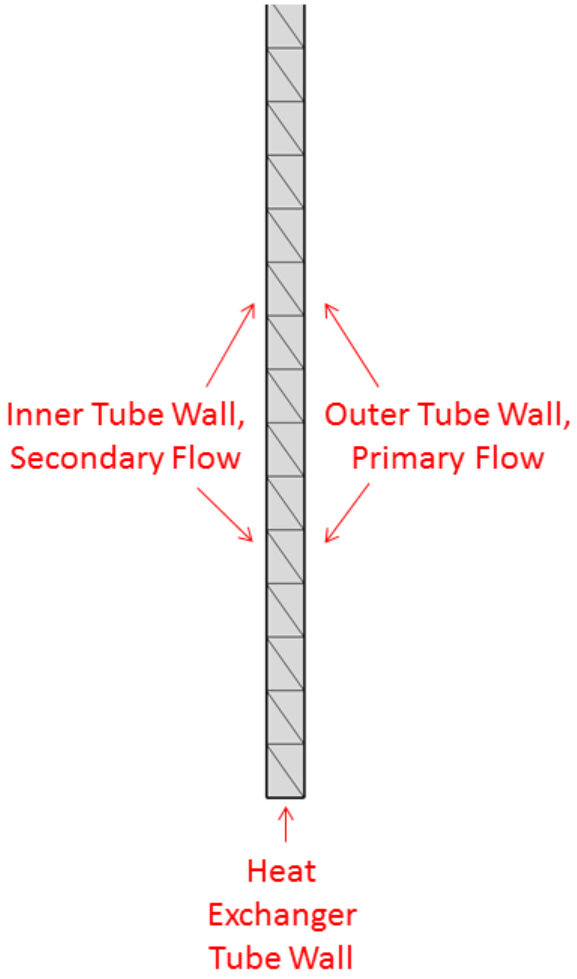

Figure 5.5: Geometry of Heat Exchanger Tube

In each pool, there are 5,700 tubes in the heat exchanger and 37,520 fuel pins in the core. We are modeling one of each, so we scale the mass flow rate proportionally to accurately model the system. For the core side of the loop, we scale the flow rate to a value corresponding to single fuel pin. This is 1/37520 th of the core's primary mass flow rate. For the heat exchanger side of the loop, we scale the flow rate to a value corresponding to a single heat exchanger tube. This is 1/5700 th of the core's primary flow rate. The point where we scale the flow rates is shown in 5.3.

5.1.3 Modeling the Sodium Pool

We account for the additional heat capacity of the sodium pool using the MATLAB function "PoolTemp". As sodium in the primary loop exits the heat exchanger, the Pipe Flow Module calls PoolTemp to bring the sodium to thermodynamic equilibrium with the current pool temperature. We set this new temperature as the inlet temperature for the core. This is a three step process. Step one increases the mass and energy of the pool as sodium enters it from the primary outlet of the heat exchanger. We use Eq. 5.6 and Eq. 5.7 to do this.

$$m_{pool,2} = m_{pool,1} + \dot{m}_{in}\Delta t \tag{5.6}$$

$$E_{pool,2} = E_{pool,1} + c_{p,in}T_{in}\dot{m}_{in}\Delta t \tag{5.7}$$

$m_{pool,1}$ is the mass of the pool at the beginning of the time step, $m_{pool,2}$ is the mass of the pool in the middle of the time step, $E_{pool,1}$ is the internal energy of the pool at the beginning of the time step, $E_{pool,2}$ is the internal energy of the pool in the middle of the time step, $\dot{m}_{in}$ is the mass flow rate of incoming sodium, ΔT is the size of the time step, and $c_{p,in}$ is the specific heat capacity evaluated at T_{in}.

The second step assumes thermodynamic equilibrium in the pool and calculates its average temperature with Eq. 5.8. This is the temperature of sodium exiting the pool and entering the core.

$$T_{out} = \frac{E_{pool,2}}{m_{pool,2}c_p} \tag{5.8}$$

c_p is the specific heat capacity evaluated at T_{in} and T_{out} is the temperature of outgoing sodium.

The third step decreases the mass and energy of the pool as sodium leaves it to enter

the core inlet. We use 5.9 and 5.10 to do this.

$$m_{pool,3} = m_{pool,2} - \dot{m}_{out}\Delta t \tag{5.9}$$

$$E_{pool,3} = E_{pool,2} - c_{p,out}T_{out}\dot{m}_{out}\Delta t \tag{5.10}$$

$m_{pool,3}$ is the mass of the pool at the end of the time step, $E_{pool,3}$ is the internal energy of the pool at the end of the time step, and $c_{p,out}$ is the specific heat capacity evaluated at T_{out}.

5.1.4 Property Data and Empirical Correlations

We supply COMSOL with the material properties for the fuel, cladding, and sodium as well as the empirical correlations for friction factor and Nusselt number. We assume the properties of the fuel, cladding, and heat exchanger tube are constant. We use the same data for the cladding as we do for the heat exchanger tube. The properties are shown in Table 5.1 [35, 36].

Table 5.1: Fuel and Clad Property Data

	TRU Fuel	ODS Cladding
Thermal Conductivity (k)	10 W/mK	30 W/mK
Density (ρ)	3861 kg/m^3	7692 kg/m^3
Specific Heat Capacity (c_p)	738.15 J/kgK	650 J/kgK

We use the ANL sodium property correlations shown in Eqs. 5.11 through 5.14 [37].

$$k = 124.67 - 0.11381 * T + 5.5226e5(T^2) - 1.1842e8(T^3) \ , \ 371 \leq T \leq 1500 \quad (5.11)$$

$$\ln(\mu) = -6.4406 - 0.3958 \ln(T) + \frac{556.835}{T} \ , \ 371 \leq T \leq 2500 \quad (5.12)$$

$$\rho = 219 + 275.32(1 - \frac{T}{2503.7}) + 511.58(1 - \frac{T}{2503.7})^{0.5} \ , \ 371 \leq T \leq 2503 \quad (5.13)$$

$$c_p = 1.6582 - 8.4790e4(T) + 4.4541e7(T^2) - 2992.6(T^{-2}) \ , \ 371 \leq T \leq 1900 \quad (5.14)$$

For friction factor, we use Eq. 5.15, the Zigrang-Sylvester approximation of the Colebrook-White correlation [38]. For the Nusselt Number, we use Eq. 5.16, recommended by Seban and Shimazaki [39].

$$\frac{1}{\sqrt{f}} = -2 \log_{10}(\frac{\epsilon}{3.7D} + \frac{2.51}{Re}(1.14 - 2 \log_{10}(\frac{\epsilon}{D} + \frac{21.25}{Re^{0.9}}))) \ , \ Re \geq 3000 \quad (5.15)$$

$$Nu = 5.0 + 0.025(RePr)^{0.8} \ , \ Pe \geq 100 \quad (5.16)$$

5.1.5 Calculation of Nodal Heat Transfer Terms

The kinetics model requires both node and pool temperatures as input. We define a node as the fission core in each pool. This includes all fuel and reflector assemblies but not the

heat exchanger and the surrounding sodium in the pool. We calculate the average node temperature using Eq. 5.17.

$$T_{node} = \frac{m_{fuel}T_{fuel} + m_{clad}T_{clad} + m_{reflector}T_{reflector} + m_{sodium}T_{sodium}}{m_{fuel} + m_{clad} + m_{reflector} + m_{sodium}} \tag{5.17}$$

T and m are the temperatures and masses of the fuel, cladding, sodium, and reflector in one of SABR's cores. COMSOL calculates T_{fuel}, T_{clad}, T_{sodium} by finding the average temperatures in the fuel, clad, and sodium domains. We assume $T_{reflector}$ is the same temperature as the inlet temperature of the sodium because there is neglible heating the reflector region. The masses of each component are hand calculated constants that we give to COMSOL.

We've already explained how we calculate the pool temperature in Eq. 5.8. We assume thermodynamic equilibrium in the pool and set $T_{pool} = T_{out}$ using Eq. 5.8.

5.2 Neutron Kinetics Model

We use a nodal neutron kinetics model to calculate the time-dependent powers of each node in SABR. We created the formulation shown below after careful consideration and literature review.

$$\frac{dn_j(t)}{dt} = \frac{(1-\beta_j)}{\Lambda_{fj}}n_j(t) + \sum_{i=1}^{6}(\lambda_{i,j}c_{i,j}) + \frac{n_j(t)}{\Lambda_{2nj}} + S_{fus,j} + \sum_{k=1}^{10}\frac{\alpha_{kj}n_k(t)}{l_{e,k}} - \frac{n_j(t)}{l_{e,j}} - \frac{n_j(t)}{l_{a,j}} \tag{5.18}$$

$$\frac{dc_{i,j}(t)}{dt} = \frac{\beta_{i,j}}{\Lambda_j}n_j(t) - \lambda_{i,j}c_{i,j} \tag{5.19}$$

$$\Lambda_{fj} = \frac{1}{V\nu\Sigma_{f,j}} \quad , \quad \Lambda_{2nj} = \frac{1}{V2\Sigma_{n2n,j}} \tag{5.20}$$

$n_j(t)$ is the neutron density of node j, β_j is the delayed neutron fraction, and $c_{i,j}$ and $\lambda_{i,j}$ represent the six groups of delayed neutron precursor densities and their respective decay constants. Eq. 5.20 defines the fission generation time Λ_{fj} and the $n, 2n$ generation time Λ_{2nj}. $n, 2n$ reactions are a non-negligible source in the system, and we must account for them due to the hard neutron spectrum. $l_{e,j}$ and $l_{a,j}$ are the neutron leakage and absorption lifetimes respectively, and the term $S_{fus,j}$ represents the neutrons contributed by the fusion plasma.

We represent neutronic coupling with a $node\ k$ to $node\ j$ coupling coefficient α_{kj}. It is the probability that a neutron emitted from the surface of $node\ k$ will impinge upon the surface of $node\ j$ before entering any other nodes. The rate of neutrons entering $node\ j$ from $node\ k$ is α_{kj} times the rate neutrons are escaping from $node\ k$, $\frac{n_k(t)}{l_{e,k}}$.

The nodal kinetics model is a series of 70 coupled, stiff differential equations. We use the MATLAB program "NodalSolve" to numerically solve this system of equations for a given time-step. NodalSolve uses MATLAB's intrinsic "ode15s" solver which efficiently solves ordinary, stiff differential equations[40].

5.3 Calculation of Nodal Kinetics Terms

MCNP6 calculates each of the nodal kinetics terms using a 3D model of SABR [41]. Fig. 5.6 and Fig. 5.7 show cross-sections of the 3D model. The model contains ten sodium pools in addition to ITER-like components such as the vacuum vessel, plasma chamber, divertor, breeding blanket, and central solenoid. For simplicity, we homogenize the ITER-like components outside of the pools. Inside the pools, we model with more detail. We homogenize the subcomponents of each pool instead of homogenizing the entire region as we did with the ITER-like components. We represent the heat exchangers as homogenized cylinders. We model the pool vessels as hollowed out trapezoidal prisms. We define any space that is inside the pool vessels but outside the cores and heat exchangers as sodium. We divide each of the cores into 125 cells and then homogenize. It's important to note that

we homogenize after subdividing the cores, not before. After we subdivide the cores, we refer to them as ”nodes”.

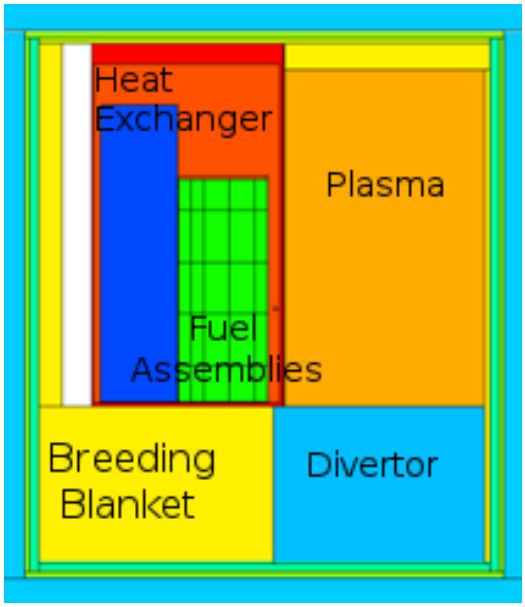

Figure 5.6: Side View of SABR MCNP Model

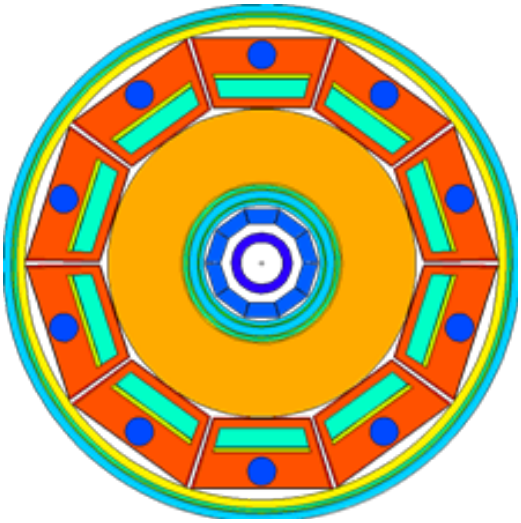

Figure 5.7: Top-Down View of SABR MCNP Model

We use different source and tally definitions depending on what kinetics terms we wish to calculate. To calculate Λ_{fj}, Λ_{2nj}, $l_{e,j}$, and $l_{a,j}$ we create an isotropic volume neutron

source in the cell labeled "plasma" in Fig. 5.6. The energies of the source neutrons are assigned using an energy spectrum for deuterium-tritium fusion neutrons. This energy spectrum is already included in MCNP6. In each of the 125 cells in each of the 10 nodes, we place tallies for flux, absorption, fission, and n,2n reactions. We also place direction-binned surface tallies on the outer surface of each node. We run 60 million particles. This gives us good enough statistical accuracy. Not all of the tallies pass MCNP's 10 statistical checks. The tallies that fail are tallies that have a very low relevance. For example, the fission reaction tally fails the statistical checks in the reflector region where is there is no appreciable fissionable material. The tallies we consider being of high relevance pass MCNP's 10 statistical checks. For example, the absorption tallies in the sodium and the fission tallies in the fuel pass all of the tests. The resulting output file is quite large and contains results for over 5000 separate tallies. We use a macro-enabled spreadsheet to automatically import the raw tally data from the MCNP output file. The spreadsheet condenses the data and calculates the effective kinetics parameters for each of the 10 nodes.

To calculate $S_{fus,j}$, we use the same source definition as before, but we change the tallies. We apply a direction-binned surface tally to the surface of each node, and we set the importance of each node to 0. Any plasma neutrons entering a node are tallied and immediately destroyed. This prevents the surface tally from double or triple counting any neutrons. We run 60 million particles, and the tallies pass all statistical checks. There are only 10 tallies in the output file, so we don't require an automated spreadsheet.

We require a bit more effort to calculate the coupling coefficients α_{kj}. It is a two part process. Part one uses the first source we described: the isotropic fusion neutron source. Instead of tallies, we use the "surface source writer" in MCNP6. The surface source writer stores the position, direction, weight, and energy of every particle crossing a designated surface. We apply the surface source writer to the surface of Node 1. In doing so, we are able to record the steady state inward and outward neutron fluxes of Node 1. We run 10 million particles. For part two, we use this recording as a surface source on the surface of

Node 1. We set the importances of all nodes to 0 and set surfaces tallies on the surface of each node. This ensures the tallies do not count a neutron more than once. We assume symmetry (α_{kj}=α_{jk}), so we only calculate this for Node 1. We run 100 million particles. There are only 10 tallies in the output file, so we don't require any automation to process the data.

5.4 Calculation of Feedbacks

Our MCNP model calculates how various perturbations affect the terms of the nodal kinetics equations. The perturbations we consider are core grid plate expansion, axial expansion, fuel bowing, Doppler broadening, and sodium voiding. The core grid plate expansion, axial expansion, and fuel bowing perturbations are manifested as changes in geometry. The sodium voiding is manifested as sodium density changes in the nodes and pools. The Doppler broadening is manifested as the requirement of different cross-section sets that have had their absorption resonances broadened. Node and pool temperature changes cause these perturbations to occur which in turn affects the terms in the kinetics equations. Table 5.2 shows how the parameters Λ_j, Λ_j, $S_{fus,j}$, $l_{e,j}$, and $l_{a,j}$ change with node temperature. Table 5.3 shows how the coupling coefficients change with pool temperature. We assume the parameters in Table 5.2 are functions only of $node\ j$'s temperature and are not affected by the temperature in adjacent nodes.

Table 5.2: Table of Kinetics Terms at Various Node Temperatures

	Node Temperature (K)			
Kinetics Term	529	829	1129	1429
$\Lambda_f\ (s)$	4.28910E-07	4.29876E-07	4.28374E-07	4.27197E-07
$\Lambda_{2n}\ (s)$	3.67211E-04	3.48010E-04	3.47831E-04	3.47205E-04
$S_{fus}\ (cm^{-3}s^{-1})$	1.97315E+11	2.00887E+11	2.04554E+11	2.08346E+11
$l_e\ (s)$	2.63793E-07	2.59782E-07	2.59171E-07	2.58622E-07
$l_a\ (s)$	5.72933E-07	5.75653E-07	5.73361E-07	5.71674E-07

Table 5.3: Table of Coupling Coefficients at Various Pool Temperatures

	Pool Temperature (K)			
Coupling Coefficient (Node 6)	529	829	1129	1429
$\alpha_{6,1}$	0	0	0	0
$\alpha_{6,2}$	0	0	0	0
$\alpha_{6,3}$	0	0	0	0
$\alpha_{6,4}$	0.00057	0.00059	0.00061	0.00064
$\alpha_{6,5}$	0.02753	0.02804	0.02865	0.02936
$\alpha_{6,6}$	0.74210	0.73755	0.73236	0.72640
$\alpha_{6,7}$	0.02753	0.02804	0.02865	0.02936
$\alpha_{6,8}$	0.00057	0.00059	0.00061	0.00064
$\alpha_{6,9}$	0	0	0	0
$\alpha_{6,10}$	0	0	0	0

For any change in temperature, the MCNP model simultaneously incorporates the effects of all the perturbation types we mentioned earlier. This is why we subdivided each node into 125 cells and homogenized their materials. The subdivision and homogenization allows us to model changes in geometry and material properties easily. We modify the material density and composition of each of the 1,250 cells in the model to reflect whatever change we desire. We have a MATLAB program "UPM" that automates this process for us. UPM takes as input the temperature of each node, the temperature of each pool, and the physical displacements of each cell (ie. geometry changes due to fuel bowing, grid plate expansion, or axial expansion). It calculates the new material densities and compositions for every cell in the model and writes this information to a text file in MCNP input format. It is easy to generate new MCNP input files for even the most complex combinations of perturbations. The next several sections describe how this MATLAB program accounts for each perturbation type.

5.4.1 Doppler Broadening

UPM uses the core temperature to choose the cross-section set to be used for that node's materials. We have Doppler broadened cross-section sets for temperatures of 600 K, 829 K, 1200 K, and 1500 K. They were produced by Dr. Chris Chapman using NJOY and the ENDF 7.0 library. These temperatures are slightly different than the temperatures used in Tables 5.2 and 5.3, but the difference is small. The isotopic composition of SABR's TRU fuel is not very sensitive to Doppler broadening. The isotopic composition of SABR's fuel can be found in the appendix of this thesis.

5.4.2 Sodium Voiding

In SABR, sodium voiding refers to two different things: voiding in the node and voiding in the pool. The sodium in the node is likely to change temperature and density at a different rate than the sodium in the pool. Sodium voiding in the node affects the absorption and

leakage terms of the nodal kinetics model. Sodium voiding in the pool affects the coupling and external source terms. UPM incorporates these changes by scaling the node and pool sodium densities based on their temperatures.

5.4.3 Grid Plate Expansion and Axial Expansion

Before MCNP tells us how changes in geometry affect the kinetics terms, we need to know how changes in temperature affect the geometry. It is easy to calculate the physical displacements caused by grid plate expansion and axial expansion. We assume the core grid plate expands and contracts isotropically with changes in temperature. We multiply the change in temperature by the coefficient of thermal expansion to find the strain. To find the x dimension displacements of a cell, we multiply the strain by a scale factor. The scale factor is the distance between the x-coordinate of the center of the grid plate and the x-coordinate of the center of the cell in question. We do this for every cell in the model. The process repeats for the y dimension as well. It is summarized in Fig. 5.8.

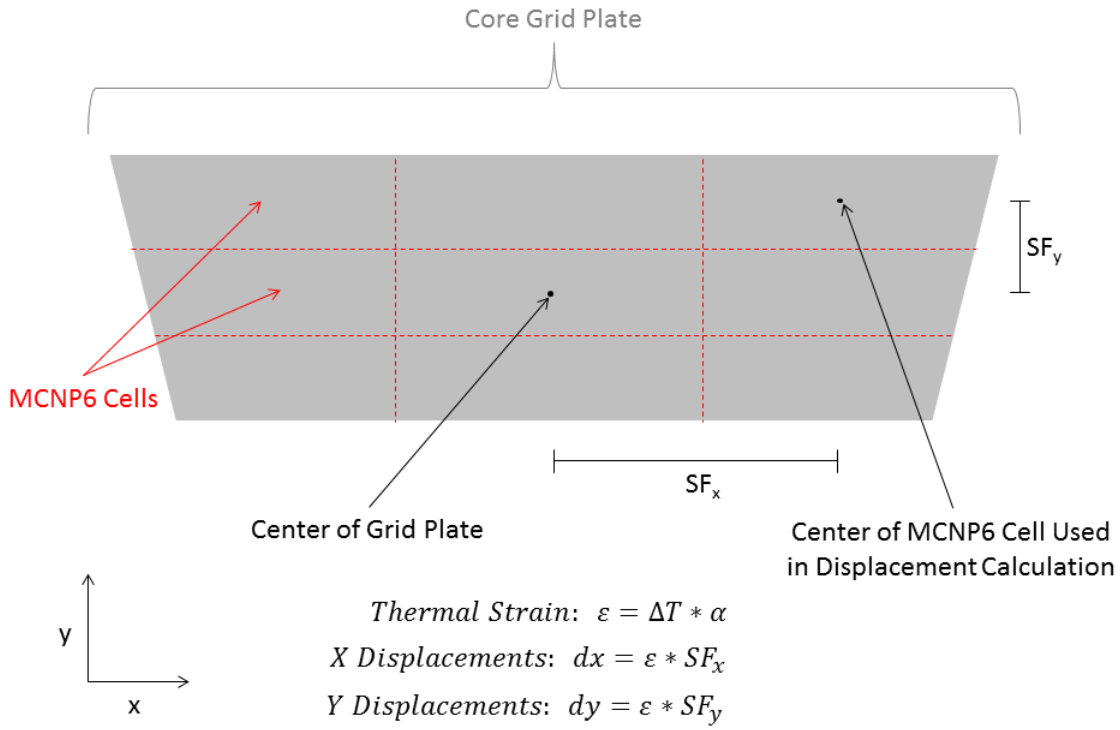

Figure 5.8: Displacement Calculation for Grid Plate Expansion

For the case of axial expansion, we employed the same method we use with the grid plate plate expansion. We calculate the strain and multiply it by a scale factor. Here, the scale factor is the distance from the bottom of the core the center of the cell in question. This gives us the z dimension displacements.

UPM uses these displacements to simulate material relocation. It does this by looping over each cell in the model and adding/removing materials where appropriate. The actual geometry of the MCNP model never changes, just the material compositions and densities of the node cells.

5.4.4 Fuel Bowing Model

UPM accounts for fuel bowing in the same way it accounts for grid plate expansion and axial expansion. It uses displacements to simulate material relocation. The difference here is that the displacements are much harder to calculate. Fuel bowing is a highly non-linear process, and it requires a sophisticated model.

We quantify fuel bowing in SABR using the Structural Mechanics Module in COMSOL Multiphysics [31]. This is a separate COMSOL model that is not a part of the dynamics model. This model calculates the fuel assembly displacements in a single core at various power-to-flow ratios. The model uses a half-core geometry as shown in Fig. 5.9 with a symmetry boundary condition to reduce computation time. The geometry contains all of the fuel assemblies and SiC flow channel inserts for a single core. Fuel pins are not included because they do not appreciably affect fuel bowing. We use the triangular swept mesh shown in Figs. 5.10 and 5.11 on both the ducts and the inserts. The model accounts for geometric non-linearity, duct-to-duct contact, and duct-to-insert contact. We use a constrained boundary condition at the bottom of the ducts. This is a simplifying assumption we use for now because SABR's grid plate has not been designed yet. When more detail is available the bottom boundary condition will need to be updated to a more realistic stiffness because the stiffness of the bottom boundary condition can have a significant impact on the fuel assembly displacements.

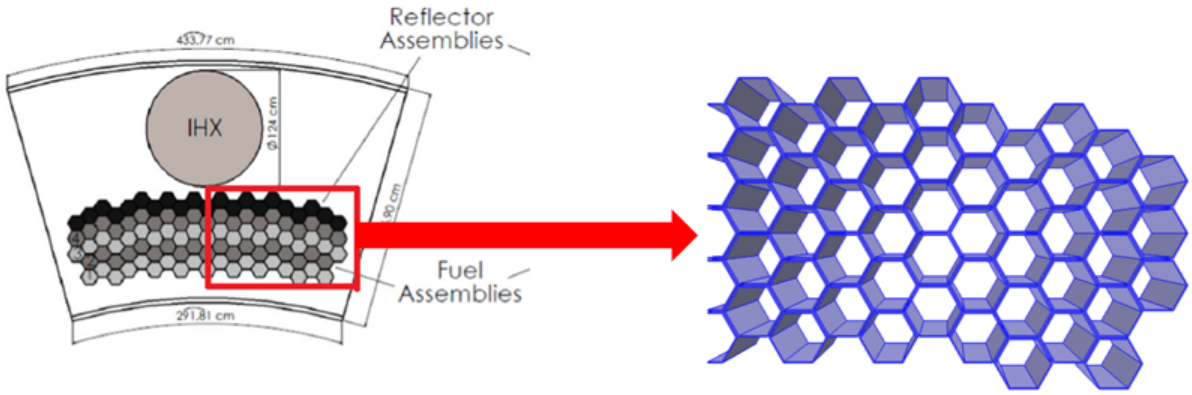

Figure 5.9: Fuel Bowing Model Geometry

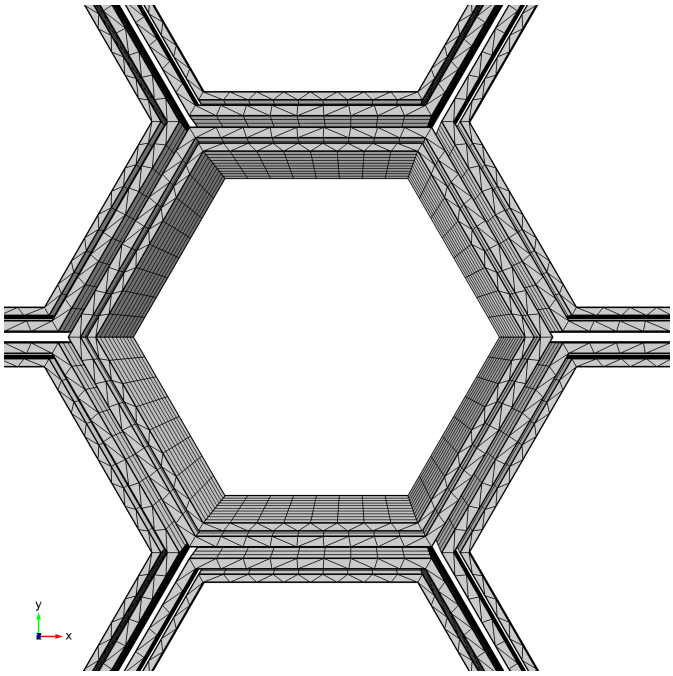

Figure 5.10: Top-Down View of Mesh

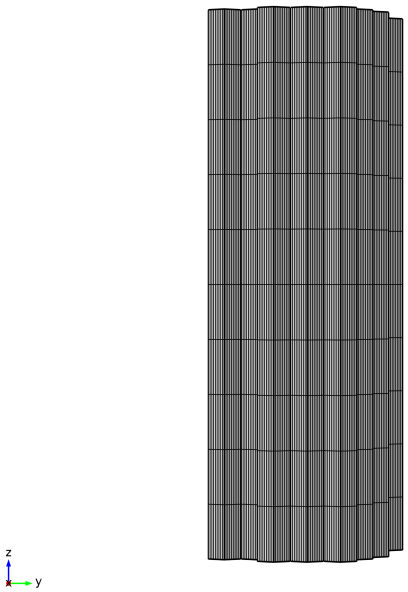

Figure 5.11: Side View of Mesh

We assign a 3D temperature distribution to the mesh using MATLAB program ”comF-Btemp”. It calculates the temperature at every mesh point on the inner surfaces of the ducts and the SiC inserts by assuming it is the same temperature as the sodium adjacent to it. The program takes in the x,y,z coordinates of each mesh point and calculates the temperature of sodium by integrating the amount of energy added to it as it travels up through the core in the z-direction. This requires the 3D power distribution of the core. Our MCNP model of SABR can give us exactly that by using FMESH tallies. This has nothing to do with the nodal kinetics model; it's just an additional task our MCNP model can perform. We break a core into 5301 cells and tally the fission reactions in each cell. We construct a 3D power distribution using the tally results. We calculate a single power profile for the reference case. We assume the profile does not change during a transient.

We calculate the fuel bowing displacements for a power-to-flow ratio of 4. This is the highest ratio we can achieve before design failure. The temperature profile and resulting displacements in the x and y dimensions are shown in Figs. 5.12, 5.13, and 5.14. We do

not consider the displacements for the z-dimension because they are accounted for in the axial expansion perturbation.

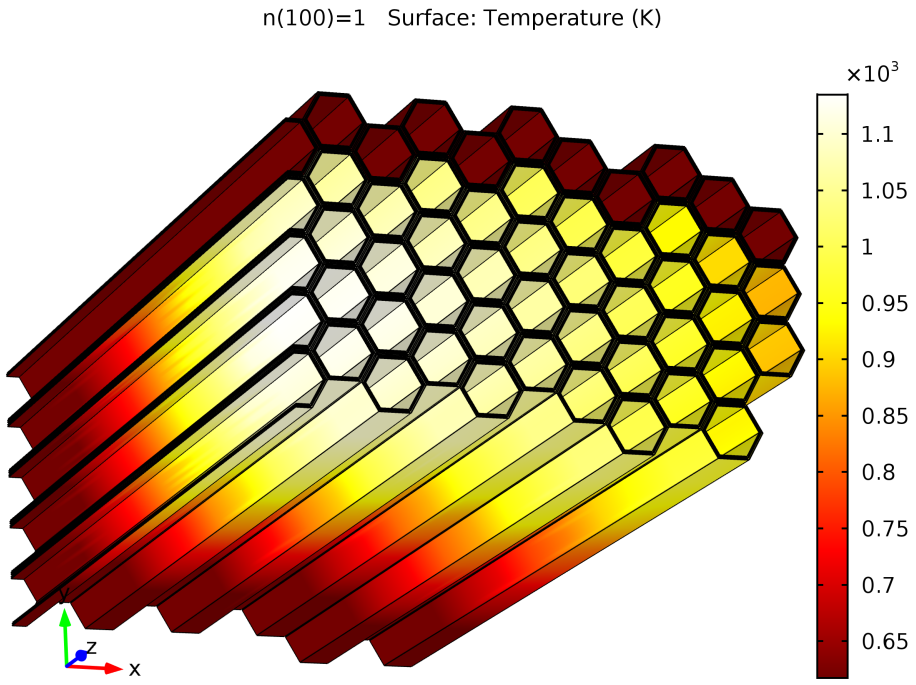

Figure 5.12: Fuel Bowing - Temperature Profile

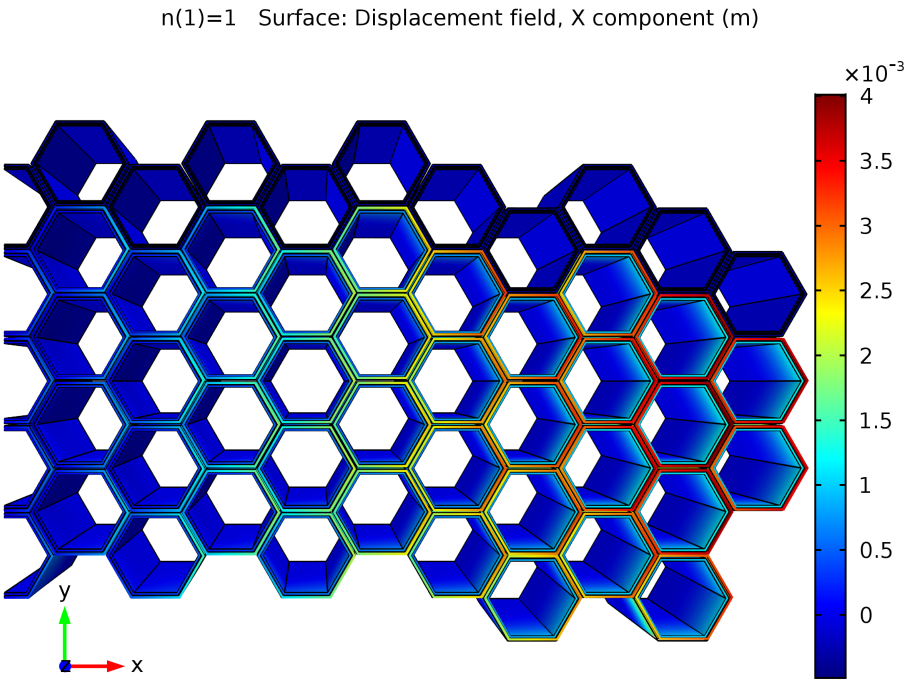

Figure 5.13: Fuel Bowing - X Displacements

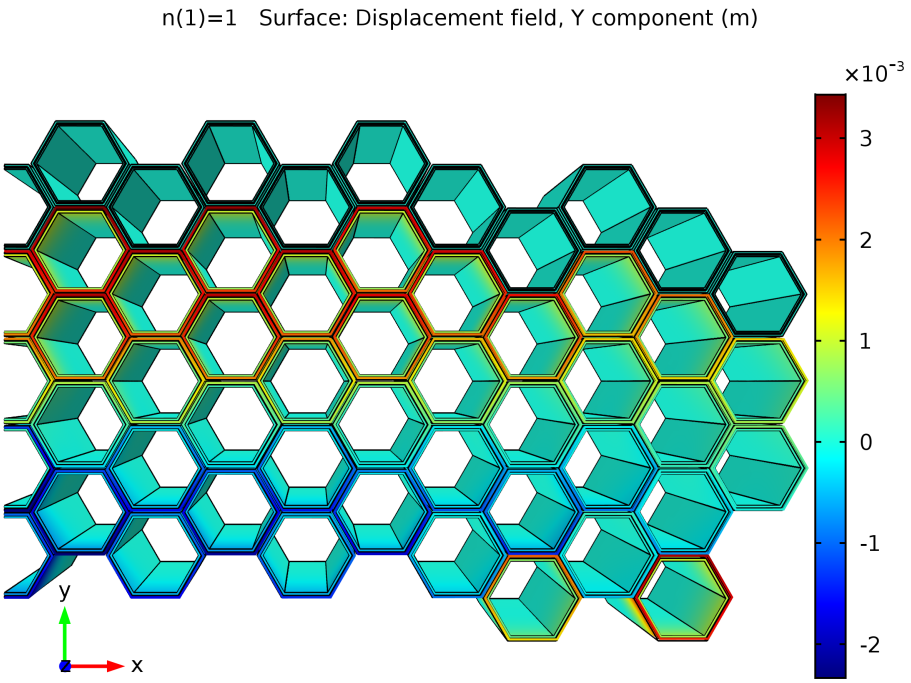

Figure 5.14: Fuel Bowing - Y Displacements

The fuel bowing for the most severe case possible is only a few millimeters. When we apply these displacements to our MCNP model, we see no appreciable change in the kinetics parameters. Because of this, we do not account for fuel bowing when performing our dynamic safety analysis of SABR.

CHAPTER 6
VERIFICATION TESTS

We have created a custom dynamics model for SABR in COMSOL Multiphysics. Like any computational model, we need to qualify it with verification and validation tests. No expermental data for SABR exists, so we are unable to perform validation tests. Instead, we settle for a number of verification tests where we compare our results to other software codes and hand calculations.

6.1 Thermal Hydraulics Model

We currently have access to a RELAP5 license, so we use it to test the thermal hydraulics component of our model. Because RELAP5 cannot handle the complexity of our SABR model, we simplify it to a single node, loop type core with no feedbacks. The remaining core geometry, composition, and thermal hydraulics conditions are identical to the SABR design. Below, we compare the steady state results and the results of six different accident scenarios. The results show our thermal hydraulics model to be just as accurate as RELAP5, and we may consider it verified.

6.1.1 Steady State

The steady state temperatures and pressure drops agree well with RELAP5. This is not surprising because we've given the COMSOL thermal hydraulics solver the same correlations for sodium properties, friction factors, and heat transfer coefficients that RELAP5 uses.

Table 6.1: Steady State Temperatures

	RELAP	COMSOL
Avg Fuel Temp (K)	725	720
Max Fuel Temp (K)	801	802
Core Inlet Temp (K)	619	619
Core Outlet Temp (K)	759	759
Secondary Inlet Temp (K)	590	590
Secondary Outlet Temp (K)	739	739
Core Pressure Drop (kPa)	70	71
Primary Side IHX Pressure Drop (kPa)	264	266
Secondary Side IHX Pressure Drop (kPa)	33	33

6.1.2 50% Loss of Flow Accident

Each core in SABR uses two electromagnetic sodium pumps. A Loss of Flow Accident (LOFA) simulates the failure of a pump in the primary loop and the resulting decrease in coolant flow. A 50% LOFA indicates the failure of only one of the two pumps. The coast down time of the pumps uses a 10 second halving time [42]. Figs. 6.1 - 6.3 compare the maximum fuel temperature, maximum primary coolant temperature, and maximum secondary coolant temperature from both COMSOL and RELAP5. The case results agree well, so we consider our model capable of accurately simulating this type of transient.

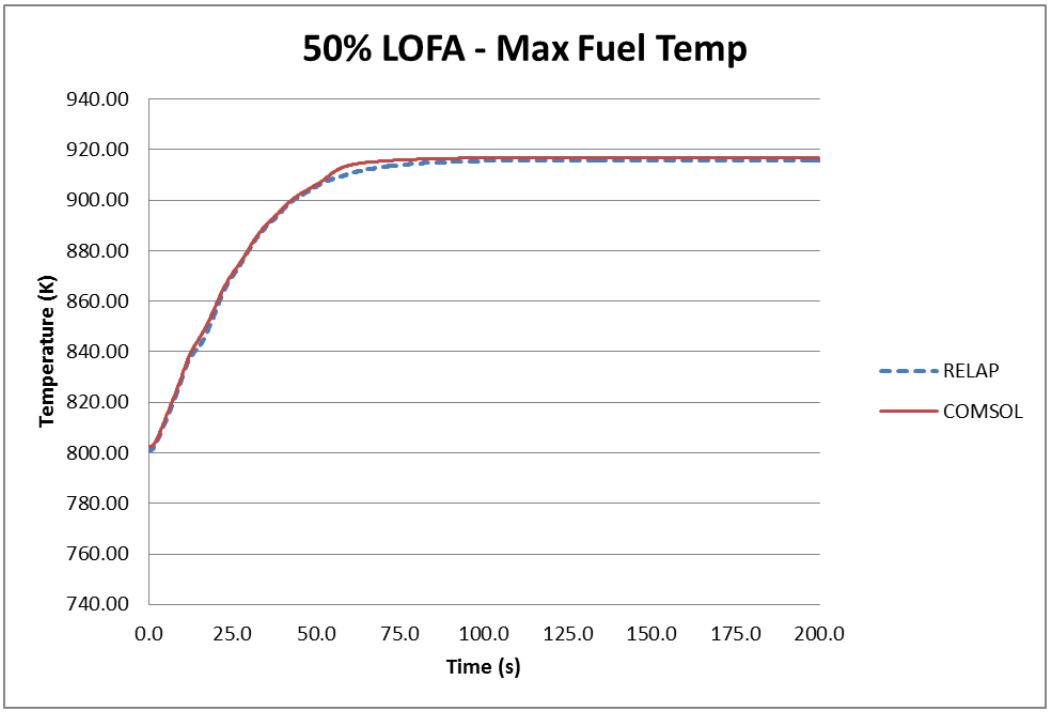

Figure 6.1: 50% LOFA - Max Fuel Temp

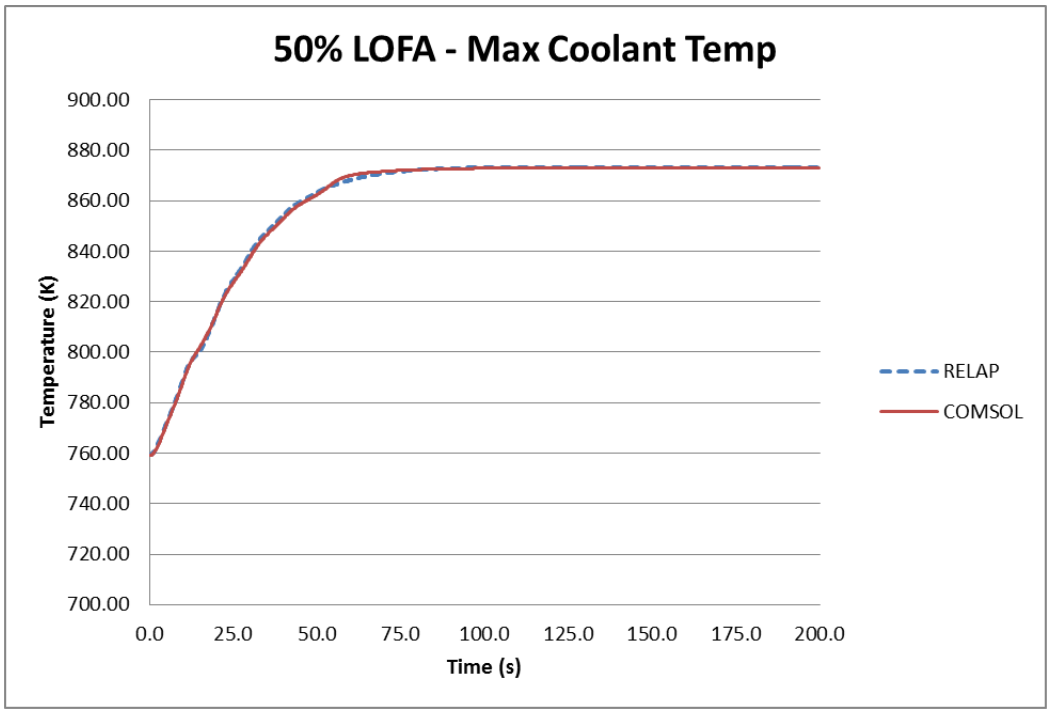

Figure 6.2: 50% LOFA - Max Coolant Temp

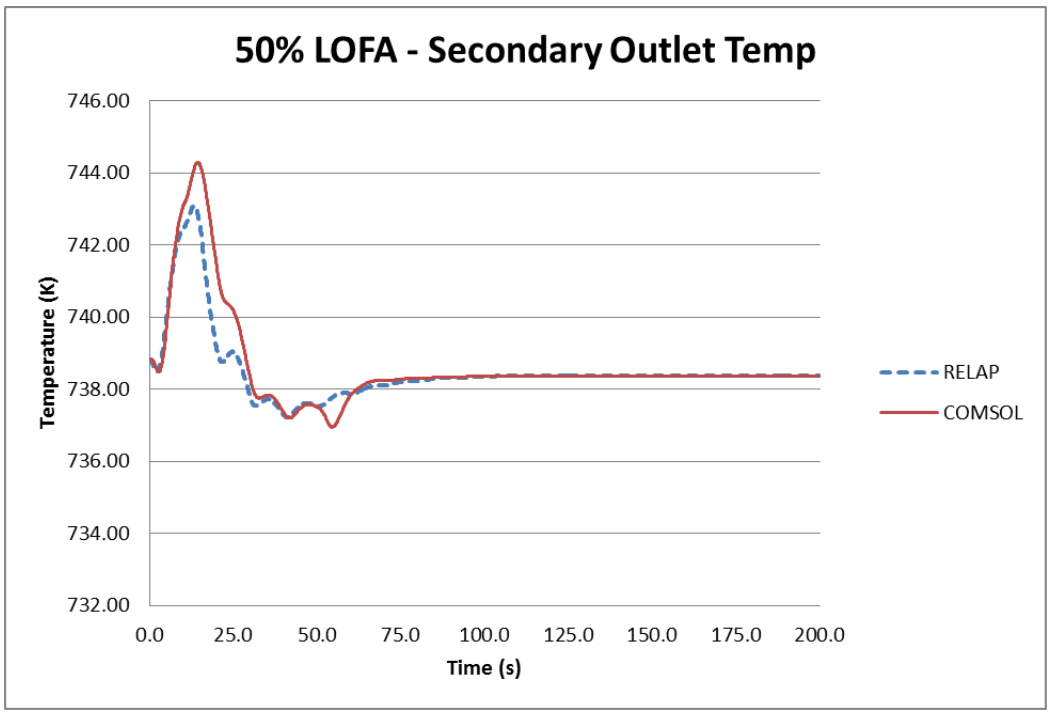

Figure 6.3: 50% LOFA - Max Secondary Temp

6.1.3 100% Loss of Flow Accident

For a 100% LOFA, both of the pumps fail simultaneously. The primary flow rate has a floor of 2% of the normal flow rate. This is the estimated amount of natural circulation in the core. Its important to note our design limits as they relate to failure. We consider our design to have failed if one of two things occur: 1) The coolant reaches its boiling point of 1156 K or 2) The fuel reaches its melting temperature of 1473 K. Figs. 6.4 - 6.6 compare the RELAP5 and COMSOL results for the case of a 100% LOFA. The RELAP5 simulation crashes due to property lookup errors after the temperatures pass these thresholds. The COMSOL model does not crash at that point, but the results beyond that are non-physical and should be ignored. The COMSOL and RELAP5 results agree well up to the point of failure, so we consider our model capable of accurately simulating this type of transient.

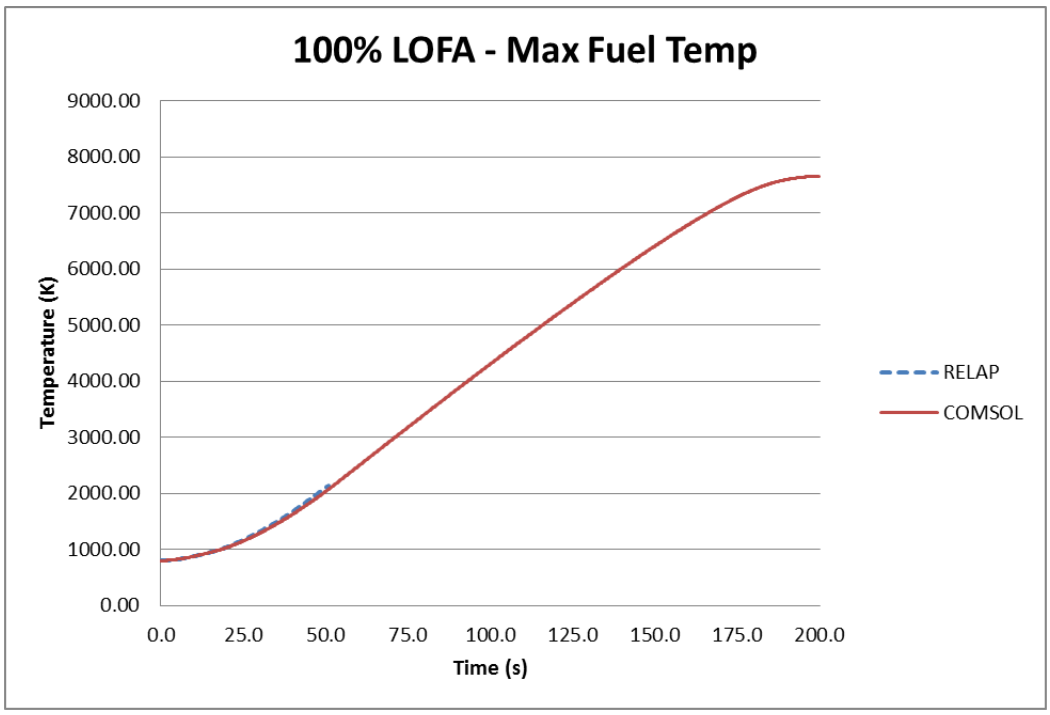

Figure 6.4: 100% LOFA - Max Fuel Temp

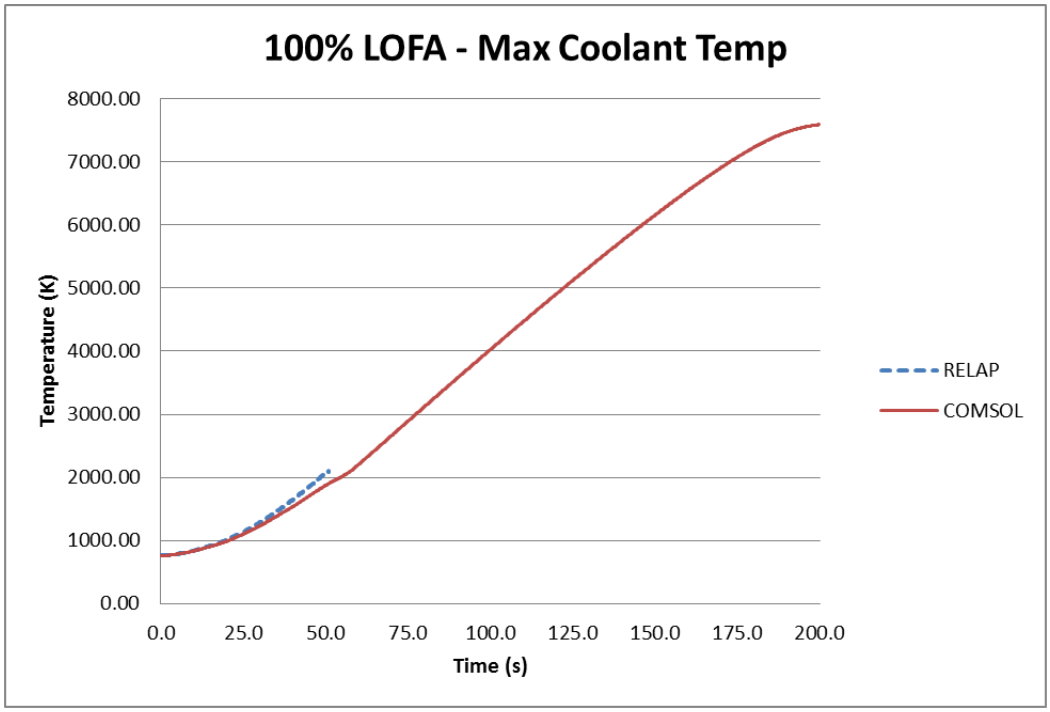

Figure 6.5: 100% LOFA - Max Coolant Temp

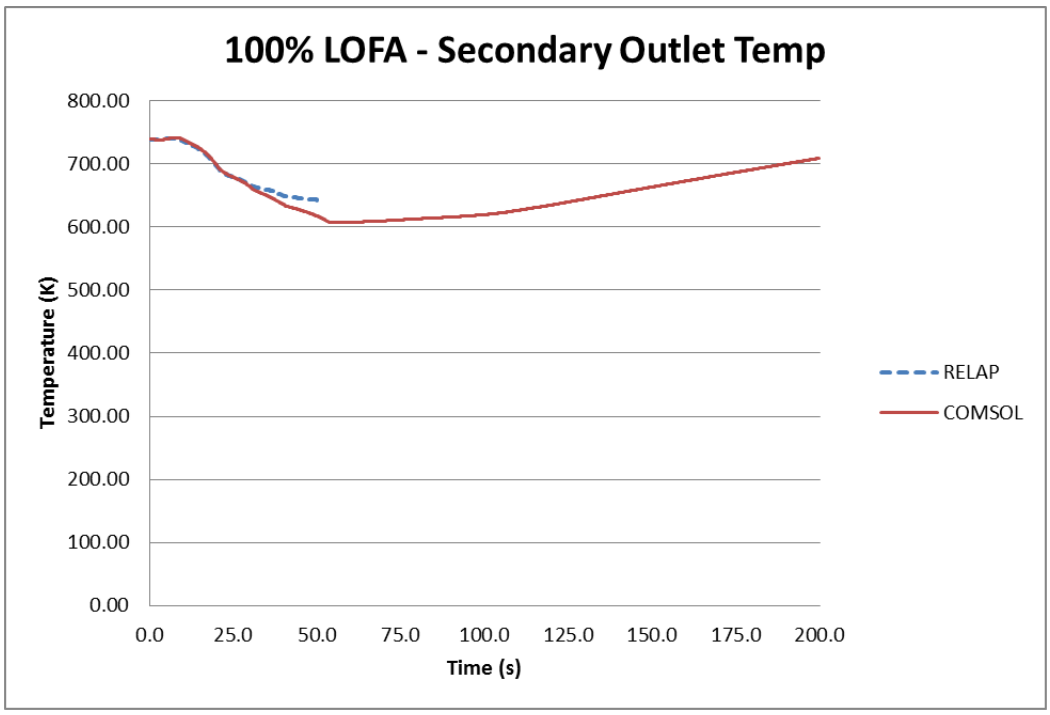

Figure 6.6: 100% LOFA - Max Secondary Temp

6.1.4 50% Loss of Heat Sink Accident

The secondary loop of each SABR core also contains two sodium pumps. A pump failure on the secondary side is referred to as a Loss of Heat Sink Accident (LOHSA). The 50% and 100% LOHSAs use the same pump coast down characteristics as the 50% and 100% LOFAs. Figs. 6.7 - 6.9 compare the RELAP5 and COMSOL results, which agree well.

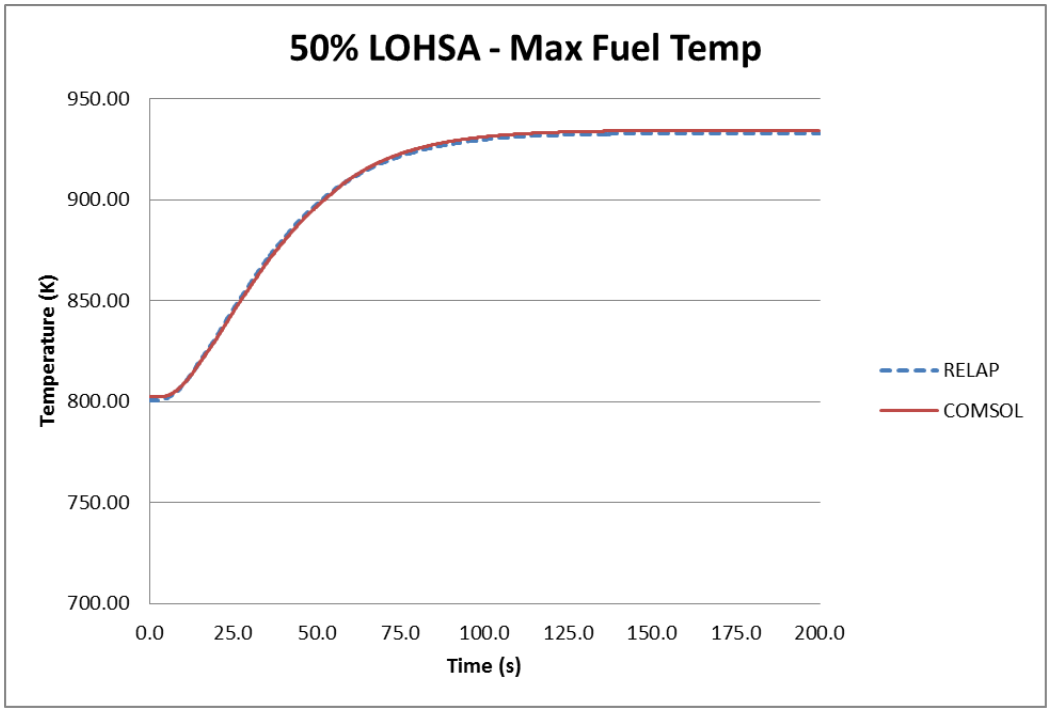

Figure 6.7: 50% LOHSA - Max Fuel Temp

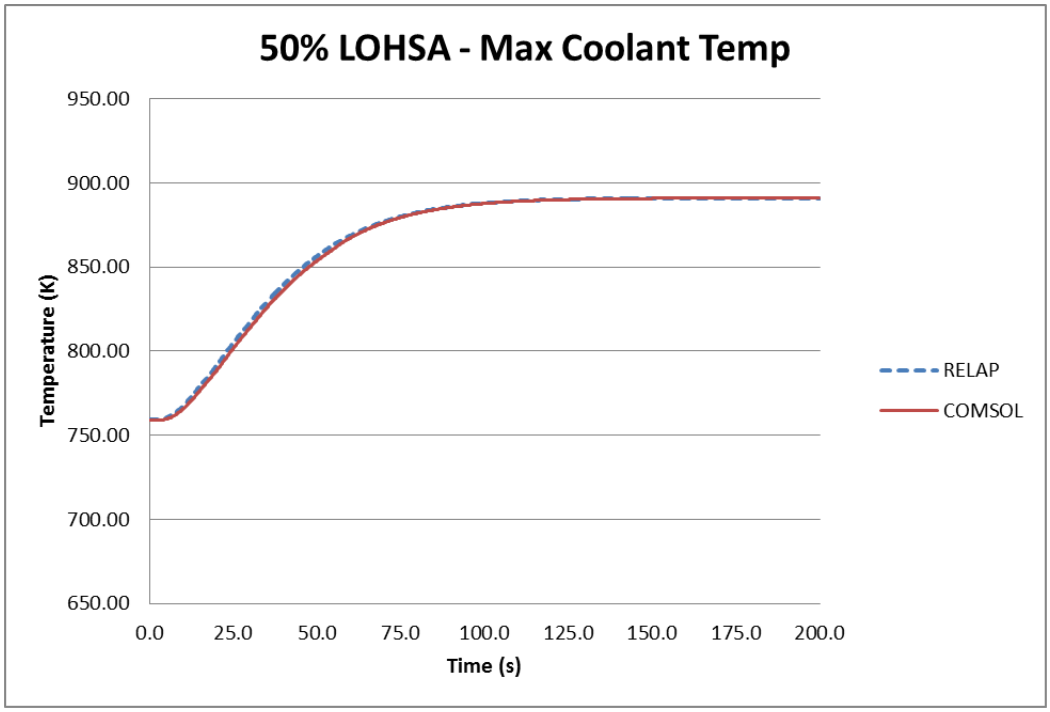

Figure 6.8: 50% LOHSA - Max Coolant Temp

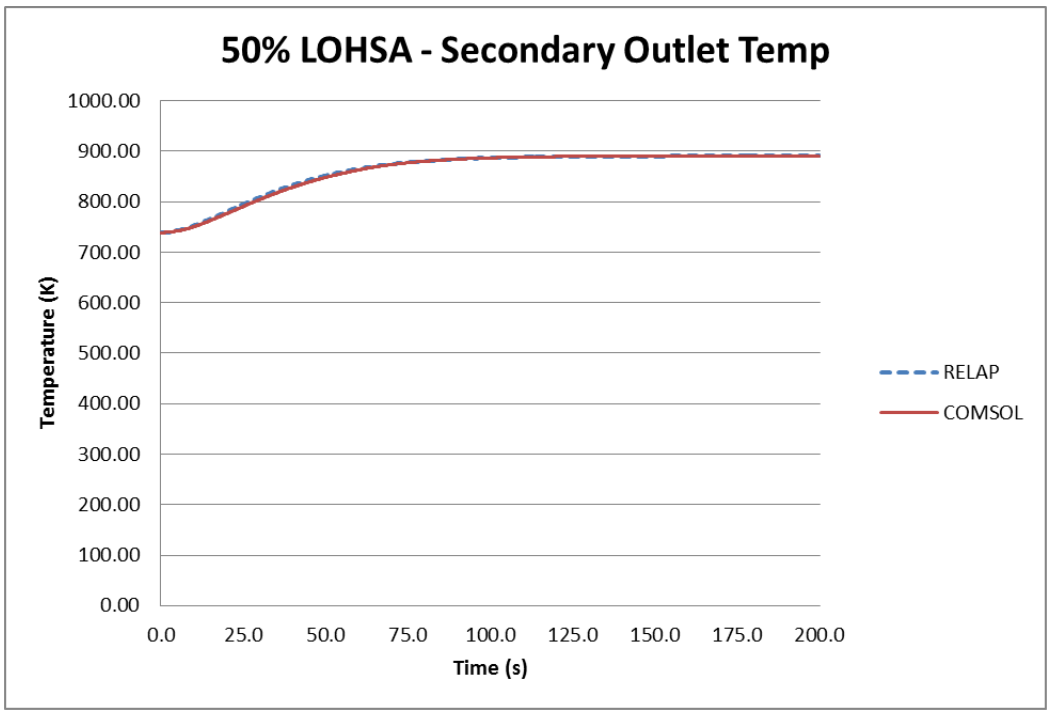

Figure 6.9: 50% LOHSA - Max Secondary Temp

6.1.5 100% Loss of Heat Sink Accident

The results presented in Figs. 6.10 - 6.12 agree well up to the point of fuel melting and coolant boiling. Once again, we assume the terminal flow rate on the secondary side is 2% of its normal flow rate.

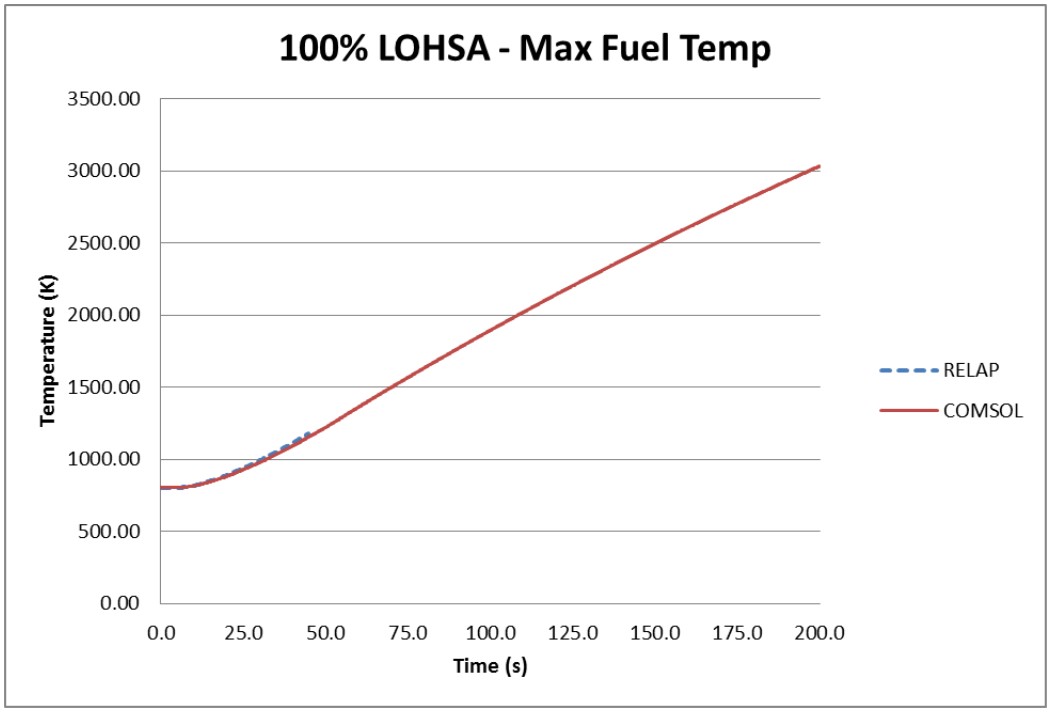

Figure 6.10: 100% LOHSA - Max Fuel Temp

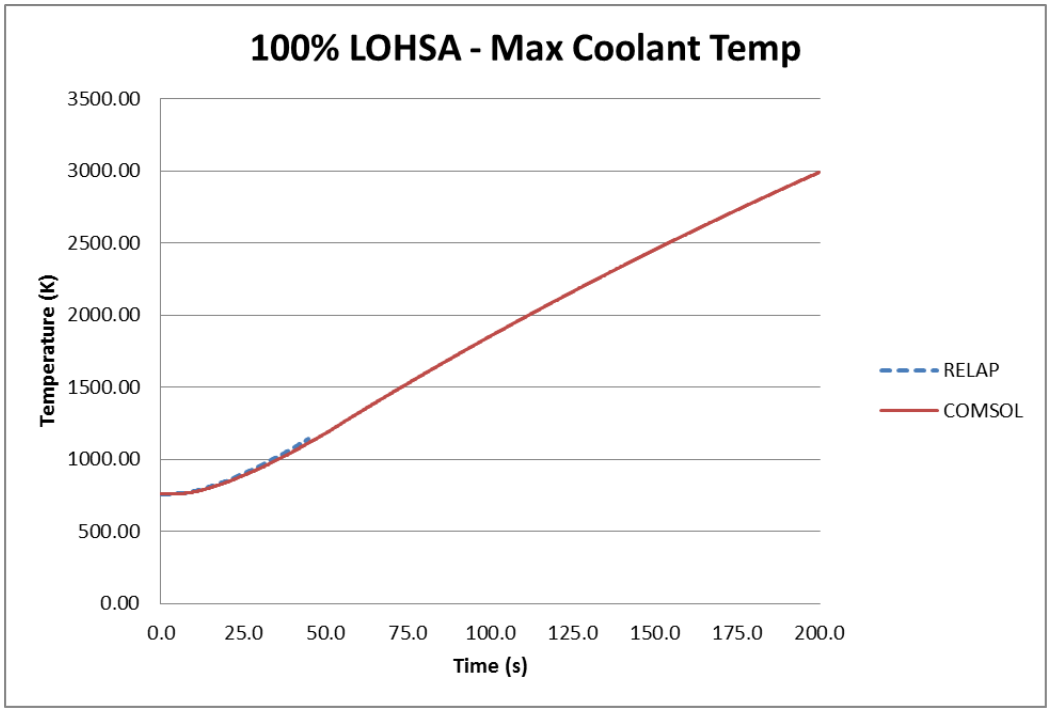

Figure 6.11: 100% LOHSA - Max Coolant Temp

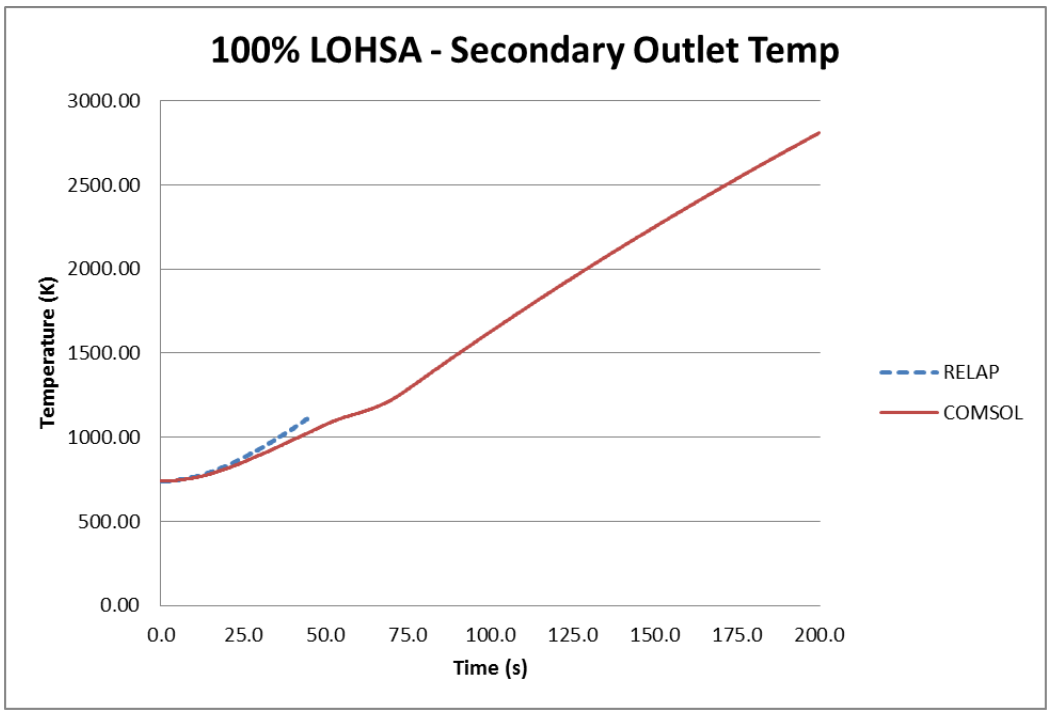

Figure 6.12: 100% LOHSA - Max Secondary Temp

6.1.6 Loss of Power Accident

A Loss of Power Accident (LOPA) refers to a loss of onsite power resulting in the immediate loss of all pumps. It is in effect a combination of a 100% LOFA and a 100% LOHSA. For this case, we keep the fusion neutron source turned on and the fusion power constant. This is a source driven system, and it is possible for the fission cores and the plasma source to have different sources of power. Figs. 6.13 - 6.15 show that the COMSOL and RELAP5 results agree well up to the point of fuel melting and coolant boiling.

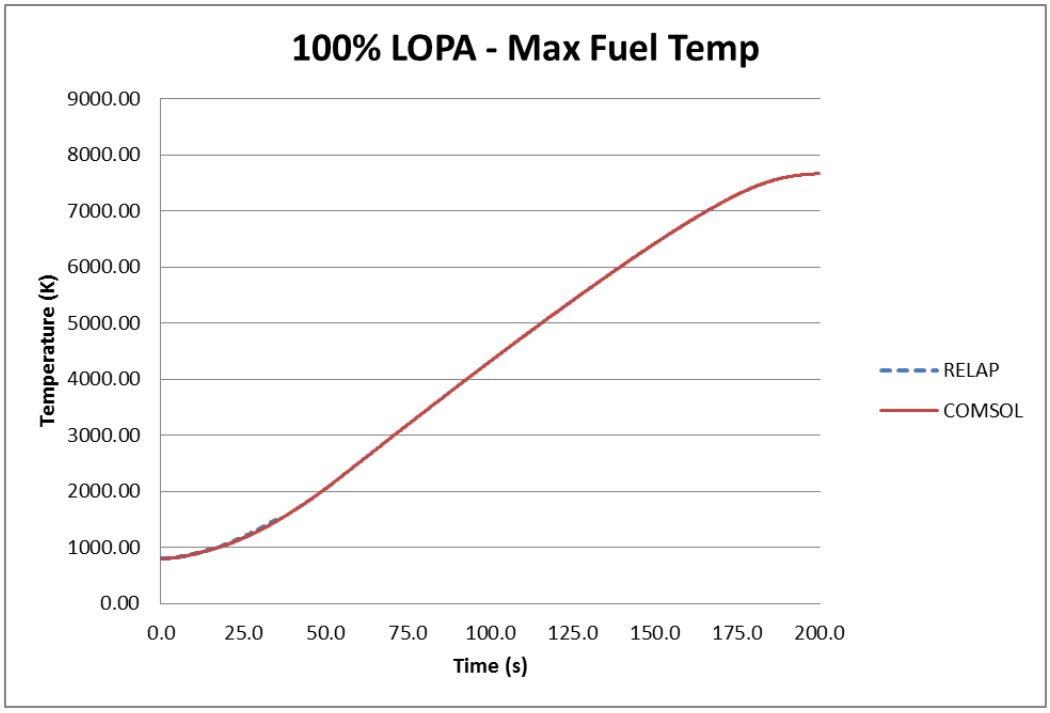

Figure 6.13: LOPA - Max Fuel Temp

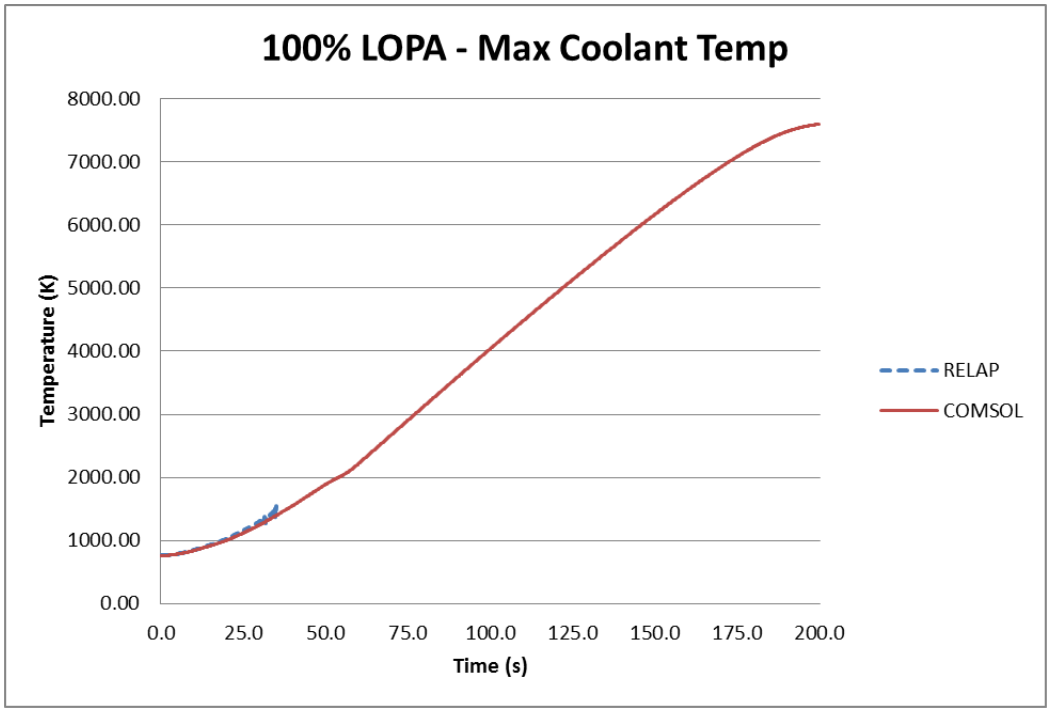

Figure 6.14: LOPA - Max Coolant Temp

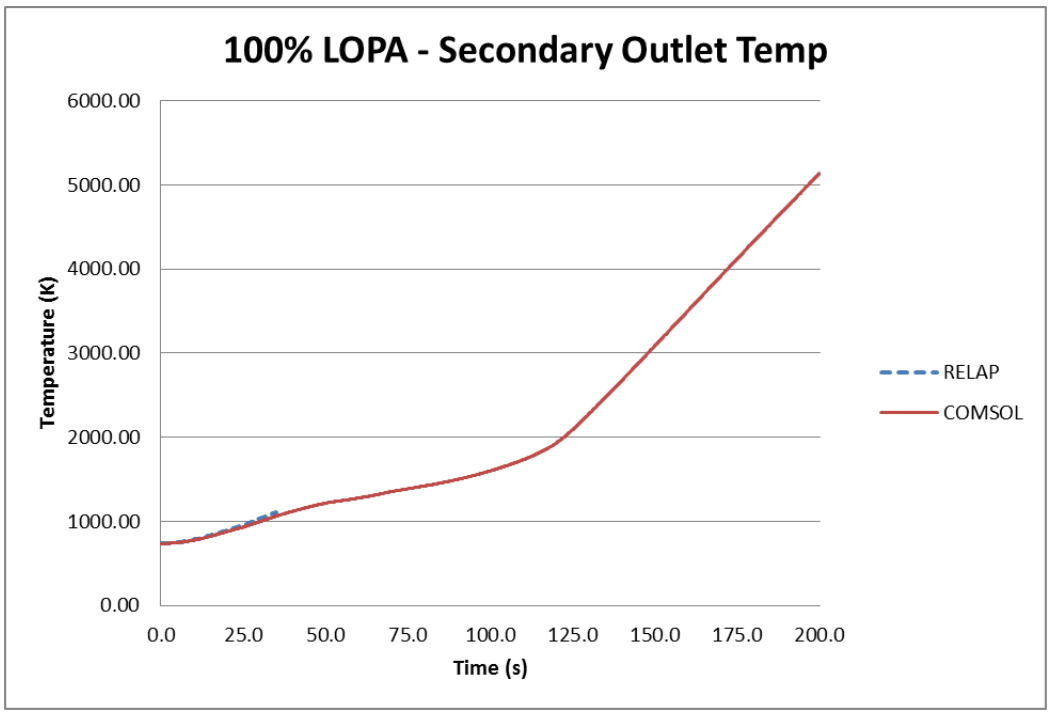

Figure 6.15: LOPA - Max Secondary Temp

6.1.7 Accidental Source Increase

SABR's external neutron source is a fusion plasma. Accidentally turning on an additional plasma heater or injecting too much fuel could cause temporary changes in the plasma power. The case of a 10% increase in fusion power, hence fusion neutron source strength, for a period of 5 seconds was simulated. Even for a very sharp change in power, the results shown in Figs. 6.16 - 6.18 agree well.

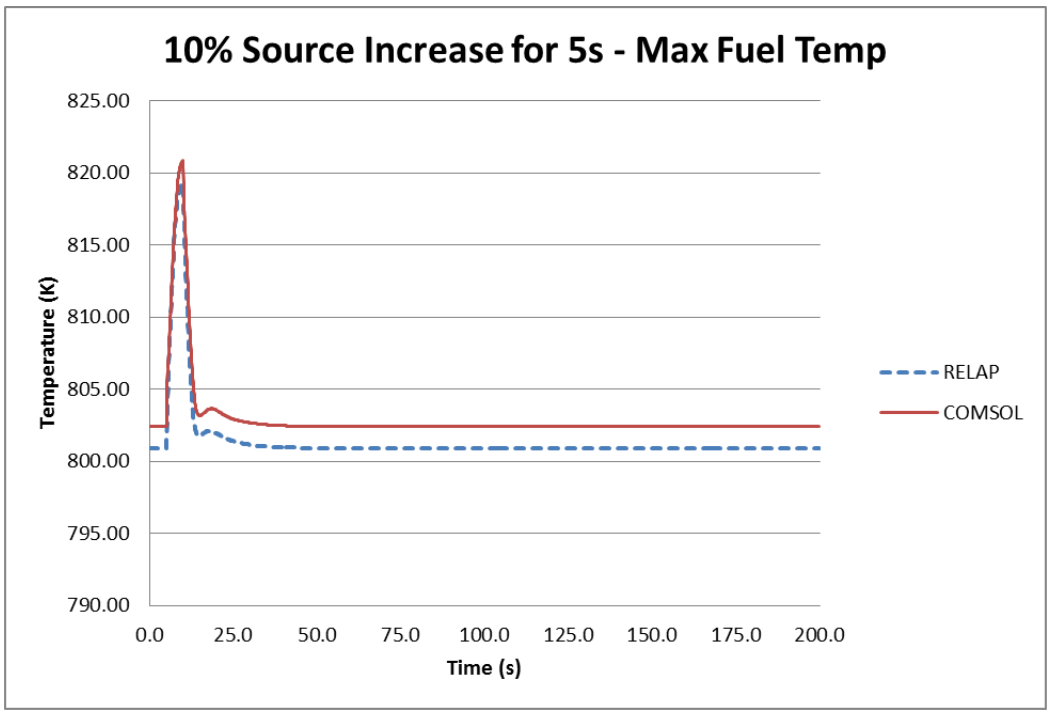

Figure 6.16: Accidental Source Increase - Max Fuel Temp

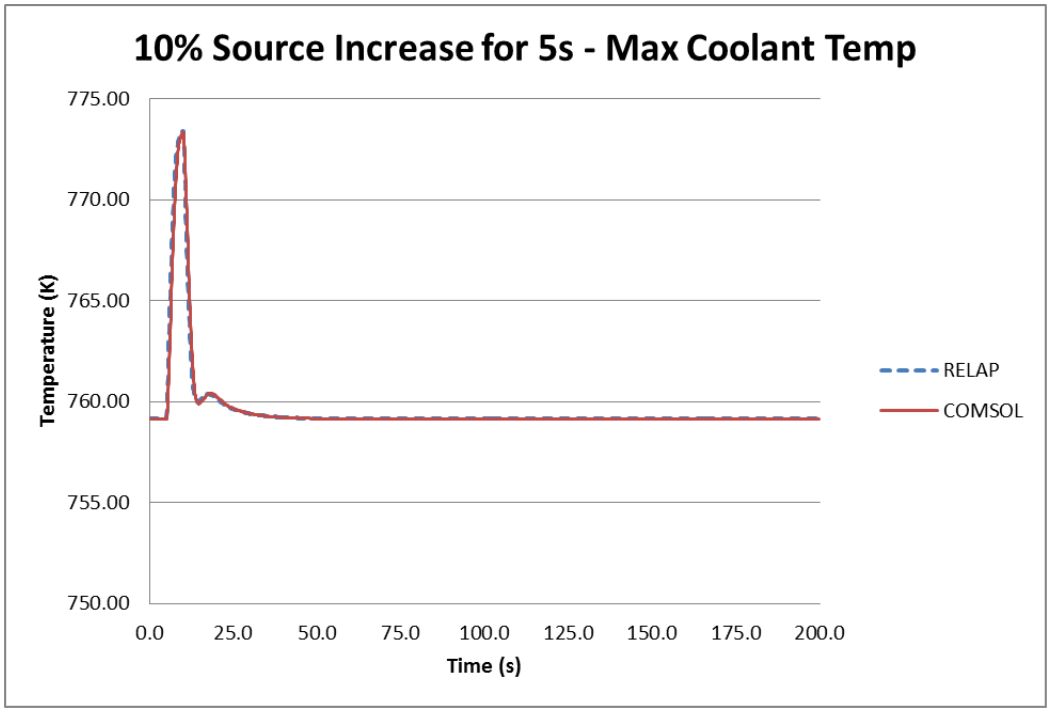

Figure 6.17: Accidental Source Increase - Max Coolant Temp

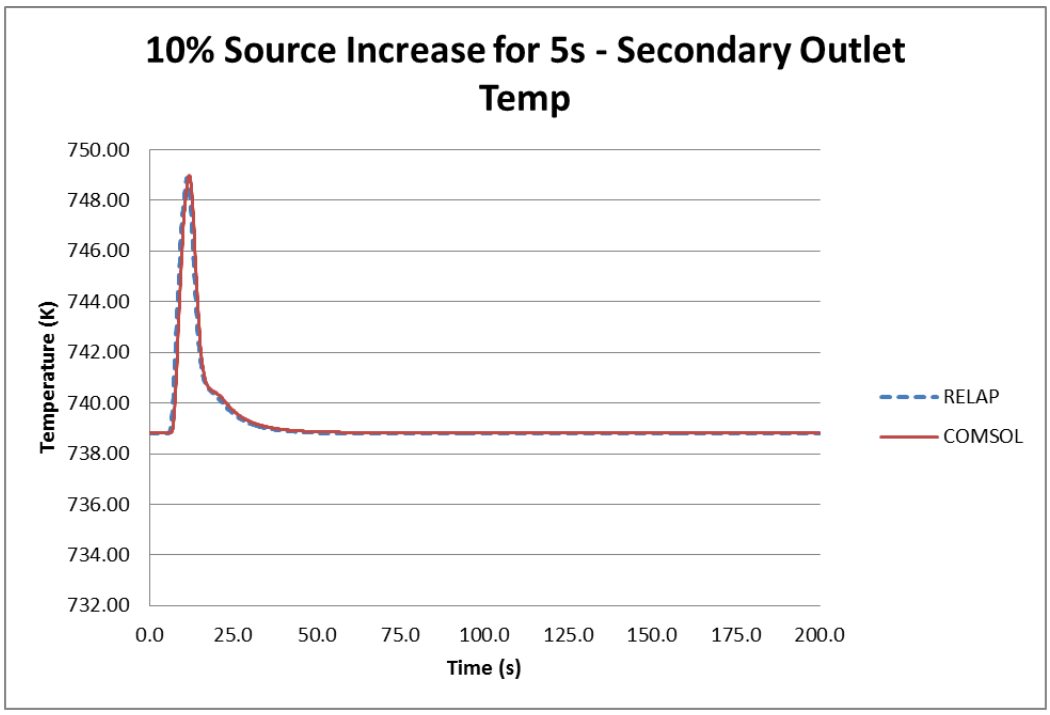

Figure 6.18: Accidental Source Increase - Max Secondary Temp

6.2 Nodal Kinetics Model

The most original part of this thesis is the nodal kinetics model. We have developed a completely original set of nodal kinetics equations. As such, this model presents several questions: Do these equations accurately represent the neutron balance? Can we correctly solve this series of coupled, stiff differential equations? Are they stable at steady state? The verification tests that follow answer these questions in the affirmative.

6.2.1 Neutron Balance

We spent a great deal of time creating the terms of our nodal kinetics equations. There are many competing nuclear reactions in each SABR core. We feel that our terms account for all of these reactions, but we need to verify it. The best way to do this is by turning our nodal model into an eigenvalue problem, using it to make an estimation of k, and then comparing that value to a k calculated by an existing code. If our neutron balance is off, we

will not accurately estimate k. If we remove the external neutron source from our equations, we can recast Eq. 5.18 to give us an estimate of SABR's k as shown below in Eq. 6.1. V_j is the volume of node j, and the other terms are the same as defined in Eq. 5.18.

We already have a model of SABR in MCNP, so we use MCNP's KCODE feature as the verification method. We make the comparison for the reference case and for several types of perturbations of arbitrary magnitude. The nodal and MCNP estimates of k fpr the reference case compare well to one another. MCNP estimates that $k = 0.97430$, and the nodal model estimates that $k = 0.97453$. A small difference of 23 pcm.

$$k_{eff} = \frac{\sum_{j=1}^{10}(\frac{n_j V_j}{\Lambda_j})}{\sum_{j=1}^{10}(\frac{n_j V_j}{l_{e,j}} + \frac{n_j V_j}{l_{a,j}} - \frac{n_j V_j}{\tau_j} - \sum_{k=1}^{10}(\frac{\alpha_{kj} n_k V_k}{l_{e,k}}))} \tag{6.1}$$

The Doppler broadening, sodium voiding, axial expansion, and grid plate expansion perturbations are roughly approximate to a 600 K increase in temperature of the node. Two different cases were run with fuel bowing. The first case (dx) shifts everything in the right two thirds of the core 10 cm to the right (away from the center of the core), and it shifts the remaining left third of the core 10 cm to the left (away from the center of the core). The second case (dy) shifts the bottom two rows of fuel 10 cm away from the core and towards the plasma, and it shifts the top two rows of fuel along with the row of reflector 10 cm away from the core and toward the heat exchanger. We model only one perturbation at a time, and we perturb only Node 1. The MCNP model of SABR and its associated tools became more developed and sophisticated after these tests were run. These results do not accurately reflect how SABR's nodes respond with increasing node temperature; that is not their purpose. Their purpose is to show that the nodal kinetics equations represent a good neutron balance. The nodal equations were not modified after these tests were run. As can be seen in Table 6.2, the results agree well, and we consider our equations to be a good neutron balance.

Table 6.2: Comparisons of Δk

	Δk (pcm)	
	KCODE	Nodal Est.
Sod. Voiding (core)	17 $\pm$ 14	7
Sod. Voiding (core + pool)	-36 $\pm$ 14	-56
Doppler Broadening	-11 $\pm$ 16	-18
Grid Plate Expansion	-37 $\pm$ 14	-62
Axial Expansion	-73 $\pm$ 10	-69
Fuel Bowing (dx)	-24 $\pm$ 8	-40
Fuel Bowing (dy)	-22 $\pm$ 8	-29

6.2.2 Numerical Solver

We wrote a MATLAB program "NodalSolve" to solve our equations over whatever time step we desire. Generally, we consider a differential equation to be stiff when it's unstable and requires very fine steps to solve. In our case, the nodal equations represent a stiff system because they are governed by multiple time constants that are different orders of magnitude. One is for prompt neutrons, which change on the order of microseconds, and the others are for delayed neutrons, which change on the order of seconds. We want to be sure this numerical method is accuractely solving our system of equations. We verify this by taking a Laplace transform of the system and comparing it's solution to the numerical solver's results. Unfortunately, our system is too complicated to be easily solved with Laplace transforms, so we simplify our equations a bit and use Mathematica to apply the transformations for us [43]. We design our cases carefully so that they are simple enough to be solved by Mathematica yet still retain the stiffness and potential stability problems of the full system. Our first case is for a single node with no delayed neutrons. It's governing

equation is shown below in Eq. 6.2.

$$\frac{dn}{dt} = (\frac{1}{\Lambda_f} + \frac{1}{\Lambda_{2n}} + \frac{\alpha_{11}}{l_e} - \frac{1}{l_a} - \frac{1}{l_e})n(t) + S_{fus} \tag{6.2}$$

The resulting Laplace solution for the steady state case is shown in 6.3. The results agree well, and the solutions differ by less than 0.003 $\%$.

$$n(t) = 474320 + 10.0229e^{-424164*t} \tag{6.3}$$

For the next case, we take the same equation as before and decrease the external source strength by 50%. The Laplace solution is shown in Eq. 6.4. Fig. 6.19 compares our results on the time scale of prompt neutrons. Our numerical estimate agrees well with the Laplace solution.

$$n(t) = 237160 + 237170e^{-424164*t} \tag{6.4}$$

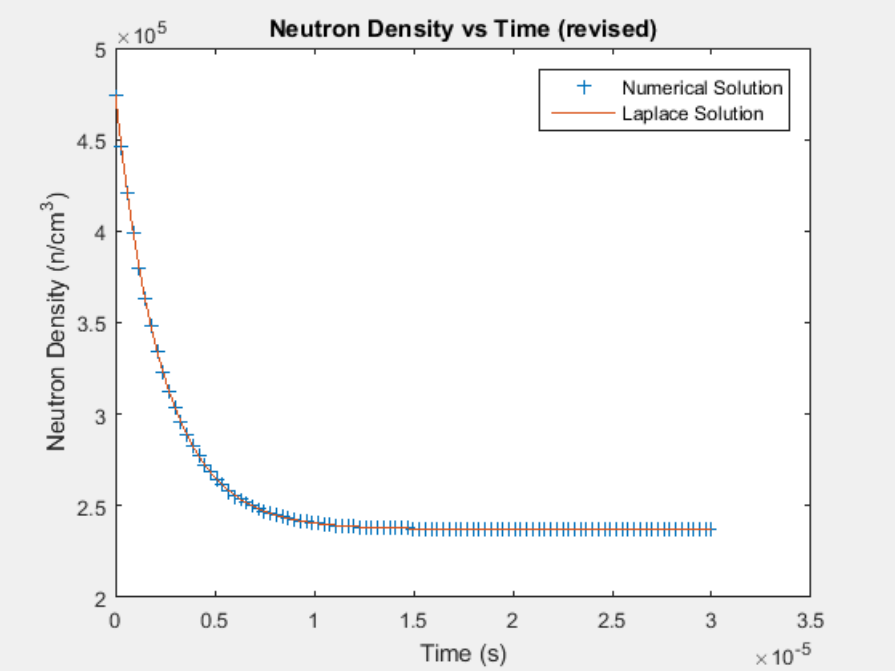

Figure 6.19: Neutron Density vs Time (No Delayed Neutrons, 50% Reduction in Source Strength at t=0)

Now we move to a problem with more stiffness. We want to confirm that our solver can handle a stiff system governed by multiple time constants. Consider a single node problem with one group of delayed neutrons. The governing equations are shown in Eq. 6.5 and Eq. 6.6.

$$\frac{dn}{dt} = (\frac{1}{\Lambda_f} + \frac{1}{\Lambda_{2n}} + \frac{\alpha_{11}}{l_e} - \frac{1}{l_a} - \frac{1}{l_e})n(t) + S_{fus} + \lambda c(t) \tag{6.5}$$

$$\frac{dc}{dt} = \frac{\beta}{\Lambda} n(t) - \lambda c(t) \tag{6.6}$$

The steady state Laplace solution is shown in Eq. 6.7. The results agree well, and the

solutions differ by less than 0.02 %.

$$n(t) = -2.73403e{-}12e^{-215581*t}(2.88044e13e^{-431161*t/2} {-} 2.28212e16e^{215578*t} {-} 1.73489e17e^{215581*t}) \tag{6.7}$$

Now we asses the transient response more thoroughly. We reduce the external source strength by 50% and compare the results on the two time scales governing the problem. The Laplace solution is shown in Eq. 6.8.

$$n(t) = 237162 + 233232e^{-431161*t} + 66245.1e^{-2.79093*t} \tag{6.8}$$

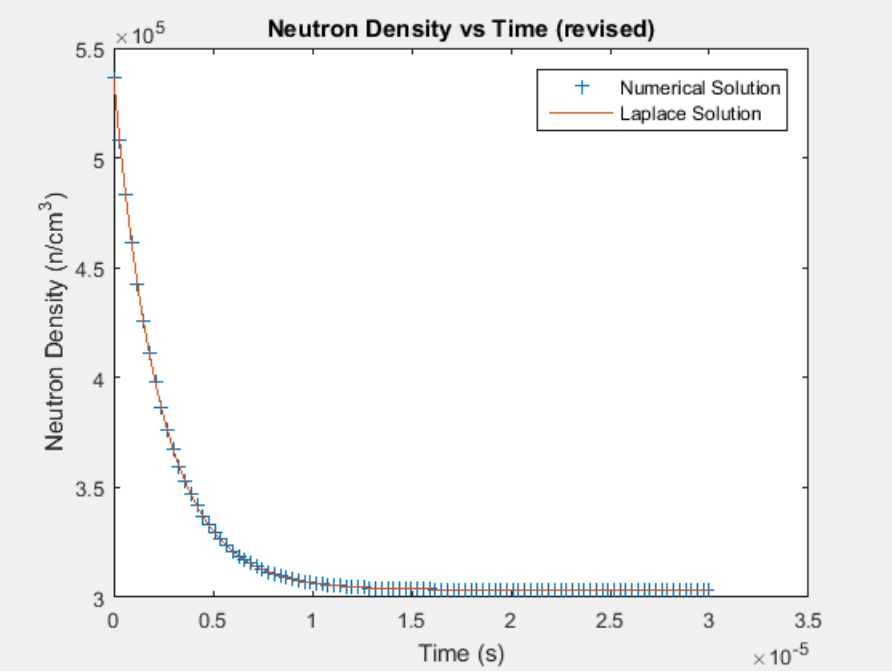

Figure 6.20: Neutron Density vs Time (1 Group Delayed Neutrons, 50% Reduction in Source Strength at t=0)

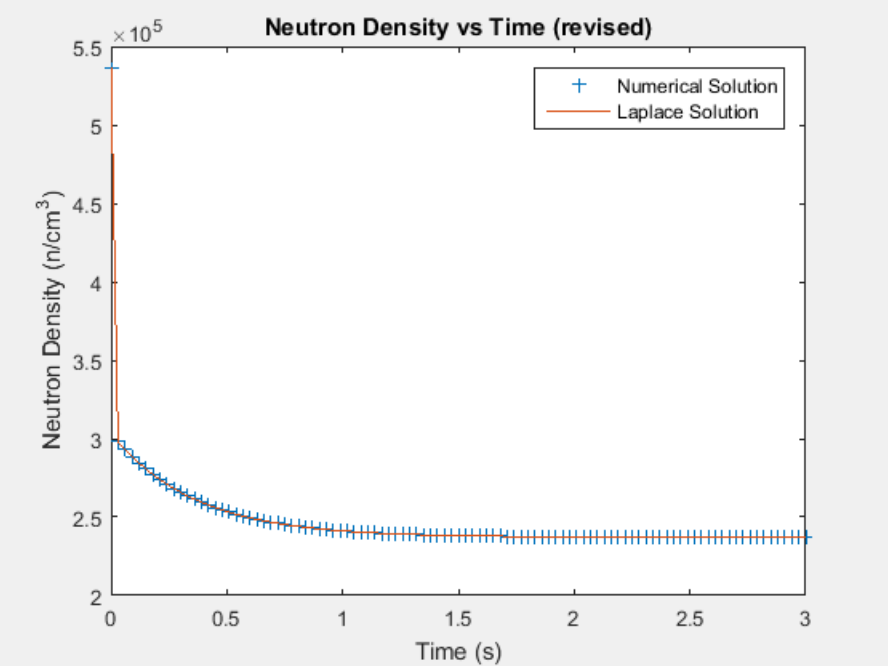

Figure 6.21: Neutron Density vs Time (1 Group Delayed Neutrons, 50% Reduction in Source Strength at t=0)

Fig. 6.20 and Fig. 6.21 show that our numerical method accurately computes the solution for all time constants in the system. In other words, our solver can fully handle the inherent stiffness of our problem.

6.3 Structural Mechanics Model

We use COMSOL to model the structural mechanics component of our fuel bowing analysis. First, we verify the mesh we are using by performing a mesh convergence study. Next, we run an IAEA structural mechanics verification problem using similar settings for the mesh and physics solvers [44].

6.3.1 Mesh Convergence Study

Given the aspect ratio of our geometry, we can use a swept mesh to increase computational efficiency. We apply a triangular surface mesh to the top surface of the ducts and sweep

it through. For the mesh convergence study, we vary the minimum and maximum element size of the surface mesh, and we vary the number of axial elements in the swept component. We choose our convergence metric to be the average x,y, or z displacement on the top surface of 3 different ducts. Each duct chosen has the maximum displacement for one of the three dimensions. Fig. 6.22 shows the ducts we use for each dimension.

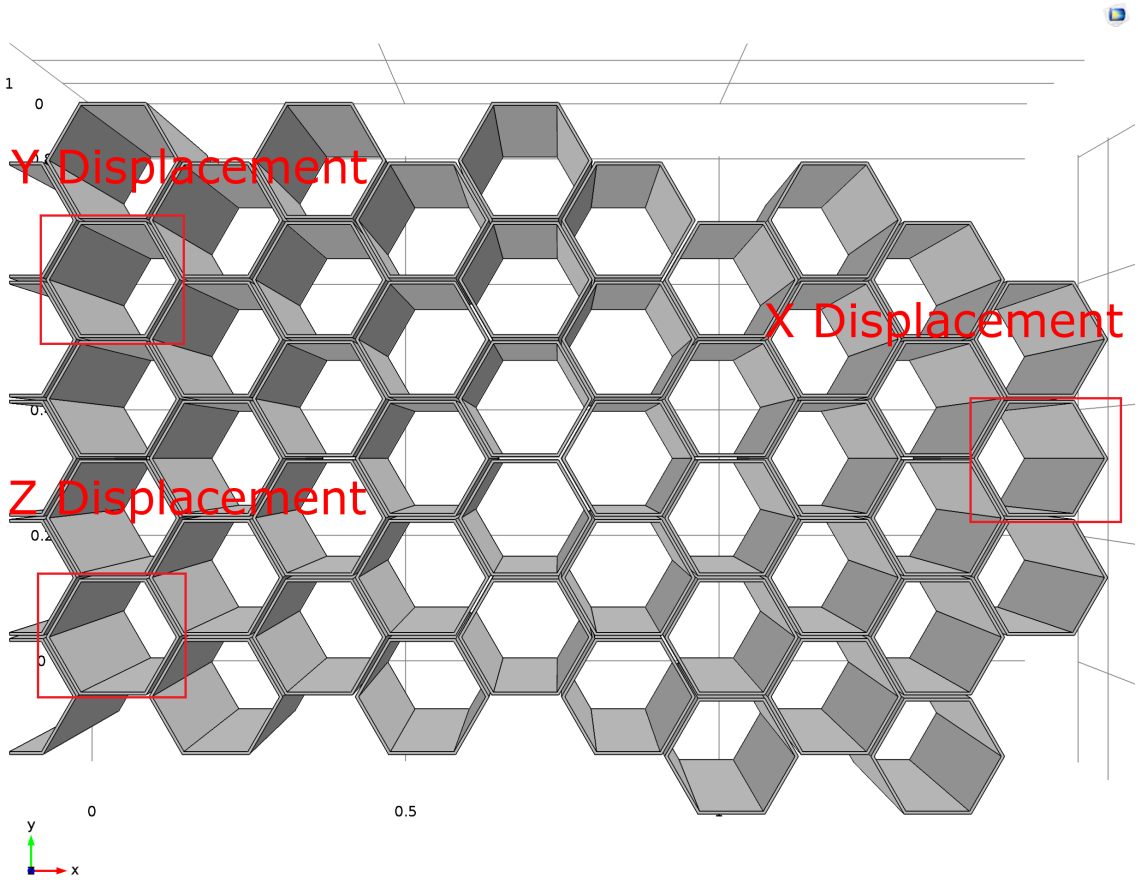

Figure 6.22: Ducts of Maximum Displacement for Each Dimension

The fuel bowing we see is on the order of 1e-3 m, so we set our convergence criterion as 1e-4 m. The tables below show that we attain convergence using 0.1/0.01 m values for max/min element size.

Table 6.3: Average X Displacement of Selected Face (m)

	Max/Min Element Size (m)			
# of Axial Elements	1.0/0.1	0.1/0.05	0.1/0.01	0.01/0.001
10	0.00354	0.00348	0.00347	0.00345
20	0.00354	0.00348	0.00347	0.00344
30	0.00354	0.00348	0.00347	0.00344

Table 6.4: Average Y Displacement of Selected Face (m)

	Max/Min Element Size (m)			
# of Axial Elements	1.0/0.1	0.1/0.05	0.1/0.01	0.01/0.001
10	0.00281	0.00280	0.00297	0.00294
20	0.00281	0.00280	0.00297	0.00294
30	0.00281	0.00228	0.00297	0.00294

Table 6.5: Average Z Displacement of Selected Face (m)

	Max/Min Element Size (m)			
# of Axial Elements	1.0/0.1	0.1/0.05	0.1/0.01	0.01/0.001
10	0.00860	0.00862	0.00863	0.00863
20	0.00860	0.00862	0.00863	0.00863
30	0.00860	0.00862	0.00863	0.00863

6.3.2 IAEA Verification Problem

We have a converged mesh, and now we want to check our physics. To do this, we use an International Atomic Energy Agency (IAEA) verification problem for structural mechanics in liquid metal fast breeder reactors. The problem solution is a hand calculation made by the IAEA's International Working Group on Fast Reactors (IWGFR) [44]. The problem contains a single fuel assembly made of stainless steel, and it uses cartesian coordinates with the origin centered on the bottom face of the duct. The z-axis is parallel with the duct axis. The duct wall is 3 mm thick with an across flats dimension of 132.9 mm. The material properties are $T_{ref} = 20\ ^\circ C$, $\alpha = 18.6e-6\ /^\circ C$, $\nu = 0.3$, and $E = 170\ GPa$. The temperature field is described by the piecewise function below with $a_0 = 212.5\ ^\circ C$, $a_1 = 0.500\ ^\circ C/mm$, $a_2 = 0.125\ ^\circ C/mm$, and $a_3 = -3.333e-4\ ^\circ C/mm$.

$$\begin{cases} 400\ ^\circ C & z \leq 1500\ mm \\ a_0 + a_1 x + a_2 z + a_3 xz & 1500\ mm < z < 2500\ mm \\ 525\ ^\circ C - \frac{50\ ^\circ C}{150 mm} x & 2500\ mm \leq z \leq 4000\ mm \end{cases}$$

We apply a similar swept, triangular mesh to the model. We use the same min/max parameters as our SABR fuel bowing model, but we refine the axial mesh a bit. The axial temperature profile in this problems varies much more strongly than the axial temperature profile of SABR. We use the same physics solvers as the SABR model, and we even include geometric nonlinearity. We calculate the x and z displacements at the very top of the assembly. The results are shown in the table below.

Table 6.6: Comparison of Displacement Estimations

	COMSOL Model	IAEA Problem	% Difference
X Displacement	-11.66 mm	-12.36 mm	5.7
Z Displacement	32.91 mm	31.86 mm	3.2

The results agree well, and we consider our structural mechanics model of SABR to be verified.

CHAPTER 7
DYNAMIC SAFETY RESULTS

When we model an accident scenario with our dynamics model, we use a maximum time step of 0.1 s. Each accident scenario is run for 125 s unless a longer time is needed. 125s is the minimum time required for the coolant flowrates to coast down and reach a constant value.

Both the primary and secondary loops of each pool both have two sodium pumps. Electromagnetic sodium pumps have no moving parts, and the flow stops almost instantly after the pump. Mechanical pumps have a flywheel that takes time to dissapate its energy. It takes tens of seconds for the flow to completely stop after the pump is turned off. SABR's EM pumps have no flywheel, but the electric motors powering them do. SABR's pump design is taken from Argonne National Lab's Advanced Burner Test Reactor [42]. The flywheel allows the flow rate to coast down slowly in the event of pump failure. We use this flywheel system for the pumps in the both the primary and secondary loops.

The flywheel motor has a ten second halving time. Figs. 7.1 and 7.2 show the coolant flowrate in either for a 50% LOFA/LOHSA and a 100% LOFA/LOHSA respectively. They are normalized to the steady state flow rates. The coastdown plots apply to both the primary and secondary cycles.

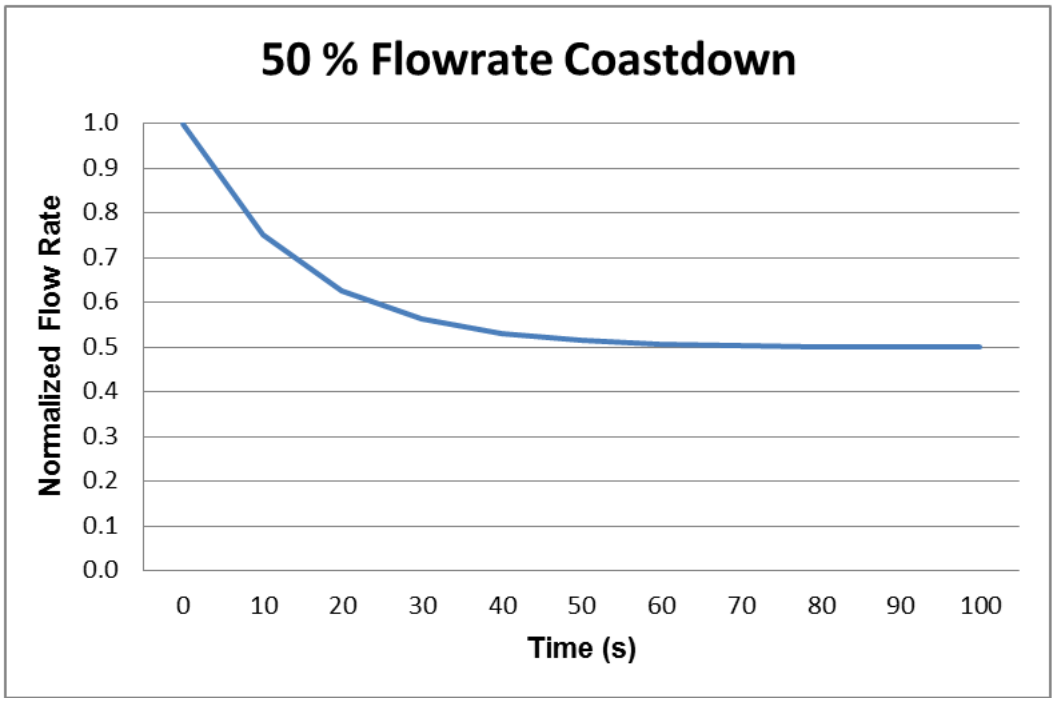

Figure 7.1: Flowrate Coastdown for Single Pump Failure

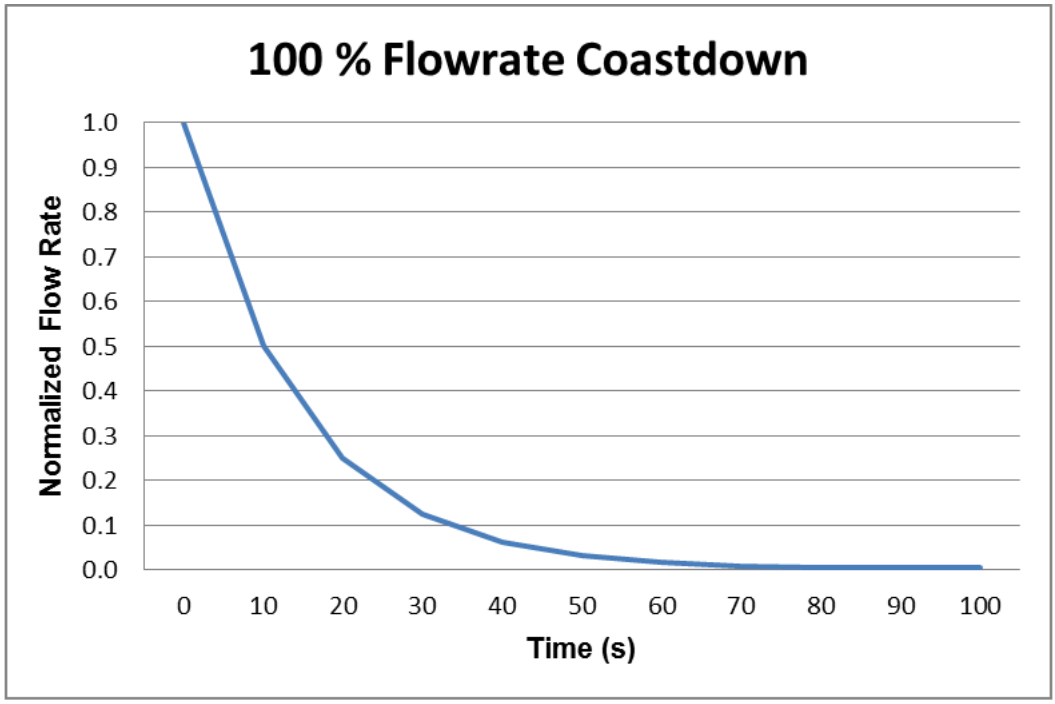

Figure 7.2: Flowrate Coastdown for Double Pump Failure

When both pumps fail, the flow rate does not coast down all the way to zero. There is some natural circulation in the core. We use the method prescribed by Todreas and Kazimi to estimate natural circulation in the primary loop [45]. It is shown in Eq. 7.1.

$$\dot{m} = (\frac{2\beta \dot{Q_H} g \Delta L \rho_o^2}{c_p R})^{\frac{1}{3-n}} \tag{7.1}$$

β is the coefficient of thermal expansion defined by $-\frac{\partial \rho}{\partial T}\frac{1}{\rho}$, $\dot{Q_h}$ is the core power, g is the acceleration due to gravity, ΔL is the height difference between the center of the core and the center of the heat exchanger, ρ is the reference density of sodium, c_p is the average heat capacity of sodium, and R is the hydraulic resistance coefficient.

This natural convection model assumes steady state conditions. We are not simulating steady state conditions, but we can still use this model. Any accident results in either failure or new steady state conditions. If the accident results in new steady state conditions, the use of the model is justified. If the accident results in failure, the use of the model is irrelevent. We are interested in determining if and when failure occurs. We are not modeling what happens after failure.

The reactor power $\dot{Q_H}$ is what drives natural circulation in the core. Different power levels result in different flow rates. We estimate the natural circulation in the core for two different power levels: full power and decay power. We have not explicitly calculated the decay power for SABR's current design. We conservatively assume a constant decay power of 7 % of full power. We base this assumption on studies of decay power in TRU fuel [46]. The minimum flow rates we use for each power are shown in Table 7.1.

Table 7.1: Minimum Flow Rates

	Full Power	Decay Power
% of Normal Flow Rate	2.0	0.5

7.1 Accidents with No Corrective Action

In this section, we examine accidents with no corrective action (control rod insertion or neutron source deactivation) taken. These results serve as a baseline in understanding SABR's inherent passive safety characteristics. The accidents start at time t=0, and they occur only in Core 1. We do not directly perturb Cores 2 through 10. Any changes in these cores are the result of the neutronic coupling between the cores.

The 50% LOFA and 50% LOHSA cases show no coolant boiling or fuel melting. The maximum fuel and coolant temperatures reached in these transients are shown in Fig. 7.3 and Fig. 7.4. The sodium boiling point is 1156 K, and the fuel melting point is 1473 K. These results indicate that SABR would survive a 50 % LOFA or LOHSA in a single core without any corrective action. However, SABR reaches the point of failure during the 100% LOFA/LOHSA/LOPA cases. Fig. 7.3 and Fig. 7.4 show that the fuel melts and the coolant boils shortly after the initiation of the accident. For a LOPA with no corrective action, we assume that the plasma does not lose power, and the fusion neutron source remains at full strength.

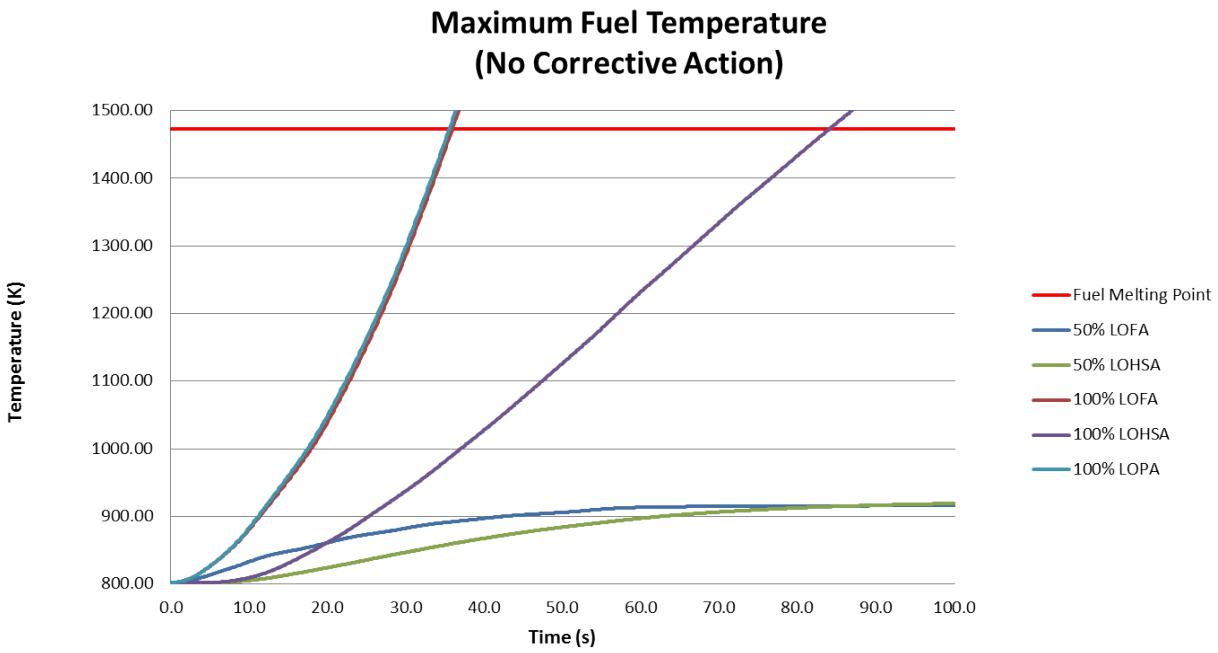

Figure 7.3: Max. Fuel Temperatures (All Uncontrolled Cases)

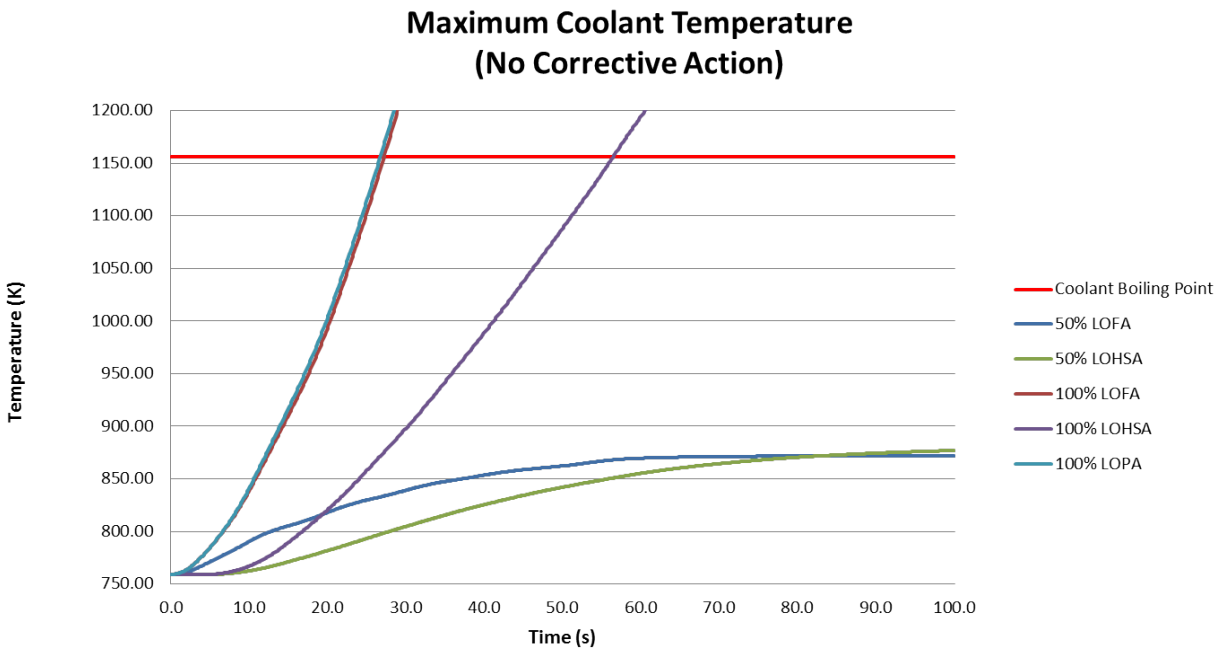

Figure 7.4: Max. Coolant Temperatures (All Uncontrolled Cases)

We also ran a 100% LOHSA case for all 10 cores and compare it to the 1 core case. It's possible that a simultaneous decrease in all core powers would reduce the power enough to avoid design failure. Unfortunately, such is not the case. Table 7.2 shows that the results are almost identical to that of the single core 100% LOHSA.

Table 7.2: Comparison of 1 Core and 10 Core LOHSAs with No Corrective Action

	Time To Coolant Boiling (s)	Time To Fuel Melting (s)
1 Core - 100 % LOHSA	56.4	84.0
10 Core - 100 % LOHSA	57.4	84.5

7.2 Accidents with Plasma Shutdown

The "100% " accidents summarized in Table 7.3 resulted in coolant boiling and/or fuel melting after about 25 seconds in the abscence of corrective action, which indicates that we have about 25 seconds to take corrective control actions.

With a subcritical reactor, one obvious control action is to turn off the neutron source. SABR's plasma is maintained by external power sources that heat the plasma and drive confining current in the plasma. Simply switching off these external power sources would reduce the neutron source strength as the plasma cooled down. Since the energy confinement time in the plasma is on the order of seconds, the neutron source strength might be expected to decay exponentially with a time constant on the order of seconds. There are constraints on ramping down magnetic fields that might lead to the necessity of slower neutron source decays. Our research group is currently examining this issue. Initial results show that the plasma power can be reduced to 0 within 10 seconds. For the purpose of the present calculations, we make the conservative assumption of an exponential decay with a time constant of 10 seconds.

Most fast reactor control systems initiate shutdown when certain parameters such as core temperature or power-to-flow ratio reach a certain value. Once the theshold is hit, the control system takes on average 2 seconds to respond. For SABR, our threshold is pump failure. When a pump fails, we conservatively assume the reactor control system takes 2 seconds to notice and another 3 seconds to respond by initiating a plasma shutdown. Thus, we initiate the plasma shutdown 5 seconds after a pump in any of the fission reactors stops.

A plot showing the fission power profile in each of the 10 cores is shown in Fig. 7.5. There are 10 lines on the plot, but they are drawn on top of each other because their powers are all the same. Even though the fusion power drops to zero, the fission power does not drop below 7%, the assumed decay power.

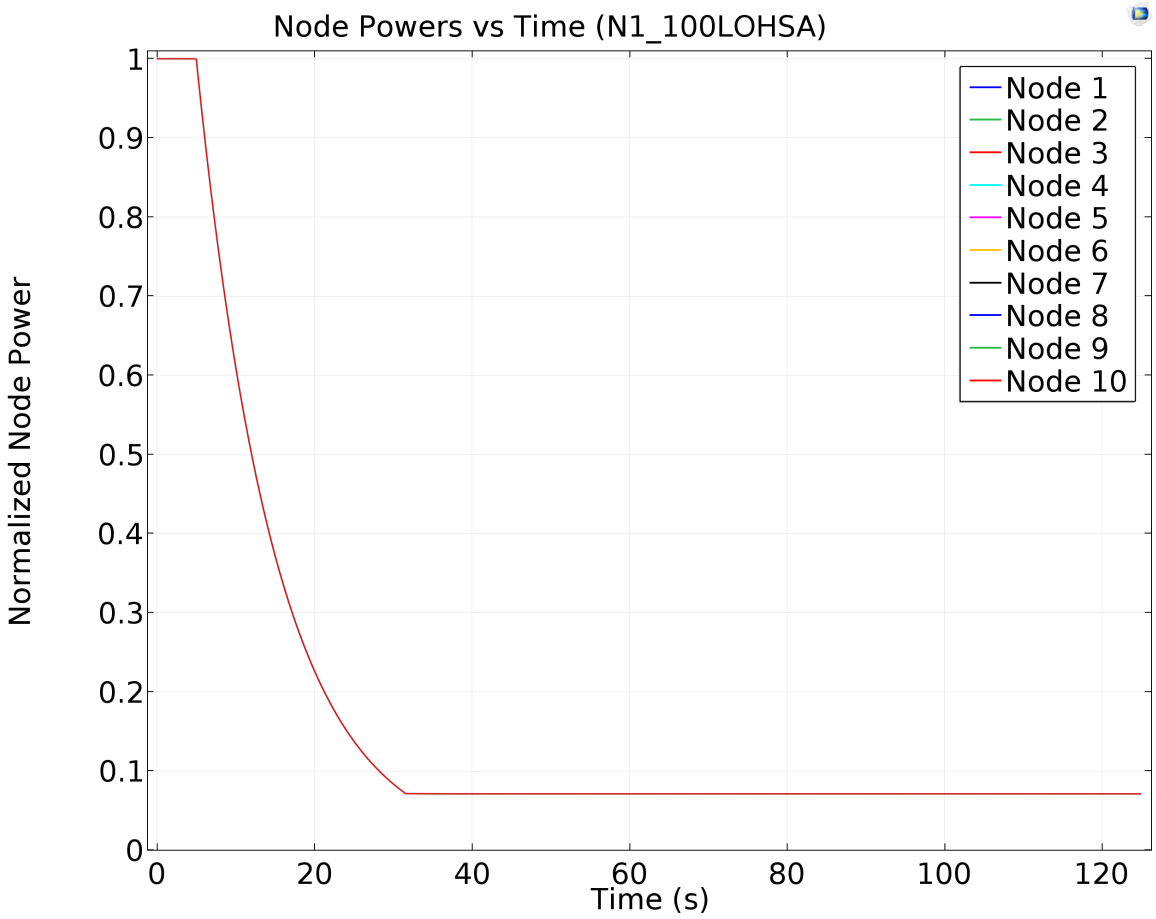

Figure 7.5: Core Powers with Plasma Shutdown

The fission reactors shut down within 30 seconds which is well before the point of failure as shown in Table 7.3. Even though the reactor is shut down, it still reaches the point of failure due to the decay power not being removed. There is not enough natural circulation to remove the residual decay power, and fuel and coolant temperatures steadily increase to the point of failure. In other words, fuel melting and coolant boiling in the 100% cases with plasma shutdown are due solely to the decay power not being adequately removed. This is a problem that hopefully can be corrected by design attention to decay heat removal.

Table 7.3: Core 1 - Time Until Failure in 100% Accidents with Plasma Shutdown

	Time To Coolant Boiling (s)	Time To Fuel Melting (s)
100 % LOFA	207.7	280.8
100 % LOHSA	685.9	1283.2
100 % LOPA	204.1	277.4

7.3 Accidents with Control Rod Insertion

In this section, we simulate the same accident scenarios but use control rod insertion as a corrective mechanism. The plasma power remains at 100%, and we insert control rods to decrease the fission power several seconds after an accident begins. We assume it takes 2 seconds for the reactor control system to notice the pump failure and 1 second to initiate a control rod drop in all 10 modular cores. We assume the control rods take 2 seconds to fully insert once they are dropped. These values are approximate to normal fast reactor control systems.

SABR's design does not include control rods, so we approximate what a control rod system for SABR would look like. We use a rod bank similar to the one in ANL's Advanced Burner Test Reactor (ABTR) [42]. The ABTR uses a bank of 10 control rods that provide up to -$40.19 of reactivity. The ABTR is a good analog because it has a power, fuel composition, and delayed neutron fraction comparable to SABR. A SABR core generates 300 MWt of power while the ABTR generates 250 MWt. SABR's fuel is TRU while the ABTR's fuel is a mixture of TRU and uranium. SABR's delayed neutron fraction is $\beta_{eff} = 0.0030$ and ABTR's is $\beta_{eff} = 0.0033$.

If we use the rod distribution shown in Fig. 7.6, we can fit 9 control rods into each SABR core. Each of the 10 control rods in the ABTR have different reactivity worths, but

here we take an average and assume each rod has the same worth. Under that assumption, each rod would be worth $4.02. We use Eq. 7.2 to convert that to a reactivity per rod of $\Delta\rho = -0.0134$. We estimate SABR's total control rod worth by dividing $\Delta\rho$ by SABR's β_{eff} and multiplying by 9 rods. We get a total control rod worth of -$39.67. This corresonds to a 15.985% decrease in the absorption lifetime l_a.

$$\$\ of Reactivity = \frac{\Delta\rho}{\beta_{eff}} \tag{7.2}$$

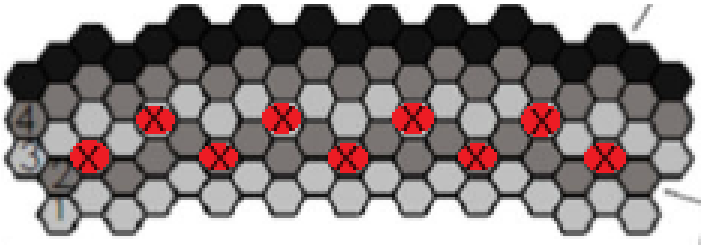

Figure 7.6: Control Rod Distribution (x)

The results shown in Tables 7.4 and 7.5 indicate that sodium boiling and fuel melting occur only for the "100% " cases. The control rods only reduce the power by 64% as shown in Fig. 7.7. This is not a large enough reduction in power to shut the core down, and the failure is caused by the active core power, not the decay power.

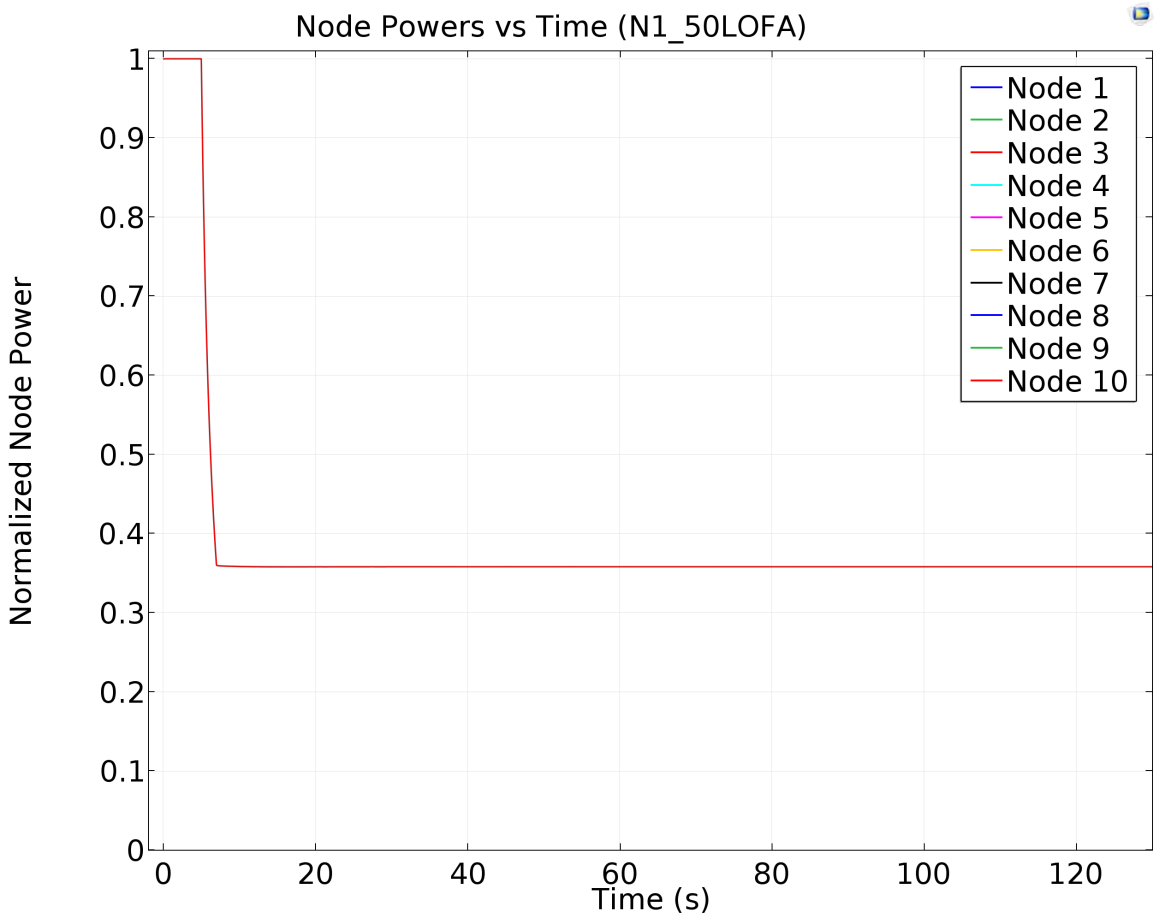

Figure 7.7: Core Powers with Control Rod Insertion

Table 7.4: Core 1 - Maximum Temperatures in 50% Accidents with Control Rod Insertion

	Max Coolant Temp (K)	Max Fuel Temp (K)
50% LOFA	772.0	813.5
50% LOHSA	759.1	802.4

Table 7.5: Core 1 - Time Until Fuel Melting in 100% Accidents with Control Rod Insertion

	Time To Coolant Boiling (s)	Time To Fuel Melting (s)
100 % LOFA	59.1	73.0
100 % LOHSA	148.4	248.5
100 % LOPA	58.3	72.2

The control rods don't provide enough negative reactivity to avoid failure in the 100% accidents. They only reduce the power by 64%. SABR would require a minimum of -$146.87 of control rod reactivity in each core to avoid failure in the 100% accidents. That is about four times the reactivity in our current control rod bank. It would appear that switching off the fusion power would be needed in addition to control rod insertion in order to avoid failure in the 100% LOFA, LOHSA, and LOPA.

7.4 Summary of Results

In this thesis, we've stated two objectives: 1) Determine if we can control SABR and safely shut it down during an accident and 2) Determine the level of passive safety in SABR. We have learned that we can control SABR and safely shut it down before it reaches the point of failure by shutting down the plasma. We have also learned that SABR's current design exhibits only a small degree of passive safety. Even if SABR is successfully shut down, the resdidual decay power is not passively removed and eventually causes SABR to fail. This identifies the need for design modifications to enhance the removal of decay heat in the event of total pump failure.

CHAPTER 8

COMPARISON WITH EBR-II PASSIVE SAFETY DEMONSTRATION

SABR does not show the same degree of passive safety that EBR-II exhibited. SABR's safety performance is different in two ways: 1) Its inability to passively remove decay heat and 2) Its need for an active shutdown mechanism. Both differences are important, but SABR's inability to remove passive decay heat is the most major difference. It is worthwhile to examine both of these differences and explain their effects.

8.1 SABR's Lack of Passive Decay Heat Removal

EBR-II was able to remove passively remove its decay while SABR is not. This is the most major difference between the safety characteristics of EBR-II and SABR, and it is for two reasons. 1) SABR's design does not present favorable conditions for natural circulation and 2) SABR does not have a passive heat exchanger.

Regarding the natural circulation, the sodium pools in SABR were not designed for optimum thermal hydraulic performance. They were designed to be integrated into an ITER fusion device. Most pool type reactors (such as EBR-II) place the heat exchanger several meters above the core to maximize the natural circulation. Natural circulation depends on several variables as shown in Eq. 8.1.

$$\dot{m} = (\frac{2\beta \dot{Q_H} g \Delta L \rho_o^2}{c_p R})^{\frac{1}{3-n}} \tag{8.1}$$

β is the coefficient of thermal expansion defined by $-\frac{\partial \rho}{\partial T}\frac{1}{\rho}$, $\dot{Q}_h$ is the core power, g is the acceleration due to gravity, ΔL is the height difference between the center of the core and the center of the heat exchanger, ρ is the reference density of sodium, c_p is the average heat capacity of sodium, and R is the hydraulic resistance coefficient.

Both EBR-II and SABR use molten sodium as the coolant so β, ρ_o^2, and c_p are likely similar between the two. We don't have readily available data on a hydraulic resistance coefficient corresponding to EBR-II, so we can't compare them. g is obviously the same between the two. The largest difference we can find between the two designs is ΔL. ΔL is 0.41 m for SABR and is 2.3 m for EBR-II [47].

8.2 SABR's Requirement of a Shutdown Mechanism

EBR-II was able to use reactivity feedbacks to shut itself down without the use of an active shutdown mechanism. SABR's reactivity feedbacks are much weaker, and that is the reason SABR requires an active shutdown mechanism. In this section, we discuss how and why the reactivity feedbacks between SABR and EBR-II are so different.

In the years leading up to EBR-II's historic demonstration of passive safety, the engineers responsible ran smaller scale tests to estimate its response to the future passive safety tests. They slowly increased the size and severity of each test to ensure the experimental data were matching their theoretical models. Remembering the experiences of EBR-I, they were eager to avoid any surprises. During this process they estimated the reactivity coefficients for EBR-II [48] which are summarized in Table 8.1. Some of the experimental data from the EBR-II passive safety tests are available, but it was not possible to directly measure the individual contributions of each reactivity feedback. We use Table 8.1 as a best possible estimate in determining which feedbacks played the larger role.

Table 8.1: Predicted Reactivity Feedbacks in EBR-II [48]

	Feedback Coeff. $(10^{-4}\$/C)$	Est. Uncertainty $(\%)$
Fuel Expansion	-4.91	11
Sodium Expansion	-11.9	7
Grid Plate Expansion	-14.5	20
Reflector Axial Expansion	-6.32	7
Control Rod Axial Expansion	-7.16	5
Doppler Broadening	-0.671	10
Fuel Bowing	9.8	25

For EBR-II, sodium and reflector expansion decrease reactivity by increasing neutron leakage from the core. Fuel and grid plate expansion decrease reactivity by moving the fuel outward into regions of lower neutron importance. Control rod expansion pushes the rods further into the core increasing parasitic neutron absorption thereby reducing reactivity. Doppler broadening decreases reactivity by reducing the fuel's ability to absorb fission-inducing neutrons. Fuel bowing increases reactivity when the fuel assemblies deform and shift the fuel in a region of higher neutron importance.

There is no exact analog to this table of reactivity feedbacks for SABR because it's a fixed source system and the effects of feedback take a different form. However, we can use the MCNP KCODE nodal k_{eff} model of Eq. 6.1 to predict changes in k_{eff}, hence reactivity feedback, from the nodal model as given in Table 6.2, which is repeated here in a modified form in Table 8.2. We can't use them to quantify the absolute strength of each feedback, but we can use them to quantify the strength of the feedbacks relative to one another.

Table 8.2: Comparisons of Δk in SABR for Various Perturbations

	Δk (10^{-3} pcm/K)
Sod. Voiding (core)	28.3 $\pm$ 23.3
Sod. Voiding (core + pool)	-60 $\pm$ 23.3
Doppler Broadening	-18.3 $\pm$ 26.7
Grid Plate Expansion	-61.7 $\pm$ 23.3
Axial Expansion	-121.7 $\pm$ 16.7

For SABR, the Doppler broadening, axial expansion, and grid plate expansion work the same way they did for EBR-II. Sodium voiding in the core hardens the neutron energy spectrum. The higher energy neutrons increase the fission to capture ratio and increase reactivity. For sodium voiding in both the pool and core, the positive spectral effect is offset by the negative effect of increased leakage of neutrons from the core. Table 8.2 does not mention control rods or fuel bowing because SABR's control rods haven't been designed yet and fuel bowing is negligible in SABR.

We've discussed how the reactivity feedbacks and SABR and EBR-II differ. The proceeding sections discuss why they differ.

8.2.1 Leakage Sensitivity

EBR-II has many more reflectors than SABR [47]. The outer edge of EBR-II's core is surrounded by several rows of steel reflectors. SABR has only a single row of steel reflectors on only one edge of its core. EBR-II's fuel pins contain upper and lower reflectors while SABR's contain none. SABR's fuel pins contain upper and lower internals consisting of stainless handling sockets that act as a mild reflector, but there is about half as much steel as there would be if there were just pure reflector there. The effect of EBR-II having more

reflectors than SABR is that EBR-II is more sensitive to neutron leakage.

Some of the strongest feedbacks in EBR-II are core axial and radial thermal expansion. While some of the negative reactivity created by these feedbacks is due to increased neutron leakage, the lion's share of negative reactivity comes from moving the fuel outward into regions of lower neutron importance. Because our compuational model homogenizes SABR's fuel, negative reactivity due to fuel expansion is accounted for in the grid plate expansion feedback.

Leakage sensitivity also causes sodium thermal expansion to be the second largest feedback in EBR-II. SABR has a small positive reactivity coefficient for sodium expansion in the core. It's slightly positive because of spectrum hardening. As the sodium expands, its ability to scatter and moderate neutrons decreases. The energy spectrum of the neutrons hardens, and the fission to capture ratio increases, yielding positive reactivity. This effect is most pronounced in the center of the core. When sodium expands in both the core and the pool of SABR, the positive reactivity from the spectrum hardening is less than the negative reactivity from the enhanced leakage from the core. As sodium density decreases, the neutron leakage from the core increases. EBR-II's sodium voiding feedback is larger than SABR's because it is more sensitive to leakage than SABR.

It is not possible to compare the fuel bowing in SABR and EBR-II. While the operators of EBR-II estimated positive reactivity coefficients for fuel bowing, the effect it had during the passive safey tests is unknown. Fuel bowing is a non-linear feedback. It's possible that while fuel bowing led to positive reactivity during the less severe tests, it could have still led to negative reactivity during the severe passive safety tests. It's impossible to know without seeing the actual deformed shapes the core assemblies took during a transient. Those data were not recorded by EBR-II's operators.

8.2.2 Control Rods

As EBR-II's control rods heat up, they thermally expand and protrude into the core and increase parasitic neutron absorption. This effect is not represented in our dynamic analysis of SABR, but it could be expected to be similar for SABR.

8.2.3 Neutron Source

A major difference between SABR and EBR-II is the presence of a neutron source. SABR is a fixed source system while EBR-II is a critical system. Reactivity feedbacks exert less influence in SABR than in EBR-II because SABR's kinetics equations are strongly dependent on the plasma neutron source term. The source term is relatively insensitive to temperature changes in the core. However, the source term of neutrons transmitted through the pool to the core is sensitive to the density of sodium in the pool. The maximum degree to which the pool temperature affects the source term of neutrons reaching the core is to increase it by 4% as the pool temperature rises from its steady state value up to its boiling point. This sodium voiding in the pool causes increased transmission of source neutrons from the plasma to the core.

When the sodium density in a SABR pool decreases, the subsequent increase in neutron source strength offsets the increase in fission neutron leakage.

CHAPTER 9
CONCLUSION

9.1 Summary of Results

The core avoids failure (no fuel melting or coolant boiling) for 50% (failure of 1 of 2 pumps) Lost of Heat Sink (LOHSA) and Loss of Flow (LOFA) accidents without any corrective action being taken. For 100% (failure of both pumps) LOFAs and LOHSAs, coolant boiling (1156 K) and fuel melting (1473 K) occur at about 25s and 35s, respectively, after pump failure unless corrective control action is taken before this time, in which case the core can be shut down without fuel melting or coolant boiling by shutting off the plasma power source. The present passive heat removal system is not sufficient to remove the decay heat and both fuel melting and coolant boiling ultimately occur unless some other means is provided for decay heat removal.

9.2 Suggestions for Future Work

9.2.1 Improve Passive Removal of Decay Heat

The most important thing to improve in SABR is to increase its ability to passively remove decay heat. The first step is increasing the vertical distance between the core and the heat exchanger to increase natural circulation. The second step is to add a passive heat exchanger to SABR's design such as a DRACS or RVACS.

A Direct Reactor Auxiliary Cooling System (DRACS) could improve natural circulation in the core during a transient. Oak Ridge National Lab designed the DRACS as part of the Fluoride Salt Cooled High Temperature Reactor [49]. The DRACS heat exchangers are capable of removing decay heat via natural circulation without any external power.

We could also add a Reactor Vessel Air Cooling System (RVACS). An RVACS removes

heat from a reactor core by drawing outside air in to circulate arround the outside of the vessel. Heat escapes the vessel through convective and radiative heat transfer to the circulating air. Such a system is possible, but it would require redesigning the pool walls to incorporate the air circulation.

9.2.2 Improve Strength of Reactivity Feedbacks

Increase Leakage Sensitivity

We know from our comparison with EBR-II that SABR is less sensitive to neutron leakage than EBR-II. We can make SABR more sensitive to leakage by improving its neutron economy. Adding more reflectors is an excellent way to do this. We could add upper and lower reflectors in the fuel pins. Neutronics analyses could determine how many reflectors could be added above and below the core without shielding the fuel from the plasma neutrons and negatively affecting the TRU burnup.

Add Control Rods

Modeling a bank of control rods in SABR will improve its safety characteristics. The thermal expansion of the rods won't be enough to make SABR passively safe, but it would be a big contribution. The thermal expansion of the control rods can provide significant negative reactivity. Our analysis of EBR-II shows they are integral part of passive safety even when not directly inserted into the core. There is plenty of room in each SABR pool to accommodate additional space in the core for control rod insertion.

Reduce Dependence on External Neutron Source

The dynamic safety results show us that the neutron source term in our kinetics equations dominates all of the other terms. An effective way to increase the strength of reactivity feedbacks is to reduce a core's dependence on the plasma neutron source. Increasing k_{eff} by adding more fuel assemblies would increase SABR's sensitivity to feedbacks and lead

to larger reductions in power during a transient. As we increase k_{eff}, we decrease the reactivity margin to a prompt supercritical power excursion. A neutronic optimization of SABR would identify the optimum k_{eff} at which to operate SABR.

Another idea would be to make the source term of neutrons transmitted to the core in the kinetics equations less dependent on the pool temperature. Currently, the source term provides "positive reactivity" with pool voiding. The strength increases up to 4% as the pool temperature approaches the boiling point. Removing the pool sodium between the plasma neutron source and the core would prevent the positive pool voiding feedback from occuring. This could be accomplished by moving the core as close to the pool wall as possible.

Increase Fuel Bowing

As we described earlier, fuel bowing does not appreciably affect reactivity in SABR because the power profile across the core is not steep enough. We may be able to increase the effect of fuel bowing if we are able to somehow change the power profile. It would be challenging to create a steep power profile because each SABR core is quite small relative to the mean free path of its neutrons. It may be possible to manually shape the power and temperature profiles to induce appreciable fuel bowing during a transient by varying the fuel composition from assembly to assembly. Assemblies toward the center of the core could be made to have a higher power than the ones on the outer edge.

There are two caveats to this approach. The first is burnup. If the assemblies operate at different power levels, they will achieve different burnup. This would be okay if SABR could continuously refuel its cores, but it can't. Each SABR pool was designed to be withdrawn when the fuel reaches its radiation damage limit. The assemblies with the highest power level reach their damage limits first. If the power profile is fairly flat, all of the assemblies will have close to the maximum achievable burn up. If the profile is steep and only a small number of assemblies operate at maximum power, we will burn less TRU than

we could have with a flatter profile.

The second caveat is the silicon carbide inserts. The thermal expansion coefficient of silicon carbide is half that of steel and its stiffness is twice that of steel. The silicon carbide will inhibit fuel bowing. It will not totally prevent fuel bowing, but it will certainly diminish it by resisting the movement of the fuel assemblies.

A neutronic and structural mechanics optimization effort would find the ideal power profile and core design that could maximize the effects of fuel bowing.

Appendices

APPENDIX A

SABR FUEL ISOTOPIC COMPOSITION - BEGINNING OF LIFE

Table A.1: Isotopic Composition of TRU-Zr Fuel

Isotope	Weight Fraction
Zr	0.4000
Pu-238	0.0084
Pu-239	0.2330
Pu-240	0.1039
Pu-241	0.0390
Pu-242	0.0156
Np-237	0.1000
Am-241	0.0829
Am-243	0.0171

APPENDIX B

INSTRUCTIONS ON REPRODUCING THE DYNAMIC SAFETY ANALYSIS

This appendix contains instructions on reproducing the work in this thesis. These instructions assume the reader is proficient in the use of Mathematica, MATLAB, MCNP6, NJOY, RELAP5, and COMSOL Multiphysics. All of the required tools and models are available on http://www.frc.gatech.edu/resources/thesis/andrew-bopp-phd-thesis-tools/ or by contacting the Georgia Tech Fusion Research Center. The reader should note these tools were not designed to be "general use" or "end user" tools. They were designed soley to aid in the completion of this thesis. Modifying any of the tools to will likely cause them to malfunction.

B.1 Verification Calculations

B.1.1 Fuel Bowing Model

We verified our COMSOL fuel bowing model by running the IAEA benchmark problem cited earlier in this thesis [44]. To run the problem, use COMSOL file "SABR FuelBowing Verification.mph". The COMSOL model requires the MATLAB file "fbVerification.m" to assign the temperature profile.

B.1.2 Thermal Hydraulics Model

The COMSOL TH verification tests can all be run at the same time using the COMSOL file "SABR DM thComparisons full.mph". The RELAP5 TH verification tests must be run individually. The RELAP5 files are named "COMSOL thComparisons LOFA 50.i", "COMSOL thComparisons LOFA 100.i", etc.

B.1.3 Kinetics Solver

To reproduce the verification of the kinetics solver, use Mathematica to Laplace transform the equations listed in the verification section of this thesis.

B.2 Fuel Bowing Calculations

Before the fuel bowing calculation can be run, the power profile in a SABR core needs to be generated using the MCNP6 file "SABR UPM FMESH". Export the FMESH data to a spreadsheet and run the MATLAB file "FMESH.m" to process the data. Running FMESH.m will generate 4 text files with all of the power profile information the fuel bowing calculation requires.

The fuel bowing calculation is a steady state analysis for a fixed P/F ratio. The calculation is repeated for various P/F ratios. Each calculation is a two step process. The first step is generating the temperature profile using the COMSOL file "SABR FuelBowing Complex TempGen.mph" and its required MATLAB file "comFBTemp.m". comFBTemp uses the FMESH power profile. Export the resulting temperature data to a text file. The second step uses COMSOL file "SABR FuelBowing Complex.mph". Import the temperature data in the text file and run the simulation.

Finally, export the displacement data from the fuel bowing calculation to a spreadsheet. The data will be called when creating the MCNP6 input file. This is described in the next session.

B.3 Reactivity Feedback Calculations

It is easy to calculate how the terms of our nodal kinetics model change with temperature and/or P/F ratio. It's a two step process. The first step is generating an MCNP6 input file representing a perturbed state of SABR, and the second step is running the file and processing its data. Generate the information needed for the input file by opening the MATLAB file

"testUPM.m" and adjusting the options documented within to simulate the desired perturbation. Copy and paste the contents of the resulting text file to the corresponding sections of the reference MCNP6 input file "SABR UPM ref". testUPM requires MATLAB files fbData.m, SurfaceIntersection.m, surfX.m, and UnifiedPertModelGen.m. We should note that SurfaceIntersection.m is a 3rd party function that calculates the vertices of intersection between two planes [50].

Before running MCNP6, the reader will need to generate new XSDIR and XSFILE files using NJOY and the ENDF 7.0 library. The transuranic isotopes listed in Appendix A must be Doppler broadened for temperatures of 300 K, 600 K, 829 K, 1200 K, 1500 K.

Once the MCNP6 file has been run, the corresponding text file can be automatically processed using the macro-enabled spreadsheet "SABR UPM Kinetics.xlsm".

The only remaining kinetics terms to calculate are the coupling coefficients. To calculate the coupling coefficients, use the MCNP6 file "SABR UPM alpha ref". First, configure the file to use the surface source writer and run it. Next, configure the file to use the surface source reader, set pool neutron importances to zero, and run the file. Manually, copy and paste the output into the "SABR UPM' Kinetics.xlsm" spreadsheet.

Performing the work above will give the user a spreadsheet of nodal kinetics terms for SABR at various temperatures and P/F ratios.

B.4 Dynamic Safety Calculations

To perform a dynamic safety analysis, open up the COMSOL file "SABR DM Template.mph" and configure it to reflect whatever accident scenario the reader desires. The dynamics model requires MATLAB files nodalSolve.m, nodalReaderGen.m, nodalDataGen, intrpCp.m, nodeX power, node1 reader.m through node10 reader.m, and pool1 temp.m through pool10 temp.m. The kinetics data generated by MCNP6 should be input to the matrix in nodalDataGen.m.

REFERENCES

[1] W. Stacey et al., "Resolution of fission and fusion technology integration issues: An upgraded design concept for the subcritical advanced burner reactor," Nuclear Technology, vol. 187, pp. 15–43, 2014.

[2] Iter, http://www.iter.org/, (Current as of Sep. 19 2016).

[3] C. Till and Y. Chang, Plentiful energy: The story of the integral fast reactor. CreateSpace Independent Publishing Platform, 2011.

[4] D. Wade et al., "The safety of the ifr," Progress in Nuclear Energy, vol. 31, pp. 63–82, 1997.

[5] C. Westfall, "Vision and reality: The ebr-ii story," Nuclear News, pp. 25–32, 2004.

[6] L. Koch, "Mechanical requirements of the lmfbr," Nuclear News, vol. 13, p. 61, 1978.

[7] H. Planchon et al., "Results and implications of the experimental breeder reactor ii inherent safety demonstration tests," Nuclear Science and Engineering, vol. 100, pp. 549–557, 1988.

[8] General u.s. nuclear info, https://www.nei.org/Knowledge-Center/Nuclear-Statistics/US-Nuclear-Power-Plants, (Current as of Jan. 13 2017).

[9] Backgrounder on the three mile island accident, https://www.nrc.gov/reading-rm/doc-collections/fact-sheets/3mile-isle.html, (Current as of Jan. 13 2017).

[10] J. Duderstadt and L. Hamilton, Nuclear reactor analysis. John Wiley and Sons, Inc., 1976.

[11] W. Stacey, Nuclear reactor physics. John Wiley and Sons, Inc., 2001.

[12] Backgrounder on chernobyl nuclear power plant accident, https://www.nrc.gov/reading-rm/doc-collections/fact-sheets/chernobyl-bg.html, (Current as of Dec. 30 2016).

[13] K. Obaidurrahman et al., "Spatial neutronic coupling aspects in nuclear reactors," Nuclear Engineering and Design, vol. 240, pp. 2755–2760, 2010.

[14] R. Avery, Theory of coupled reactors, Proc. of Second UN Intl. Conf. on the Peaceful Uses of Atomic Energy, 1958.

[15] H. Murray et al., "Stability of coupled core reactors by the second method of liapunov," Journal of Nuclear Energy Parts A/B, vol. 20, pp. 729–734, 1966.

[16] A. Belleni-Morante, "The kinetic behavior of a reactor composed of g loosley coupled cores: Integral formulation," Journal of Nuclear Energy Parts A/B, vol. 18, pp. 549–559, 1964.

[17] Overview of trace v5.0, Regulatory Information Conference, 2007.

[18] Relap5-3d introduction, `http://www4vip.inl.gov/relap5/relap5-3.htm`, (Current as of Sep. 19 2016).

[19] Sas4a/sassys-1 software description, `http://www.ne.anl.gov/codes/sas4a/`, (Current as of Sep. 19 2016).

[20] Purdue advanced reactor core simulator, `https://engineering.purdue.edu/PARCS`, (Current as of Sep. 26 2016).

[21] R. Al-Chalabi, "Nestle: A nodal kinetics code," Transactions of the American Nuclear Society, vol. 68, 1993.

[22] Sas-dif3dk description, `http://www.ne.anl.gov/codes/sasdif3dk/`, (Current as of Sep. 26 2016).

[23] Y. Gohar, "Fusion solution to dispose of spent nuclear fuel, transuranic elements, and highly enriched uranium," Fusion Engineering and Design, vol. 58-59, pp. 1097–1101, 2001.

[24] J. McWherter, Molten salt breeder experiement design bases, Oak Ridge National Laboratory, ORNL/TM-3177, 1970.

[25] R. Thoma, Chemical feasibility of fueling molten salt reactors with puf_3, Oak Ridge National Laboratory, ORNL/TM-2256, 1968.

[26] T. Mehlhorn et al., "Fusion-fission hybrids for nuclear waste transmutation: A synergistic step between gen-iv fission and fusion reactors," Fusion Engineering and Design, vol. 83, pp. 948–953, 2008.

[27] H. Wu et al., "A fusion-fission hybrid reactor with water-cooled pressure tube blanket for energy production," Progress in Nuclear Energy, vol. 64, pp. 1–7, 2013.

[28] M. Kotschenreuther et al., "Fusion-fission transmutation scheme - efficient destruction of nuclear waste," Fusion Engineering and Design, vol. 84, pp. 83–88, 2009.

[29] T. Sumner, "Dynamic safety analysis of the sabr subcritical transmutation reactor concept," Nuclear Technology, vol. 171, pp. 123–135, 2010.

[30] Z. Yu et al., "Feasibility study if applying the passive safety system concept to fusion-fission hybrid reactor," Fusion Engineering and Design, vol. 89, pp. 370–377, 2014.

[31] Comsol multiphysics, http://www.comsol.com/comsol-multiphysics, (Current as of Sep. 19 2016).

[32] Matlab overview, http://www.mathworks.com/products/matlab/, (Current as of Sep. 19 2016).

[33] COMSOL, Comsol multiphysics reference manual v5.2, 2015.

[34] Why all these stresses and strains? https://www.comsol.com/blogs/why-all-these-stresses-and-strains/, (Current as of Feb. 10 2017).

[35] S. Hayes and M. Meyer, Personal Communication (2007) w/ Argonne National Lab.

[36] J. Cole et al., Developing and evaluating candidate mtls. for gen. iv supercritical water reactors, Idaho National Laboratory, INL/EXT-06-01382, 2006.

[37] J. Fink and L. Leibowitz, Thermodynamic and transport properties of sodium liquid and vapor, Argonne National Laboratory, ANL/RE-95/2, 1995.

[38] D. Zigrang and N. Sylvester, "A review of explicit friction factor equations," Trans. of ASME, vol. 107, pp. 280–283, 1985, Journal of Energy Resources Technology.

[39] R. Seban and T. Shimazaki, Trans. of ASME, vol. 73, p. 803, 1951.

[40] Matlab function "ode15s" description, https://www.mathworks.com/help/matlab/ref/ode15s.html, (Current as of Feb. 10 2017).

[41] Lanl monte carlo working group, https://mcnp.lanl.gov/, (Current as of Sep. 19 2016).

[42] Y. Chang et al., Advanced burner test reactor preconceptual design report, Argonne National Laboratory, ANL/ABR-1, 2008.

[43] Wolfram mathematica, https://www.wolfram.com/mathematica/, (Current as of Dec. 26 2016).

[44] I. A. E. Agency, Verification and validation of lmfbr static core mechanics codes, part i, IAEA International Working Group on Fast Reactors, IWGFR/75, 1990.

[45] N. Todreas et al., Nuclear systems, volume 2. Hemisphere Publishing Corporation, 1990.

[46] A. Rineiski, "Decay heat production in a tru burner," Progress in Nuclear Energy, vol. 50, pp. 377–381, 2008.

[47] L. Koch, Ebr-ii: An integrated experimental fast reactor nuclear power station, Report Authorized by Argonne National Laboratory, N/A.

[48] W. Lehto et al., "Safety analysis for the loss of flow and loss of heat sink without scram tests in ebr-ii," Nuclear Engineering and Design, vol. 101, pp. 35–44, 1987.

[49] A. Qualls et al., Fluoride salt-cooled high-temperature demonstration reactor point design, Oak Ridge National Laboratory, ORNL/TM-2016/85, 2016.

[50] Mathworks file exchange, `http://www.mathworks.com/matlabcentral/fileexchange/48613-surface-intersection`, (Current as of Mar. 15 2017).